I. PROJECTED G1 WAVEFUNCTIONS FOR He_2

II. LOCALIZED WAVEFUNCTIONS FOR H_2O, OH, AND O

Thesis by

Steven Lawrence Guberman

In Partial Fulfillment of the Requirements

For the Degree of

Doctor of Philosophy

California Institute of Technology

Pasadena, California

1973

(Submitted November 7, 1972)

To Mom, Dad and Stan

ACKNOWLEDGMENTS

First I wish to thank all the past and present members of the MQM group for many spirited and enlightening discussions and for the use of their computer programs and subroutines. In this regard I am especially grateful to Dave Huestis, Bob Ladner, Thom Dunning, Richard Blint, Vince Gutschick, Al Fordyce Wagner, and Ivar T. Zambatz.

I want to express my deep gratitude to Bill Goddard for his invaluable advice and criticism generously offered throughout the course of this research.

I am quite grateful to those here at Caltech and in Pasadena who aided in my escaping the grasp of the Selective Service System, Local Board No. 38A.

I thank Dr. Soe Aung for first bringing to my attention the interesting problems associated with the excited states of He_2. This occurred while savoring various culinary delights during "dinner" at the Greasy. The need for quotes is self-explanatory.

I am also much indebted to Adria Larson for her help in preparing correspondence, applications, etc., over the last few years.

For financial support I thank the Woodrow Wilson Fellowship Foundation and Caltech.

Finally I thank the cities of Pasadena and Los Angeles for generating enough smog to keep me indoors preparing this thesis.

ABSTRACT

I. The low-lying excited states of He_2 have been examined using projected Generalized Valence Bond wavefunctions. Two types of interactions are shown to be important in understanding the anomalous maxima and the general shapes of the curves. The interaction between core orbitals on opposite centers is important at small R whereas at large R the dominant interaction is between core and Rydberg orbitals on opposite centers. The latter effect is expressible in terms of the exchange kinetic energy and arises from the repulsion between singlet coupled pairs of orbitals. This is described simply in terms of the shapes of the Rydberg orbitals. The results in general agree favorably with experiment where such comparison can be made.

II. Localized wavefunctions obtained from applying an external localization criterion to orbitals resulting from the GF method are reported for H_2O, OH, and O. The shapes and angles between the orbitals are described in some detail. It is shown that the resulting GF orbitals change in a chemically reasonable manner as we proceed from O to OH to H_2O.

TABLE OF CONTENTS

PART I

PROJECTED G1 WAVEFUNCTIONS FOR He_2

A. INTRODUCTION

In the recent past considerable progress has been made here at Caltech in developing wavefunctions which not only provide a near quantitative description of chemical systems but which most importantly provide for a readily interpretable description.[1a] This latter emphasis has led to the development and application of improved independent particle wavefunctions.[1b] Such wavefunctions consist of orbitals each of which is viewed as containing an electron which moves in an average field due to all the other electrons. This interpretation is a direct consequence of the variational principle.[1c] Each electron is considered as a separate interacting entity allowing for a description of just what the individual electrons are doing in atoms and molecules. This feature of independent particle wavefunctions has been shown to provide a powerful interpretive tool for understanding chemical systems.[2] The development of the Generalized Valence Bond or GI method has further enhanced this interpretability by overcoming many of the problems associated with Hartree-Fock wavefunctions. Thus our objective has been not to calculate wavefunctions, etc. to umpteen decimal places but instead to provide an understanding of chemical systems which often cannot be attained experimentally or by other theoretical methods. The excited states of He_2 investigated here by the spatially projected G1 method afford one such opportunity. These states have several characteristics which although discovered experimentally have remained only poorly understood. Some of these are discussed

immediately below while others are discussed in later sections.

In 1924 Theodore Lyman[3] reported his observations of the spectra excited by a continuous discharge through helium gas. In addition to seeing a line at 584.4 Å corresponding to the $1\ ^1S \rightarrow 2\ ^1P$ atomic transition, he also saw a "line" of diffuse character (sometimes shaded toward the red) at 600.3 ± 0.6 Å. Although Lyman expressed some doubt that the "line" was due to helium he found that as the purity of the helium was increased the intensity of the line did not change much with respect to the lines of the $1\ ^1S \rightarrow n\ ^1P$ series. Also, the line did not, in general, overlap the dipole forbidden line $1\ ^1S \rightarrow 2\ ^1S$ at 601.4 Å. This forbidden line was only present in violent disruptive discharges whereas the "line" at 600.3 was strong in continuous discharges. Lyman could offer no explanation for the origin of the "line".

Unfortunately, progress was slowed by the presence of a Ne line, $(2p)^6\ ^1S \rightarrow (2p)^5\ (5s)\ ^1P$, which falls at 600.03 Å. Since Ne is a frequent impurity[4] in He, it could be excited by collisions with excited He atoms. As a result several workers[5a] proposed that the line observed by Lyman was a Ne line. The origin of Lyman's anomalous line was finally attributed to He after investigations[5b, c] of more highly purified gas.

In 1935, J. L. Nickerson[6] confirmed the helium origin of the line and found that the intensity of the 600 Å band varied approximately as the first power of the current (although he did not state the range of current). From this he concluded that the band came from a molecular

state formed from a ground state atom and an atom excited by collision with an electron. In view of Kruger's[5c] work, in which it was found that the forbidden line at 601.4 Å never appears without the band, the pertinent excited atomic state was taken to be $2\ ^1S$. Nickerson also identified other bands arising from transitions between lower vibrational levels of this molecular state ($A\ ^1\Sigma_u^+$) to the repulsive $X\ ^1\Sigma_g^+$ as comprising the continuum observed by Hopfield.[7a]

Now Nickerson was left with one problem. The molecular transition $A\ ^1\Sigma_u^+ \rightarrow X\ ^1\Sigma_g^+$ at 600.019 Å occurs with an energy of 385 cm^{-1} greater than the forbidden atomic transition. This led Nickerson to consider the possibility of a maximum in the upper A state occurring at large internuclear distances (above the nearly horizontal part of the ground state curve). But there are no curves of the same symmetry near enough to the A state to result in an avoided crossing leading to a potential maximum. Thus Nickerson ended his paper without being able to offer an explanation for the origin of the 600 Å band.

Since this early work there have been many theoretical and experimental investigations into the excited states of He_2. Most of these will be discussed later. It has now been well established that although the ground state of He_2 is primarily repulsive (exhibiting only a van der Waals minimum of 8.75×10^{-4} eV at 2.9 Å)[7b] many of the excited states are bound with respect to the corresponding excited states of the separated atoms. We will show here that many of the curves have potential maxima between 1.5 Å and 3.5 Å and in addition have a minimum near 1 Å with a binding energy of up to 2 eV.

The primary objective of this investigation is to examine the nature of the interactions responsible for the shapes of the excited state potential curves. Since Nickerson's paper, several theoretical and experimental investigations have confirmed the existence of a potential hump in the $A\,^1\Sigma_u^+$ state of He_2. But in spite of this there has still been no explanation offered for its origin. Such an explanation, in terms of nonbonding interactions, is offered here. In addition, the origin of the maxima in other curves and the other interactions leading to their general shapes is also discussed.[8]

In the following section we will first discuss the wavefunctions, their general characteristics, and other details of the method. In section C the resulting potential curves, orbitals, etc. are presented, the nature of the important interactions are explained, and the results are compared with spectroscopic data and calculations reported by others. In section D we discuss the application of the ideas discussed here to two additional systems. Finally, in the last section we will discuss dissociative recombination and associative ionization in terms of our potential curves and the observations of others.

B. THE WAVEFUNCTIONS

1. Form of the Wavefunctions

The Hartree-Fock (HF) method for electronic wavefunctions leads to orbitals in terms of which the wavefunction may be readily interpreted, but for many systems, including the excited states of He_2, it leads to an

improper description at large R. In these cases the HF wavefunction does not dissociate to the correct separated atom limit. The configuration interaction (CI) method can lead to a proper description of the potential curves but cannot be interpreted as easily as HF. Here we use wavefunctions closely akin to valence bond (VB) wavefunctions except that a different orbital is used for each electron, we solve for all orbitals self-consistently at each internuclear distance, and there are no orthogonality constraints between orbitals. Such wavefunctions are referred to here as generalized valence bond (GVB) wavefunctions, or more specifically, as spatially projected G1 wavefunctions.[9]

In this description the wavefunction for an excited singlet state of the He atom is described as

$$\mathcal{A}\{[\phi_{\bar{c}}(1)\phi_{v}(2) + \phi_{v}(1)\phi_{\bar{c}}(2)]\alpha\beta\} \qquad (1)$$

(where $\mathcal{A}$ is the antisymmetrizer) and denoted as in Fig. 1a. Here $\bar{c}$ is a 1s-like core orbital and v is the excited orbital (v = 2s for the $2\,^1S$ state and v = 2p for the $2\,^1P$ state, see Fig. 2). Orbital $\phi_{\bar{c}}$ is very nearly the same for the various states of the He atom. The ground state also has the form in (1) but in this case both orbitals are 1s-like core orbitals.

At large R the GVB wavefunction for the ground state of He_2 has the form

$$\mathcal{A}\{[\phi_{c\ell}\phi_{c'\ell} + \phi_{c'\ell}\phi_{c\ell}][\phi_{cr}\phi_{c'r} + \phi_{c'r}\phi_{cr}]\alpha\beta\alpha\beta\} \quad , \qquad (2)$$

which we will denote as in Fig. 1b, where $\phi_{c\ell}$ and $\phi_{c'\ell}$ and He $1\,^1S$ orbitals on the left and ϕ_{cr} and $\phi_{c'r}$ are He $1\,^1S$ orbitals on the right.

For the case of an unexcited atom on the left and an excited one on the right, the wavefunction is denoted as in Fig. 1c, where the $\bar{c}$ is not quite equivalent to c or c′. The wavefunction of Fig. 1c must be combined (as in Fig. 1de) with another having inversions of these orbitals to obtain excited states having g or u symmetry. The wavefunctions of Fig. 1de are now written as (omitting the normalization constant)

$$\Psi_{g,u} = \mathcal{A}\{([\phi_{c\ell}\phi_{c'\ell} + \phi_{c'\ell}\phi_{c\ell}][\phi_{\bar{c}r}\phi_{vr} + \phi_{vr}\phi_{\bar{c}r}] \pm [\phi_{cr}\phi_{c'r} + \phi_{c'r}\phi_{cr}][\phi_{\bar{c}\ell}\phi_{v\ell} + \phi_{v\ell}\phi_{\bar{c}\ell}])\alpha\beta\alpha\beta\} \quad (3)$$

Thus for each internuclear distance we take the wavefunctions of the excited states of He_2 to have the form shown in (3) and Fig. 1d or 1e, and we solve for the orbitals self-consistently. As a result the orbitals for a g state (Fig. 1d, + sign in (3)) are not exactly the same as those for the corresponding u state (Fig. 1e, - sign in (3)). The core orbitals (c, c′, and $\bar{c}$) change only very slightly from state to state, and in our discussions we will ignore changes in the core orbitals (see Fig. 3).

The wavefunction shown in (3) can also be written as:

$$\Psi_{g,u} = P_{g,u}G_1^{\gamma}\phi_{c\ell}\phi_{c\ell'}\phi_{\bar{c}r}\phi_{vr}\,\alpha\beta\alpha\beta \quad (4)$$

As a result our wavefunction is the same as the G1 wavefunction[9a] except for the presence of the spatial projection operator, $P_{g,u}$ ($P_{g,u} = 1 \pm i(1)i(2)i(3)i(4)$) where i is an inversion operator. Thus, just as with the G1 wavefunction, we retain an independent particle interpretation of the orbitals. This proof[9a] of this is the same as that for the G1 wavefunction

with the replacement of $P_{g,u}G_1^{\gamma}$ for G_1^{γ}. Also the proofs[10a] for the existence of uppers bounds on the exact energies for excited states calculated by G1 wavefunctions can easily be extended to cover the self-consistent projected wavefunctions discussed here. Our approach to solving for the self-consistent orbitals in a CI-like manner (see below) makes for an obvious application of the Hylleraas-Undheim and McDonald Theorem[11] for upper bounds to the exact excited energies calculated by our SCF wavefunctions. Note that such an application cannot be made for the wavefunctions constructed from orbitals which are not determined self-consistently.

2. Method

In order to solve for the orbitals the wavefunction was written as a CI wavefunction by expanding one of the four orbitals in terms of its basis functions:

$$\Psi_{g,u} = P_{g,u}G_1^{\gamma}\left(\sum_i^N C_i^{vr}\phi_{c\ell}\phi_{c\ell'}\phi_{\bar{c}r}\chi_i\right)\alpha\beta\alpha\beta \qquad (5)$$

We proceed in the usual manner by forming the Hamiltonian matrix except that now the matrix is formed over the following functions (when solving for ϕ_v)

$$P_{g,u}G_1^{\gamma}\phi_{c\ell}\phi_{c\ell'}\phi_{\bar{c}r}\chi_i \qquad (6)$$

Expanding G_1^{γ}, each matrix element is now given by

$$H_{ij} = \langle\phi_{c\ell}\phi_{c\ell'}\phi_{\bar{c}r}\chi_i\,|H|\,P_{g,u}O_{11}^{\gamma}\phi_{c\ell}\phi_{c\ell'}\phi_{\bar{c}r}\chi_j\rangle \quad . \qquad (7)$$

Thus for N basis functions we need to calculate N(N+1) G1 energies in

order to form the H matrix. In addition, we also calculate the N(N+1) elements of the overlap matrix, S, over the functions shown in (6). For each orbital we solve the matrix equation

$$HC = SC\Lambda \ . \qquad (8)$$

The new orbital is then placed into (8) and we solve for another orbital. This continues until all four orbitals have converged. Since we solve for one orbital at a time all of the needed integrals do not change when we proceed to solve for another orbital. The current program provides for eliminating the recalculation of these integrals although the time savings is small. In addition, this approach does not involve third and fourth order density matrices (see section C. 2.) and is considerably simpler than other approaches.[9c, 10a] Nevertheless, its major drawback is that we solve for only one orbital at a time leading to a considerable time expenditure before convergence is reached. The time needed to solve for one orbital is roughly N(N+1)/12 seconds on an IBM 370/155 computer.

3. Basis Set

The basis set consisted of 6 s-type, 2 p-type, and 1 d-type contracted Gaussian on each He constructed from a primitive set of 13 1s-type, 6 2p-type, and 4 3d-type Gaussians. The exponents and contraction coefficients are shown in Tables I and II. The first ten exponents in the s set were obtained from Huzinaga.[12] Three additional diffuse basis functions were added keeping the ratio of the exponents constant. The first five p exponents shown in Table II were taken from Table VI of Huzinaga[12] and scaled by a factor of 1.06524 to be appropriate for He.

The scale factor was obtained using an estimate of the He 2p orbital energy obtained from Moore.[13] The sixth p exponent was determined from the ratio of the fourth and fifth exponents. Finally the four d exponents were taken from the set of 3s exponents given in Table VII of Huzinaga and were rescaled by a factor of 1.001146 in order to be appropriate for He.

The contraction coefficients were determined from G1 calculations on the atomic states using the primitive basis. The 1s and 1s′ contractions were determined from a 13s calculation on $1\,^1S$ giving an energy of -2.877985 a.u. The $\overline{1s}$ and 2s contractions are the two orbitals obtained from a 13s calculation on $2\,^2S$ giving an energy of -2.143465 a.u. The 3s is the valence orbital also obtained from a 13s calculation on $3\,^1S$ yielding an energy of -2.059201 a.u. The thirteenth s primitive was allowed to remain free. The p contraction was determined from a ⟨4s, 6p⟩ calculation. Here the 4s set consisted of the $\overline{1s}$, 2s, 3s and s″ functions shown in Table I. This contraction was used because the early exploratory calculations were done with Bob Ladner's G1 program[9c] which restricted the number of basis functions to 14 and necessitated an unsymmetrical basis set on the nuclei. This contraction was kept for the symmetrical basis used here and differs by only 3×10^{-5} a.u. from the energy calculated for $2\,^1P$ with a ⟨6s, 6p⟩ basis. The energy for ⟨4s, 6p⟩ $2\,^1P$ was -2.122410 a.u. The last p function was left free. The d contraction was obtained from a ⟨4s, 4d⟩ calculation on $3\,^1D$. The s set was the same as that used for $2\,^1P$. We obtained an energy of -2.054738 a.u. for $3\,^1D$. This was 3×10^{-4} a.u. worse than that for ⟨6s, 4d⟩. It should be pointed out that the d functions used here are

$3d_{z^2}$ (i.e., $\propto z^2 e^{-\xi r^2}$).

C. INTERPRETATION

There are essentially two types of interactions responsible for the shapes of the He_2^* potential curves. There is a long range exchange interaction ($R > \approx 5.0$ Bohr) which often results in small repulsive maxima and a short range interaction ($R < \approx 5.0$ Bohr) which determines the shape of the curves at small R. In order to understand these effects this analysis of the excited states will utilize two types of potential curves. The first type, to be discussed later, is obtained from fully self-consistent results using the wavefunction shown in (3) and Fig. 1de. The second type is obtained from a frozen orbital (FO) wavefunction. This wavefunction is that shown in (3) and Fig. 1de except that at each internuclear separation, R, the orbitals are now restricted to be those self-consistently obtained at $R = \infty$. The FO curves will be seen to be quite useful in that they exhibit many of the important features of the SCF curves and allow us to understand the pertinent interactions without having to consider the simultaneous self-consistent readjustment of the orbitals. In addition, the gross features of several of the self-consistent curves will be seen to arise from avoided crossings of FO curves. Before proceeding further we note that FO potential curves will be designated as $\phi_v = n\ell$ or $v = n\ell$, $^{1,3}\Sigma^+_{g,u}$(FO) while SCF curves are designated as $^{1,3}\Sigma^+_{g,u}(n\ell)$ where $n\ell$ is the $R = \infty$ limit of the Rydberg orbital.

1. Short Range Interaction--The Three Electron Core

In Fig. 4 we show several FO curves[14a] corresponding to the approach of a ground state He atom to He(1s, 2s) ^1S, He(1s, 2p) ^1P, He(1s, 3s) ^1S, He(1s, 3p) ^1P, He(1s, 3d) ^1D, and $He^+(1s)$ ^2S. We note that without exception as R is decreased each state due to the inversion symmetry splits into two states one of which is repulsive while the other is attractive. Note also that the three electron FO curves show the purely repulsive nature of the $^2\Sigma_g^+$ state of He_2^+ and the attractive nature of $^2\Sigma_u^+$.

In order to understand these short range interactions we must first consider the large size of the excited Rydberg orbitals compared to the three core-like orbitals. This is shown in Table III where we have chosen $\langle z^2 \rangle^{\frac{1}{2}}$ somewhat arbitrarily as an indication of the relative sizes of the orbitals. We see that the smallest of the Rydberg orbitals, the 2s orbital, is more than four times "larger" than the 1s' He core orbital. Thus as the two He centers approach each other in Fig. 4, for R less than the size of ϕ_v, but greater than the size of the core orbitals we find that ϕ_v is approximately equally shared by both heliums and where ϕ_v was a separated atom s or d orbital we can take $\phi_{vr} \approx \phi_{v\ell}$ in the wavefunctions denoted by Fig. 1de. For these g states the wavefunction can now be written as in Fig. 1f. Factoring ϕ_v out of the wavefunction leads to the three electron wavefunction shown in Fig. 1g. This describes the repulsive $^2\Sigma_g^+$ state of He_2^+ already mentioned and shown in Fig. 4. The same procedure applied to Fig. 1e leads to the attractive three electron $^2\Sigma_u^+$ state shown in Fig. 1h.

Consider now the v = 2s FO curves shown in Fig. 4. In the u state, which is denoted as the A state, the interaction of the three core orbitals is attractive and as a result the 4 electron curve is attractive. In the corresponding g state the core orbitals interact repulsively leading to a repulsive 4 electron curve. This may also be viewed by noting that we may write our wavefunction as

$$\Psi_{g,u} = G_1^{\gamma} \Phi_{g,u} \, \alpha\beta\alpha\beta \tag{9}$$

where we have

$$\Phi_{g,u} = \phi_{c\ell}\phi_{c'\ell}\phi_{\bar{c}r}\phi_{vr} \pm \phi_{cr}\phi_{c'r}\phi_{\bar{c}\ell}\phi_{v\ell} \tag{10}$$

and the orbitals are those obtained self-consistently at R = ∞. Taking ϕ_{vg} and ϕ_{vu} to be symmetry functions we have:

$$\begin{aligned} \phi_{v\ell} &= C_1\phi_{vg} - C_2\phi_{vu} \\ \phi_{vr} &= C_1\phi_{vg} + C_2\phi_{vu} \end{aligned} \tag{11}$$

Substituting (11) into (10) we obtain

$$\Phi_g = C_1\Phi_g^+\phi_{vg} + C_2\Phi_u^+\phi_{vu} \ , \tag{12}$$

$$\Phi_u = C_1\Phi_u^+\phi_{vg} + C_2\Phi_g^+\phi_{vu} \tag{13}$$

where we have for the spatial He_2^+ wavefunctions

$$\Phi_g^+ = \phi_{c\ell}\phi_{c'\ell}\phi_{\bar{c}r} + \phi_{cr}\phi_{c'r}\phi_{\bar{c}\ell} \tag{14}$$

$$\Phi_u^+ = \phi_{c\ell}\phi_{c'\ell}\phi_{\bar{c}r} - \phi_{cr}\phi_{c'r}\phi_{\bar{c}\ell} \ . \tag{15}$$

From normalization of $\phi_{v\ell}$ and ϕ_{vr} and their overlap we determine C_1 and C_2:

$$C_1^2 = (1 + S_{\ell r})/2, \qquad C_2^2 = (1 - S_{\ell r})/2 \tag{16}$$

where $S_{\ell r} = \langle \phi_{v\ell} / \phi_{vr} \rangle$.

Thus from the overlap of the excited orbital with its inversion on the opposite center one can determine at a particular R the amount of g or u core character in our wavefunction. At $R = \infty$ we have from (16) $C_1^2 = 0.5$ and $C_2^2 = 0.5$. The values of C_1^2 and C_2^2 are important for distances smaller than about 8.0 Bohr where the $^2\Sigma_u^+$ and $^2\Sigma_g^+$ He_2^+ curves begin to split appreciably (see Fig. 4). From Table IV we see that for the v = 2s FO wavefunction $S_{\ell r}$ increases with decreasing R leading to a large value of C_1 at R = 2.2. Thus the frozen wavefunction for v = 2s has almost entirely a repulsive g core for the 4 electron g state and an attractive 3 electron u core for the 4 electron u state. This leads the v = 2s $^1\Sigma_g^+$ (FO) state to be totally repulsive while the v = 2s $^1\Sigma_u^+$ (FO) state is attractive as shown in Fig. 4. Note also from Table IV that the FO and SCF results are similar for v = 2s $^1\Sigma_u^+$ but quite different for v = 2s $^1\Sigma_g^+$ at small distances. This is also seen in Figs. 5 and 6 where we show the SCF and FO curves together. Thus the FO results provide for a reasonable description of the A state but are not adequate for v = 2s $^1\Sigma_g^+$ at small distances. We will come back to this later.

For v = 2p and R less than the size of v but greater than the size of core orbitals we can take $\phi_{vr} \approx -\phi_{v\ell}$. Thus our wavefunction now

takes the form shown in Fig. 1jk and the results are qualitatively the opposite from v = 2s. We now find that the 4 electron g state has the attractive core while the u state has the repulsive core. This is shown in Fig. 4. The large barrier in the v = 2p $^1\Sigma_g^+$ (FO) curve is due to an exchange effect which will be discussed later. Note that for v = 2p in Table IV, $S_{\ell r}$ is positive at large distances but decreases and becomes increasingly negative at smaller R. At large distances only the two lobes of the same sign overlap whereas (retaining the same phases) at smaller distances lobes of opposite sign overlap leading to a negative overlap as shown below.

Small R Large R

From Table IV we see that this results in $^1\Sigma_g^+$ (FO) having mostly unfavorable core at large R and favorable core at small R. Thus at large R (e.g., 5.8 Bohr) where $^2\Sigma_g^+$ and $^2\Sigma_u^+$ are already split we would expect $^1\Sigma_g^+$ (FO) to be first more repulsive than $^1\Sigma_u^+$ and then cross $^1\Sigma_u^+$ falling beneath it at smaller R. This does indeed happen and can be seen in Fig. 4. But it must be pointed out that this provides only a small contribution ($\approx$ 12%) to the splitting of $^1\Sigma_g^+$ (FO) and $^1\Sigma_u^+$ (FO), v = 2p at R = 5.8. This is because C_1 and C_2 are quite close to 0.5 and $^2\Sigma_g^+$ and $^2\Sigma_u^+$ are

nearly equally split at R = 6.2, 5.8 as seen in Table IV. In addition we see from Fig. 2 that the v = 2p curves start to split appreciably before $^2\Sigma_g^+$ and $^2\Sigma_u^+$ split. Thus the splitting of these curves at large R and the major contribution at smaller R ($> 4.2\ a_0$) appear to be an effect of the spatial projection involving ϕ_v.

From Table IV we see that for v = 3p, $C_2 > C_1$ for $R \leq 8.0$ and as a result we would not expect this effect to cause the FO curves to cross as we did for v = 2p. But as in the case of v = 2p we find $^1\Sigma_g^+$ to be attractive at small R and $^1\Sigma_u^+$ to be repulsive.

From Fig. 4 we see that for the n = 3 states the splitting of the states occurs at nearly the same R as for $^2\Sigma_{g,u}^+$ in agreement with what has been said above. Data for v = 3s and 3d are also shown in Table IV and the conclusions are as expected.

These results apply equally well to $^3\Sigma$ states. For R small enough so that $\phi_{vr} \approx \phi_{v\ell}$ or $\phi_{vr} \approx -\phi_{v\ell}$ these states lead to the same combinations of $^2\Sigma_u^+$ and $^2\Sigma_g^+$ components of He_2^+ as for the $^1\Sigma$ states.

From the above considerations we expect that for FO, v = npπ, $^1\Pi_g$ will be attractive at small R and $^1\Pi_u$ will be repulsive while the reverse will hold for v = ndπ. For v = 2pπ, 3pπ and 3dπ these predictions have been confirmed for $^3\Pi_u$ and $^1\Pi_u$ states by the CI calculations of B. K. Gupta and F. A. Matsen,[15] and those of J. C. Browne.[16] In addition, Ginter[17] has observed experimentally that the v = 2pπ $^3\Pi_u$ state appears to have a large maximum since the fourth vibrational level is observed which is at an energy approximately equal to the separated atom $1s^2\ ^1S + (1s, 2p)\ ^3P$ limit. As predicted here (and confirmed by

calculations in Refs. 15 and 16) a large maximum in $v = 2p\pi\ ^3\Pi_u$ or $^1\Pi_u$ would be caused by the repulsive $v = 2p\pi$ curve avoiding a curve crossing with the attractive curve of the same total symmetry from $v = 3d\pi$. The above results have also been confirmed by calculation for $v = 2p\ ^1\Pi_g$ and $^1\Pi_u$ by B. K. Gupta et al.[18]

Thus in summary we see that of the two couplings resulting from a specific excited state of He_2 one leads to attractive He_2^+-like core-core interactions and one leads to repulsive core-core interactions. The sign of the resulting interaction depends upon the symmetry of ϕ_v, i.e., $^{3,1}\Sigma_u^+$ is favorable for $v = 2s,\ 3s,\ 3d$ and $^{3,1}\Sigma_g^+$ is favorable for $v = 2p,\ 3p,\ 4f$. In addition for $v = 2p\ ^{3,1}\Pi_g$ is favorable and for $v = 3d\ ^{3,1}\Pi_u$ is favorable. Further experimental and theoretical results relating to the discussion here will be presented when we discuss the SCF curves in section C. 3.

2. Exchange Interactions Involving the Rydberg Orbital

A wavefunction of the form shown in Fig. 1b consisting of a singlet pair on the left and a singlet pair on the right leads to a repulsive interaction in the energy curve (the well-known repulsion of closed shells) as long as van der Waals correlation effects are ignored. Thus considering the excited states in the form shown in Fig. 1c, we would expect all of these states to be repulsive for large R (assuming the orbitals to be σ-like, i.e., not orthogonal by symmetry).

We will proceed to examine this repulsive effect by considering the exchange kinetic energy, T^X. We define T^X as

$$T^X = T - T^{c\ell} \tag{17}$$

where T is the total kinetic energy and $T^{c\ell}$ is a classical kinetic energy defined by

$$T^{c\ell} = \sum_{i=1}^{n} \langle i | t_i | i \rangle \quad . \tag{18}$$

Here n is the number of electrons and $t_i = -\frac{1}{2}\nabla_i^2$. $T^{c\ell}$ is therefore the total kinetic energy for a classical Hartree-type wavefunction which does not invoke the Pauli principle.

C. W. Wilson and W. A. Goddard III[19] have discussed the importance of the exchange kinetic energy in bonding. In a study of H_2, He_2 ($\chi\ ^1\Sigma_g^+$) and six other small molecules they found that T^X was the important factor in determining bond formation. It is well-known that the total kinetic and potential energies are poor indicators of binding.

In addition a partition of the potential energy into nuclear-nuclear, nuclear-electron and electron-electron terms is not useful since, e.g., for He_2 these terms vary approximately as 4/R, -8/R, 4/R, respectively at large R whether or not the system is bound. But for H_2 Wilson and Goddard found that for a partition of the total energy into an exchange part, E^X, and a classical part, $E^{c\ell}$, that the exchange part dominated the classical part and for H_2 ΔE^X provided two-thirds of the binding energy (for SCF wavefunctions ΔE^X did not always dominate $\Delta E^{c\ell}$ in other systems). A further partition of E^X into V^X, the nuclear-electron exchange energy, $2^X_{e\ell}$, the exchange part of the electron-electron energy and T^X showed that T^X dominated V^X and $2^X_{e\ell}$ and in addition had the correct sign to determine bonding for all the systems considered. Here V^X is defined as in (17) and (18) except that we replace t_i with $-z_A/r_{Ai}$ $- z_B/r_{Bi}$ where A and B denote the nuclei and z is the nuclear charge. We define $2^X_{e\ell}$ as:

$$2^X_{e\ell} = 2_{e\ell} - 2^{c\ell}_{e\ell} \tag{19}$$

where

$$2^{c\ell}_{e\ell} = \sum_{i>j} \langle ij \left| \frac{1}{r_{12}} \right| ij \rangle \quad , \tag{20}$$

and involves only coulomb integrals. Also it was found that for H_2 T^X was quite insensitive to self-consistent adjustment of the orbitals and in addition, for all molecules studied, the general conclusions reached from consideration of T^X were the same for SCF and frozen wavefunctions. Before proceeding with a discussion of exchange effects in He_2^* it is important to show that these ideas are also valid for He_2^*.

In Tables V-X we show the partition of the energy and the changes in the various components as R is decreased from infinity. Since we are interested in explaining the origin of maxima which occur in the potential curves at large R we only give energies at large R. In addition, in order to simplify the discussion we have calculated the energies in Tables V, VI, VIII-X with frozen unprojected wavefunctions. Since we are at large R these energies are similar to those obtained from projected SCF wavefunctions. In Table VII we show for comparison some SCF energies.

First we note from Tables V-X that for the frozen wavefunctions $E^{c\ell}$ ($E^{c\ell} = T^{c\ell} + V^{c\ell} + 2^{c\ell}_{e\ell}$) opposes E, decreasing when E increases and increasing when E decreases. In all frozen cases $\Delta E^{c\ell}$ remains negative at these distances. On the contrary the total exchange energy E^X ($E^X = T^X + V^X + 2^X_{e\ell}$) parallels E for the frozen wavefunctions. Also ΔE^X dominates $\Delta E^{c\ell}$ and therefore also dominates the total frozen energy. But in agreement with the results of Wilson and Goddard we find these results change considerably for SCF wavefunctions. In Table VII we see that with the exception of $^1\Sigma_u^+(2p)$ $\Delta E^{c\ell}$ is positive. In addition ΔE^X, although remaining positive here for ΔE positive, no longer always dominates $\Delta E^{c\ell}$ and thereby ΔE. Thus the $\Delta E^{c\ell} - \Delta E^X$ partition is somewhat erratic for these excited states and appears to confirm earlier results[19] on other systems.

Further examination of the tables shows that for the frozen wavefunctions ΔT^X always dominates ΔE^X and ΔE. In addition it has the same sign as ΔE and always parallels ΔE. The remaining parts of the

frozen exchange energy, ΔV^X and $\Delta 2^X_{e\ell}$ always have a sign opposite to ΔE and always change in opposition to ΔE. For the SCF wavefunctions we see that both ΔV^X and $\Delta 2e\ell^X$ are somewhat erratic. Nevertheless ΔT^X remains positive and is always greater than ΔE (although SCF effects have reduced $\Delta T^X/\Delta E$). The relevance of ΔT^X to bonding is further shown in Figs. 8, 9 and 10 where we show ΔT^X and E for the frozen and SCF wavefunctions of C $^1\Sigma_g^+$ (2s), $^1\Sigma_g^+$ (2p), and $^1\Sigma_g^+$ (3s). From the Figures it is seen that T^X always follows E. This occurs even for the multiple minima in the SCF $^1\Sigma_g^+$ (3s) curve. Thus T^X appears to play an important role here in determining bonding. We will now proceed to analyze the maxima in our potential curves at large R in terms of pair-wise contributions to T^X.

It has been shown[19] that for a spatially unprojected G1 wavefunction we can write,

$$T^X = \sum_{i>j}^{n} T^X_{ij} \tag{21}$$

where

$$T^X_{ij} = -\frac{1}{N} S_{ij} D^j_i \tau_{ij} \ . \tag{22}$$

Here N is the normalization constant for the total wavefunction, S_{ij} is the overlap integral between orbitals i and j and τ_{ij} is given by

$$\tau_{ij} = t_{ii} + t_{jj} - 2t_{ij}/S_{ij} \tag{23}$$

where t_{ii} is the integral shown in (17). D^j_i is a first-order density

matrix.[9a] D_i^j is expressed in terms of orbital overlaps and is important here because of the non-orthogonality of the orbitals. Thus for the spatially unprojected wavefunction we can express the total kinetic energy as

$$T = \frac{1}{N} \sum_{i,j}^{n} D_i^j t_{ij} \quad . \tag{24}$$

Note that for a Hartree-Fock wavefunction we have $D_i^j = \delta_{ij}$ in (24). In addition to overlaps, D_i^j also contains the coefficients, $U_{r_1\sigma}$, of the permutation σ which appears in the spatial part of the G_1 operator shown in (4). In evaluating spin independent energy integrals over G_1 wavefunction we only need to consider[9a] part of the G_1 operator, namely O_{11}. Thus for the total overlap in the denominator of a G_1 energy expression we write

$$\text{DENOM} = \langle \Phi | O'_{11} \Phi \rangle \tag{25}$$

where Φ is a product of spatial orbitals ($\Phi = \phi_1 \phi_2 \ldots \phi_n$) and

$$O'_{11} = \sum_{\sigma} U_{11\sigma}\sigma \quad . \tag{26}$$

In (26) σ is an operator which permutes the electrons in Φ and $U_{11\sigma}$ is the 11 element of the matrix representation for σ. O'_{11} differs from the usual O_{11}[9a] by a constant factor. Getting back to D_i^j we also define[9a] D_i^j as the coefficient of $\phi_j^*(j)\phi_i^*(j)$ in

$$\langle \Phi \left| \sum_{\sigma} U_{11\sigma}\, \sigma\, \Phi \right\rangle^{\dagger} \tag{27}$$

where the dagger indicates that we do not integrate over electron j. In order to understand the nature of the pairwise contributions in Eq. (22) let us further examine D_i^j. For a four electron, spatially unprojected G1 wavefunction we have the general expression

$$D_i^j = S_{ij}\, U_{11}(i,j) + \sum_{k\neq j,i} U_{11}(k,i,j) S_{ki} S_{kj}$$

$$+ U_{11}(i,j)(k,\ell) S_{k\ell}^2 S_{ij} + \sum_{\substack{k\neq \ell \\ k,\ell \neq i,j}} U_{11}(k,\ell,i,j) S_{kj} S_{k\ell} S_{\ell i} \quad . \tag{28}$$

Substituting for the U_{11}'s and c, c', $\bar{c}$ and v(where c, c' are core orbitals on the left He and $\bar{c}$, v are the core and valence orbitals on the right He) for i, j we obtain the D_i^j's that concern us here:

$$D_c^v = -\tfrac{1}{2} S_{cv} - \tfrac{1}{2} S_{c\bar{c}} S_{\bar{c}v} - \tfrac{1}{2} S_{cc'} S_{c'v}$$

$$+ S_{c'\bar{c}}^2 S_{cv} + S_{c'v} S_{c'\bar{c}} S_{c\bar{c}} - \tfrac{1}{2} S_{\bar{c}v} S_{cc'} S_{c'\bar{c}} \tag{29a}$$

$$D_{c'}^v = -\tfrac{1}{2} S_{c'v} - \tfrac{1}{2} S_{c'\bar{c}} S_{\bar{c}v} - \tfrac{1}{2} S_{cc'} S_{cv}$$

$$+ S_{c\bar{c}}^2 S_{c'v} + S_{cv} S_{c\bar{c}} S_{c'\bar{c}} - \tfrac{1}{2} S_{\bar{c}v} S_{c\bar{c}} S_{cc'} \tag{29b}$$

$$D_c^{\bar{c}} = -\tfrac{1}{2} S_{c\bar{c}} - \tfrac{1}{2} S_{cc'} S_{c'\bar{c}} - \tfrac{1}{2} S_{cv} S_{\bar{c}v}$$

$$+ S_{c'v}^2 S_{c\bar{c}} + S_{c'\bar{c}} S_{c'v} S_{cv} - \tfrac{1}{2} S_{\bar{c}v} S_{c'v} S_{cc'} \tag{29c}$$

$$D_{c'}^{\bar{c}} = -\tfrac{1}{2} S_{c'\bar{c}} - \tfrac{1}{2} S_{cc'}S_{c\bar{c}} - \tfrac{1}{2} S_{c'v}S_{\bar{c}v}$$

$$+ S_{cv}^2 S_{c'\bar{c}} + S_{c\bar{c}}S_{cv}S_{c'v} - \tfrac{1}{2} S_{\bar{c}v}S_{cv}S_{cc'} \qquad (29d)$$

$$D_{c}^{c'} = S_{cc'} - \tfrac{1}{2} S_{c\bar{c}}S_{c'\bar{c}} - \tfrac{1}{2} S_{cv}S_{c'v}$$

$$+ S_{\bar{c}v}^2 S_{cc'} - \tfrac{1}{2} S_{c'\bar{c}}S_{\bar{c}v}S_{cv} - \tfrac{1}{2} S_{c'v}S_{\bar{c}v}S_{c\bar{c}} \qquad (29e)$$

$$D_{\bar{c}}^{v} = S_{\bar{c}v} - \tfrac{1}{2} S_{c\bar{c}}S_{cv} - \tfrac{1}{2} S_{c'\bar{c}}S_{c'v}$$

$$+ S_{cc'}^2 S_{\bar{c}v} - \tfrac{1}{2} S_{cv}S_{cc'}S_{c'\bar{c}} - \tfrac{1}{2} S_{c'v}S_{cc'}S_{c\bar{c}} \quad . \qquad (29f)$$

Note that in Eq. s (29) there are two patterns of signs. Equations (29a)-(29d) have the same pattern and are for density matrices between orbitals in different rows of Fig. 1c. Equations (29e) and (29f) have a different pattern of signs and are for density matrices between orbitals in the same rows of Fig. 1c.

Now let us examine (29) to see which terms are important for He_2. As an example we use the FO unprojected wavefunction at R = 6.2 for v = 2s. There are six overlaps to consider in (29) and of these, those involving one center are constant with R for the FO wavefunctions and relatively large: $S_{cc'} = 0.8789$ and $S_{\bar{c}v} = -0.0814$ (for SCF C $^1\Sigma_g^+$(2s) $S_{cc'} = 0.8785$ and $S_{\bar{c}v} = -0.0791$). In addition, those involving overlap between the core orbitals on the left and the Rydberg orbital on the right are also relatively large: $S_{cv} = 0.08460$ and $S_{c'v} = 0.1601$ (for SCF C $^1\Sigma_g^+$, $S_{cv} = 0.02739$ and $S_{c'v} = 0.06423$). Thus SCF

relaxation of the orbitals tends to substantially reduce S_{cv} and $S_{c'v}$. This decreases the magnitude of the maximum in the SCF potential curve compared to FO. The smallest overlaps are those between cores on opposite centers: $S_{c\bar{c}} = 0.00057$ and $S_{c'\bar{c}} = 0.00220$ (compared to $S_{c\bar{c}} = 0.00060$, $S_{c'\bar{c}} = 0.00014$ for C $^1\Sigma_g^+$ SCF). Now returning to (29a) the terms on the right-hand side (proceeding from left to right) are given by -0.04230, 0.00002, -0.07033, 0.00000, 0.00000, 0.00000. For C $^1\Sigma_g^+$ SCF we obtain -0.01369, 0.00005, -0.02821, 0.00000, 0.00000, 0.00001. Thus both SCF and frozen wavefunctions allow us to replace (29a) with a good approximation:

$$D_c^v \approx -\tfrac{1}{2}(S_{cv} + S_{cc'}S_{c'v}) \quad .$$

Since $S_{cc'} \approx 1$ we can make a further approximation and take

$$D_c^v \approx -\tfrac{1}{2}(S_{cv} + S_{c'v}) = -\bar{S}_{c,c',v} \quad . \tag{30a}$$

Thus D_c^v is given by the opposite sign of the average of the overlaps of the Rydberg orbital with the cores on the opposite center. Similar considerations follow for $D_{c'}^v$, and we also obtain

$$D_{c'}^v \approx -\bar{S}_{c,c',v} \quad . \tag{30b}$$

Since $S_{c'v} > S_{cv}$ we expect (30b) to be a slightly better approximation than (30a). For the FO wavefunction we find (from Eq.s 29a and 29b) $D_c^v = -0.1125$, $D_{c'}^v = -0.1171$ and $-\bar{S}_{c,c',v} = -0.1223$. For SCF C $^1\Sigma_g^+$ we have similarly $D_c^v = -0.04188$, $D_{c'}^v = -0.04412$ and $-\bar{S}_{c,c'v} = -0.04581$. Because of the negative sign (due to v and c,c′ being in different rows of

Fig. 1c) in Eq. s (30a) and (30b) and because $\overline{S}_{c,c',v}$ remains positive and increases as we decrease R at these distances, $T^X_{c,v}$ and $T^X_{c'v}$ will lead to increasing positive contributions to T^X as R decreases. From Table XI we see that these pairwise contributions are indeed the dominant contributions to T^X at large R. It is also seen in Table XI that both τ_{cv}, $\tau_{c'v}$, and N vary only slowly with distance compared to S_{cv} and $S_{c'v}$. Thus we may write

$$T^X_{cv} \propto S_{cv}\overline{S}_{cc'v} \tag{31}$$

$$T^X_{c'v} \propto S_{c'v}\overline{S}_{cc'v} \quad . \tag{32}$$

Equations (31) and (32) express the repulsive interactions in the energy due to the overlap of singlet coupled pairs on opposite heliums. Since the core orbitals are quite localized about their centers (see Fig. 3) we should therefore be able to predict the location of maxima in our frozen curves from a knowledge of the amplitude of the Rydberg orbital as a function of the distance from its center. These amplitudes are shown in the plots of Fig. 3. We will come back to this later.

In Eq. (29c) we find that the terms on the right-hand side are given by -0.00028, -0.00096, 0.00343, -0.00001, -0.00003, 0.00570. Thus we may write (29c) roughly as

$$D^{\bar{c}}_{c} \approx -\tfrac{1}{2} S_{cv}S_{\bar{c}v} - \tfrac{1}{2} S_{\bar{c}v}S_{c'v}S_{cc'} \quad .$$

Taking $S_{cc'} \approx 1$ we have,

$$D^{\bar{c}}_{c} \approx -\tfrac{1}{2} S_{\bar{c}v}(S_{cv} + S_{c'v}) = -S_{\bar{c}v}\overline{S}_{c,c',v} \quad . \tag{30c}$$

Because of the first two terms on the right-hand side of Eq. (29c), Eq. (30c) is not as good an approximation as Eqs. (30a) and (30b). For this reason Eq. (30c) is only reasonable at large distances. Because $S_{\bar{c}v}$ is negative, we note from Eq. (22) $T^x_{c\bar{c}}$ will be negative at large distances (see Table XI). But at smaller distances $S_{c\bar{c}}$ and $S_{c'\bar{c}}$ will be large and the first two terms in (29c) will overwhelm the other terms as S_{cv} and $S_{c'v}$ become small. Nevertheless at the large distances of interest here, $S_{c\bar{c}}$ is small and because of the factor $S_{\bar{c}v}$, $D^{\bar{c}}_c$ will be small compared to D^v_c and $T^x_{c\bar{c}}$ is negligible compared to T^x_{cv} (see Table XI). Similar considerations follow for $D^{\bar{c}}_{c'}$ in Eq. (29d).

The major contribution to $D^{c'}_c$ in Eq. (29e), $S_{cc'}$, remains constant with R. The third term adds a small negative contribution which is a factor of about 100 smaller than $S_{cc'}$. All other terms can be neglected except for the fourth term on the right-hand side of Eq. (29e) which is positive and constant with R. Since $\tau_{cc'}$ is constant with R we find that the most rapidly changing term in Eq. (22) is N and this leads to the small negative or bonding character of $\Delta T^x_{c,c'}$ with R.

For $D^v_{\bar{c}}$ we see in Eq. (29f) that the first and fourth terms are constant with R and provide the major contributions. All other terms in $D^v_{\bar{c}}$ are at least a factor of 100 smaller. Because τ is negative here N now causes $T^x_{\bar{c}v}$ to increase with R. Nevertheless $\Delta T^x_{\bar{c}v}$ is small compared with T^x_{cv} and $T^x_{c'v}$.

Returning to the FO curves in Fig. 4 we now have enough information to discuss their general shapes and the maxima. In Table XII

we show the energies obtained for FO $^1\Sigma_g^+$ and $^1\Sigma_u^+$. From Table XII we see that for v = 2s at, e.g., R = 10.0 Bohr, both $^1\Sigma_g^+$ and $^1\Sigma_u^+$ are still split by the same amount (0.00076 a.u.) as at R = ∞ while the potential curves of both states are 0.00032 a.u. above their energies at R = ∞. Because this splitting is approximately constant with R at large distances and because both curves are approximately equally repulsive, the major contribution to the rise in the curves is not due to the spatial projection operator at these large distances.

As a result we have discussed v = 2s above with the results of an FO spatially unprojected wavefunction. For such a wavefunction Eq. (21) holds. As discussed above the rise in both the v = 2s $^1\Sigma_g^+$ and $^1\Sigma_u^+$ curves is due to the interaction between the diffuse Rydberg orbital and the core orbitals on the opposite He. In Fig. 2 we see that the 2s orbitals [14b] for $^1\Sigma_g^+$ and $^1\Sigma_u^+$ have their maximum amplitudes near 3.25 Bohr and 2.52 Bohr, respectively. Nevertheless, from about 3.5 Bohr out to R = ∞ both curves are quite similar. Thus both the g and u v = 2s orbitals should have increasing and equal overlaps with the core orbitals on the opposite center as R is decreased. We expect this interaction to be increasingly repulsive until 3.25 Bohr and 2.52 Bohr where it will reach a maximum for the g and u curves, respectively. At smaller distances the overlap of the Rydberg orbital with the opposite cores will also decrease and this interaction will be less repulsive (for R > 1.5 Bohr for $^1\Sigma_g^+$ (FO) and R > 0.5 Bohr for $^1\Sigma_u^+$ (FO)). Now since the core orbitals are quite localized[20] (see Fig. 3) and therefore somewhat spiked in shape relative to the diffuse Rydberg orbital we expect to find

that the overlap between the Rydberg orbital and the opposite cores will be approximately directly proportional to the amplitude of Rydberg orbital. We find that at R = 10.0, 8.0, and 6.2 Bohr, the amplitudes for all three orbitals shown in Fig. 3(b) are 0.00399, 0.00899, and 0.01758 a.u., respectively. The equal amplitudes of all three orbitals further justifies our use of the spatially unprojected wavefunction to analyze T^X at these distances. These numbers all differ by a factor of about 5 from the values of S_{cv} and a factor of 10 from the values of $S_{c'v}$ shown in Table XI. Thus the overlap of the Rydberg orbital with the opposite cores is to a good approximation directly proportional to the amplitude of the Rydberg orbital. Thus we have related the repulsive interaction described here to the shape of the Rydberg orbital. This will prove useful in understanding the magnitude of this repulsive interaction in the higher excited states.

In Fig. 4 we see that v = 2s $^1\Sigma_u^+$(FO) reaches a maximum (0.00471 a.u.) at 4.89 Bohr. Beyond this point the favorable core-core interactions ($^2\Sigma_u^+$) already discussed overwhelm the unfavorable interactions of the Rydberg orbital and the potential curve falls to give a minimum near 2.3 Bohr. On the other hand for v = 2s $^1\Sigma_g^+$(FO) the repulsive interactions involving the Rydberg electron at large R are supplemented at smaller R ($R < \approx 6.2$ Bohr) by repulsive ($^2\Sigma_g^+$) core-core interactions. As a result $^1\Sigma_g^+$(FO) is totally repulsive as seen in Fig. 4. This is also shown in Fig. 7 where we have plotted $^2\Sigma_g^+$(FO) so as to have the same R = ∞ limit as v = 2s $^1\Sigma_g^+$(FO). Here we see that $^1\Sigma_g^+$ rises before $^2\Sigma_g^+$ because of the repulsive Rydberg core interactions.

At smaller R($R < 3.2$ Bohr) the Rydberg orbital has a reduced overlap with the cores on the opposite center and essentially surrounds both centers. The Rydberg interactions then become less important and both curves approximately coincide, showing the repulsive core-core interactions.

For v = 2p, as described in Ref. 14 $^1\Sigma_g^+$, $^1\Sigma_u^+$ and $^1\Sigma^+$ wavefunctions all yield identical energies and orbitals at $R = \infty$. In Fig. 4 we note that the v = 2p $^1\Sigma_g^+$ (FO) curve has a much larger maximum (0.03783 a.u.) than v = 2s $^1\Sigma_u^+$ (FO) at smaller R, 3.92 Bohr. In addition both u and g curves rise at large R and the splitting remains small until about 4 Bohr. Thus this rise at large R cannot be due to the spatial projection operator. Its origin can be understood by examining Table XI and Fig. 2b.

To understand the size of the hump in v = 2p $^1\Sigma_g^+$ (FO) we once again refer to the shape of the Rydberg orbital. We see in Fig. 2b that the amplitude of ϕ_v = 2p reaches a maximum at 2.16 Bohr (this is quite similar to a hydrogenic 2p which has its maximum at 2.0 Bohr) and is always greater in amplitude than ϕ_v = 2s for distances greater than 2.16 Bohr. For ϕ_v = 2p, the amplitudes at R = 10.0, 6.2, and 4.2 are 0.00706, 0.02849, and 0.05113, respectively. The square of these amplitudes are approximately directly proportional to T^x_{cv} and $T^x_{c'v}$. Assuming equal proportionality factors, we take the square of the ratio

of the amplitudes of ϕ_v = 2p to ϕ_v = 2s at R = 10,0, 6.2, and obtain 3.131 and 2.626, respectively. The corresponding ratios of T^x_{cv} are 3.028, 2.454 while for $T^x_{c',v}$ they are 2.901 and 2.307, respectively. Thus we see that we can account for the difference in the magnitude of the maxima for ϕ_v = 2s and ϕ_v = 2p by simply considering the shapes of the two orbitals.

As seen in Fig. 2b, ϕ_v = 2p continues to rise in amplitude at smaller distance. At R = 4.2 the amplitude of ϕ_v = 2p is 1.64 times larger than that for ϕ_v = 2s. Thus we would expect T^x and therefore ΔE to be roughly 2.7 times larger for ϕ_v = 2p than ϕ_v = 2s. Upon examining Fig. 4 and Table XII we see that ΔE for ϕ_v = 2p is about a factor of 9 greater than ΔE for ϕ_v = 2s. This factor can be understood by reexamining the core-core interactions which we discussed previously. Table XIII shows that at R = 4.2 Bohr $^2\Sigma_g^+$ and $^2\Sigma_u^+$ are split from E(∞) by about 0.013 a.u. But the effect of the core is quite different for v = 2s and v = 2p. At R = 5.0 for v = 2p (see Table IV), there are almost equal amounts of favorable and unfavorable core. As a result the important interaction here is the T^x interaction of the Rydberg orbital and the core-core interaction plays only a small role. Nevertheless the latter interaction eventually becomes important at smaller R and causes ϕ_v = 2p $^1\Sigma_g^+$ (FO) to fall for R < 3.9 Bohr. In contrast to this Table IV shows that ϕ_v = 2s $^1\Sigma_u^+$ (FO) already has a substantial predominance of favorable core and little unfavorable core near R = 5.0. Here the core-core interactions are important and begin to overwhelm the T^x Rydberg interactions at R = 5.0 Bohr causing the maximum in

the ϕ_v = 2s curve to occur at larger R than for ϕ_v = 2p. In addition, the difference in the variation with R of overlaps of Rydberg orbitals on opposite centers causes the core-core interaction to be important at smaller R for ϕ_v = 2p as compared to ϕ_v = 2s. This allows the unfavorable T^X interaction of ϕ_v = 2p with the opposite cores to give rise to a substantially larger maximum at smaller R for ϕ_v = 2p. This is quite clearly shown in Fig. 7 where the large T^X Rydberg-core interaction causes the v = 2p $^1\Sigma_u^+$ (FO) curve to rise sooner than $^2\Sigma_g^+$ (FO) and indeed to be much more repulsive than v = 2s $^1\Sigma_g^+$ (FO).

For the n = 3 FO curves we proceed with a similar analysis. From Fig. 2 we see that the ϕ_v = 3s $^1\Sigma_g^+$, $^1\Sigma_u^+$ and $^1\Sigma^+$ orbitals are quite similar for r > 3 Bohr. This is also true for ϕ_v = 3d and holds at all r for ϕ_v = 3p as already discussed. Note that since the maximum amplitude for these orbitals occurs at large r we expect to find a maximum in the potential curves at large R. Since the core splitting is negligible at these distances we should find that the distances at which there is a maximum in the amplitude of the orbital should be approximately the internuclear distance where there is a maximum in the potential curve. In addition, except for ϕ_v = 3d, the amplitudes are less than those for the n = 2 orbitals and hence we would expect to find only small maxima.

Examination of the spline-fitted curves shown in Fig. 4, obtained from the points shown in Table XII, shows that the maximum in the ϕ_v = 3s, $^1\Sigma_g^+$ (FO) potential curve is 0.00267 a.u. for 9.76-9.83 Bohr (the spline fitted curve is flat to six decimal places in the energy here).

Note that this fit is mainly based on the three points at R = 15.0, 10.0 and 8.0. For ϕ_v = 3s, $^1\Sigma_u^+$ (FO) we have a maximum of 0.00259 a.u. at 9.78-9.85 Bohr. Figure 2c shows that for ϕ_v = 3s both $^1\Sigma_u^+$ and $^1\Sigma_g^+$ have maximum amplitudes at 9.80 Bohr and thus the correlation to the maximum in the potential curves is quite good.

Similarly for ϕ_v = 3p the maximum in the $^1\Sigma_g^+$ (FO) potential curve is 0.00283 a.u. at 10.47-10.54 Bohr. While in $^1\Sigma_u^+$ (FO) it is 0.00300 a.u. at 10.51-10.54 Bohr. The maximum in ϕ_v = 3p comes at 11.00 Bohr. For $^1\Sigma_g^+$ (FO) the energy at R = 11.0 Bohr is 0.00279 a.u. above the value at R = ∞ and thus considering that we use only 3 points at wide separation in our spline fit the agreement between the position of the amplitude maximum and the energy maximum is quite good.

From Table IV we see that at R = 5.8 Bohr there is a predominance of favorable core for ϕ_v = 3s, 3d $^1\Sigma_u^+$ and ϕ_v = 3p $^1\Sigma_g^+$. Thus for the n = 3 states the core splitting will become evident in the potential curves near this R. Figure 2d shows that the amplitude of ϕ_v = 3d has a maximum at 5.65 Bohr. As a result the FO potential curve will cross ϕ_v = 3p and will be increasingly repulsive until the splitting of the cores becomes important near 5.8-6.2 Bohr. This is indeed the case as seen in Fig. 4. Just as the slope of the potential curve begins to decrease near 6.0 Bohr as the unfavorable T^x Rydberg-core interaction reaches a peak the interaction of the cores splits the g and u potential curves. Note though that the ϕ_v = 3s, 3p curves have zero amplitude near 5.5 Bohr and 6.3 Bohr, respectively. Thus the unfavorable T^x Rydberg-core interactions will decrease to zero here and the potential curves

will begin to fall close to the R = ∞ energies just as the core splitting becomes important. This is shown in Figs. 4 and 7.

This concludes the discussion of the frozen curves. We have seen that by considering the symmetry of the 3 electron core and the overlap of Rydberg orbitals on opposite centers we have been able to account for the shapes of the potential curves at R $<$ ≈6.2 Bohr. By considering the exchange kinetic energy between the Rydberg orbital on one center and the core orbitals on the other center as determined by the shape of the Rydberg orbital we have been able to account for the energy variation at large R. These results will be essential to our discussion of the SCF orbitals in the next section.

3. The SCF States

The total energies for the SCF states are given in Tables XIV and XV. These energies are plotted in Fig. 11 and with the frozen energies in Figs. 5 and 6. Also the positions and magnitude of the maxima and minima in the SCF states are summarized in Table XVI. In Tables XVII and XVIII we show some orbital coefficients.

a. The A $^1\Sigma_u^+$ state.

The A $^1\Sigma_u^+$ state has been the most widely discussed excited state of He_2. It is the second lowest excited state (lying above a $^3\Sigma_u^+$) and is the source of the 600 Å bands mentioned in the Introduction. These bands, seen in both absorption[21a, b, 22] and emission[4, 23], are due to transitions between X $^1\Sigma_g^+$ and quasibound vibrational levels of the A state which lie above the dissociation limit and below the maximum

in the A state potential curve. In addition much interest has centered on the A state because through transitions to the repulsive $X\ ^1\Sigma_g^+$ state it provides for a continuum light source[24] in the windowless vacuum ultraviolet ($\sim$ 600-1100 Å). In spite of this interest and as mentioned in the Introduction, little has been previously reported toward understanding the origin of the maxima and the general shapes of the He_2 excited states.

In Fig. 6 we see that the FO curve and the SCF curve for $A\ ^1\Sigma_u^+$ are quite similar and indeed the FO curves provide for a reasonable description of the A state. Because the FO curve reproduces the maximum in the A state, this maximum cannot be due to an avoided curve crossing. This is also seen by inspection of the right-hand column of Fig. 12 where we show a contour plot of the ϕ_v orbital in a plane containing the He nuclei. We see that the ϕ_v orbital retains its 2s character at all distances while polarizing away from the incoming He as R is decreased. Note that at small R, ϕ_v encloses the two He nuclei. The rise in the potential curve is caused by the nonbonding interaction expressed in terms of T^x and the overlaps between the Rydberg orbital and the cores on the opposite center. This has been discussed in Section C2. SCF readjustment of the orbitals reduces the size of the maximum by about one-half to 0.00223 a.u. (0.0607 eV). This is reflected by the decrease in T^x which is shown at R = 6.2 in Tables V and VII for the FO and SCF wavefunctions, respectively. In addition, S_{cv} decreases from 0.085 for the FO wavefunction to 0.018 for the SCF wavefunction. (Note that because the SCF wavefunction contains a

spatial projection operator, Eq. (21) which is appropriate for a spatially unprojected wavefunction does not apply.) Compared to the FO wavefunction the maximum now comes at larger R (by about 1 Bohr) at 5.82 Bohr and is quite broad as seen in Table XV. Since we would expect the atomic contribution to the correlation energy to remain approximately constant between infinity and R = 5.8 Bohr our value for the magnitude of the maximum is probably of the order of 10 to 20% larger than the actual value. There have been several experimental estimates for the maximum. By fitting a potential for the A state to intensity data taken from the spectra of Tanaka and Yoshino,[21a] Sando and Dalgarno[25] predict a hump height of 0.049 eV ± 0.01 eV at 3.1 Å (5.86 Bohr). In addition their curve is quite broad in the vicinity of the maximum in agreement with the curve calculated here. Other experimentally derived estimates are 0.05 ± 0.01 eV,[26] 0.059 eV,[21a] 0.03 ± 0.03 eV at 3.0 ∓ 0.3 Å,[27] 0.05 eV at 3.1 Å,[28] and 0.06 eV.[21b] Thus the position and magnitude of the maximum calculated here is in excellent agreement with the experimental results.

There have also been a number of theoretical calculations on the A state. Buckingham and Dalgarno[29] performed the first such calculation obtaining a maximum of 0.26 eV at about 4 Bohr. They used a wavefunction which was similar to the FO wavefunction discussed here except that each orbital was represented by a single Stater basis function. They pointed out that electron exchange was important at large distances and that the maximum which they obtained arose from the "overlapping of the electron distributions of the separate atoms."

They did not go into any further detail on this and did not present a detailed partition of the energy.

Browne[30] used a 2-term CI wavefunction for the A state. Using orbitals constructed from single basis functions with optimized exponents, he obtained a hump height of 0.174 eV at 5.0 Bohr and a minimum at 2.07 Bohr with D_e = 1.9 eV. Allison, Browne, and Dalgarno[31] investigated the A state with a 3-term CI wavefunction in which their orbitals were also constructed from basis functions. One of their configurations contained a diffuse (Slater exponent = 0.485) 2p basis function for the Rydberg orbital. They obtained a smaller hump than Browne of 0.084 eV at 6 Bohr. Scott et al.[32] used both a 4 and 17-term CI wavefunctions obtaining maxima of 0.154 eV and 0.153 eV at 5.26 Bohr and 5.22 Bohr. Note though that although the 17-term wavefunction provided for additional polarization of the core (with tight $p\sigma$ functions) over that found in the 4-term wavefunction, it did not provide for much additional polarization of ϕ_v. This may explain why both CI wavefunctions gave similar barrier heights. He obtained D_e = 1.62 eV for the 4-term wavefunction and 1.72 eV for the 17-term wavefunction demonstrating in part the effect of the additional core polarization in the larger wavefunction. S. Mukamel and U. Kaldor[33] have performed two CI calculations using 209 and 124 configurations. The former wavefunction had a tight $2p\sigma$ function (exponent = 2.462) and no other polarization functions. It gave a hump of 0.087 eV at 5.3 Bohr and a D_e of 2.306 eV with a minimum at 1.966 Bohr. The 124-term wavefunction had a tight $2p\pi$ function and no $2p\sigma$'s. It gave a larger value

for the maximum (0.1487 eV at 5.1 Bohr) and a smaller D_e (1.947 eV with a minimum at 2.01 Bohr). The many interacting terms in these wavefunctions makes it somewhat difficult to make a definitive statement although it appears that the lack of $2p\sigma$'s in the 124-term wavefunction probably contributed in large part to the worse value for D_e and the maximum.

The D_e [$D_e = E(R = \infty) - E(R = R_{MIN})$] given by our calculation (see Table XVI) is 1.883 eV (with $R_{MIN} = 2.07$ Bohr) and is not in good agreement with the experimentally derived values of 2.345 ± 0.005 eV[26] and 2.50 eV.[28,34] We have performed a full CI calculation at R = 2.2 Bohr for the A state. The CI wavefunction (having 160 configurations) was constructed from the eight occupied orbitals of the SCF wavefunction obtained at R = 2.2 Bohr. (The SCF wavefunction is equivalent to an 8-term CI wavefunction built from the SCF orbitals.) The energy of the CI wavefunction was only 0.00043 Bohr lower than the SCF energy. Since the CI wavefunction includes configurations which contain the GF spin coupling in addition to the G1 spin coupling this result indicates the unimportance of spin couplings other than G1 at this distance (using projected G1 orbitals). Thus in line with the discussion of other calculations given above it appears that the absence of tight $2p\sigma$'s in our basis set which are needed for core polarization at small distances is in large part the cause of the error in D_e.

Since there are no avoided curve crossings involved in determining the shape of the A $^1\Sigma_u^+$ potential and since the Rydberg orbital is

quite diffuse we would expect the binding to be determined almost entirely by the three electron core. Thus we obtain D_e = 0.07229 a.u. (1.967 eV) with R_{MIN} = 2.18 Bohr for $X\ ^2\Sigma_u^+$ (see Table XIII). Thus D_e and R_{MIN} differ by about 5% from values calculated for $A\ ^1\Sigma_u^+$. This idea is further supported by the work of Ginter and Battino[35] who find from their spectral data and the atomic term levels of Moore[13] that the D_e values for the A state and $X\ ^2\Sigma_u^+$ differ by only 5 cm^{-1} (0.0006 eV).

Our calculated R_{MIN} is 2.07 Bohr which is about 5% larger than the experimental value of 1.963 Bohr. Typically, GVB wavefunctions lead to an R_e about 3-8% larger than the experimental value.

Calculating the experimental ionization energy of $A\ ^1\Sigma_u^+$ from the estimate of the height of N = 0, v = 0 level of the $X\ ^2\Sigma_u^+$ ground state above N = 0, v = 0 level of $A\ ^1\Sigma_u^+$ given by Ginter and Battino[35] and the zero point energies[36,37] we obtain 0.14606 a.u. From the SCF curves we obtain 0.14114 or an error of about 3.4%. This reflects a roughly equal treatment of the cores near $R = R_{MIN}$ and the correlation error at $R = \infty$ for both states.

In order to see a free-bound transition in absorption from $X\ ^1\Sigma_g^+$ it is necessary that the ground state not become appreciably repulsive until R is less than the position of the maximum in the upper state. At 300°K we find $KT = 9.5 \times 10^{-4}$ a.u. which corresponds to about R = 4.2 Bohr on the $X\ ^1\Sigma_g^+$ curve (see Fig. 11). This is within the maximum calculated for the A state but not within the maxima calculated for several higher states. We will return to this later in order to explain the absence of certain bands in the absorption spectra. By correcting for the difference in the correlation error at $R = \infty$ in $X\ ^1\Sigma_g^+$ and $A\ ^1\Sigma_u^+$

using atomic energies from Moore[13] we find that at $R = R_{MAX}$ for $A\ ^1\Sigma_u^+$ and T = 300 °K the transition $X\ ^1\Sigma_g^+ \rightarrow A\ ^1\Sigma_u^+$ occurs at 601.01 Å. This is quite close to the first absorption line seen by Tanaka and Yoshino[21a] at 600.012 Å.

b. The $C\ ^1\Sigma_g^+$ state.

In our discussion of the FO curves we observed that the g state arising from $\phi_v = 2s$ was totally repulsive due to the repulsive Rydberg-core interaction at large R (as in $A\ ^1\Sigma_u^+$) and repulsive core-core interaction at small R. Since there are higher FO g states which have attractive core-core interactions it is natural to expect the SCF curves to exhibit an avoided crossing near where the FO curves cross. This can be seen to be the case in Fig. 5 where the FO curve for $\phi_v = 2s\ ^1\Sigma_g^+$ crosses with the attractive curve for $\phi_v = 2p\ ^1\Sigma_g^+$. In addition the SCF curve for $\phi_v = 2s$, $C\ ^1\Sigma_g^+$, is attractive with $R_{min} = 2.17$ Bohr and $D_e = 0.02368$ a.u. (0.64437 eV). A large maximum occurs at R = 3.90 Bohr with $E_{max} = 0.00796$ a.u. (0.21660 eV). Note that the FO curves cross at R = 3.29 Bohr near the maximum in the SCF curve. The avoided curve crossing is further shown in the left-hand column of Fig. 12 where we show ϕ_v for the SCF state. Note that (except for the inner node[14b] in ϕ_v for $C\ ^1\Sigma_g^+$ which is present at $R = \infty$) ϕ_v for both $C\ ^1\Sigma_g^+$ and $A\ ^1\Sigma_u^+$ are quite similar for $R > \sim 5.4$ Bohr. Both orbitals polarize away from the opposite center as R decreases reducing their overlap with the opposite core orbitals. For $R < 5.4$ Bohr, ϕ_v for $C\ ^1\Sigma_g^+$ changes smoothly to a 2p orbital reflecting the avoided curve

crossing while ϕ_v for A $^1\Sigma_u^+$ remains a 2s orbital. The effect of the avoided crossing was noted earlier when we examined the occupation numbers for the three electron core of the SCF C $^1\Sigma_g^+$ state in Table IV. At small R the FO v = 2s g curve has mostly unfavorable core whereas the SCF curve has mostly favorable $^2\Sigma_u^+$ core.

Ginter[36] has reported eleven bands for the transition C $^1\Sigma_g^+ \rightarrow$ A $^1\Sigma_u^+$. He finds R_{min} = 2.072 a.u. which is about 5% smaller than the value calculated here. Although no value for D_e is reported, Ginter has been able to observe the emission spectra only to v = 5 in the C state. He also suggests that the similar c $^3\Sigma_g^+$ state predissociates by v = 5 or 6. This is an indication of the smaller well depth ($E_{max} - E_{min}$) in the C state compared to the A state. For the C state our calculated well depth is about one-third the size of that for the A state. From the Deslandres table and the ω_e given by Ginter one can estimate a lower bound on the experimental well depth of 0.03555 a.u. This value is about 12% larger than that calculated here (see Table XVI). As seen in Fig. 5 the small well depth in the C state occurs because the bottom of the well for ϕ_v = 2p $^1\Sigma_g^+$ (FO) does not fall very much below the v = 2s, R = ∞ limit. From the zero point energies and $\nu_{(0-0)}$ Ginter reports 11050.8 cm^{-1} (0.050351 a.u.) for the difference between the minima of the C and A states. We calculate 0.046279 a.u. or an error of about 8%.

Buckingham and Dalgarno[29] used the same method previously described in their calculation on the A state and obtained a totally repulsive potential for the C state. This is reasonable since their

wavefunction was similar to the FO wavefunction reported here. Allison, Browne and Dalgarno[31] performed a 5-term CI calculation on the C state and also obtained a totally repulsive curve. Their choice of configurations did not allow for the avoided curve crossing described above. The only previous calculation giving an attractive well was by J. C. Browne[30] who reported single configuration FO-type calculations for $\phi_v = 2s, 2p\ ^3\Sigma_g^+$, a two configuration calculation on c $^3\Sigma_g^+$ and a 3 configuration on C $^1\Sigma_g^+$. His single configuration calculations showed the attractive nature of $\phi_v = 2p\ ^3\Sigma_g^+$ (FO) with a large maximum and the totally repulsive curve for $\phi_v = 2s\ ^1\Sigma_g^+$ (FO). His two and three configuration calculations showed the avoided crossing arising from the crossing of the single configuration curves. Although his potential curve for C $^1\Sigma_g^+$ was not smooth in the vicinity of the maximum he reported a hump of ≈ 0.7 eV at R = 4.5 a.u.

Mulliken[38] has offered an explanation for the appearance of large maxima in some of the He_2 potential curves. He claims that states for which the principal quantum number of the Rydberg orbital at the united atom limit is greater than the corresponding quantum number at the separated atom limit will have large "obligatory" humps. He takes the united atom limit of the Rydberg orbital to be important near R_e. For cases in which the Rydberg orbital is unpromoted large humps are not expected (e.g., A $^1\Sigma_u^+$). For the C state, Mulliken takes the united atom limit of the Rydberg orbital (based on the H_2^+ correlation diagram) to be $3p\sigma$ and thus expects a large hump since $\phi_v = 2s$ at $R = \infty$. We have seen though that the repulsive part of the potential

curve arises from the unfavorable Rydberg-core interactions and are indeed present in the FO curve with ϕ_v = 2s. The SCF energy curve for the C state falls as the Rydberg orbital becomes 2p-like. The orbital remains 2p-like (although diffuse) and unpromoted into our smallest separation at 1.8 Bohr beyond the minimum. It is interesting to note that Ginter[36] has observed that the term defect (assuming a principal quantum number n = 3) for the C state is quite large (δ = 0.715). (The term defect, δ, is defined by

$$T = 0.5/(n - \delta)^2 \qquad (32)$$

where T is the difference between the energies of the v = 0 levels of the C and X $^2\Sigma_u^+$ states.) In view of the results reported here this is quite reasonable since the Rydberg orbital is 2p-like at R_e and not 3p-like as had been previously assumed (see Figs. 12 and 13a).[36, 38, 39]

c. The $^1\Sigma_g^+$ (2p) state.

As has been previously discussed the FO curve for v = 2p $^1\Sigma_g^+$ rises to high maximum due to the core-core interactions and a repulsive Rydberg-core interaction. At smaller R it falls to a minimum due to the attractive core-core interactions. In Fig. 5 we see that the SCF curve has essentially the same shape as the FO curve with a maximum at R = 3.52 Bohr (see Table XVI) of almost equal magnitude (0.03769 a.u. compared to 0.03783 a.u. for the FO curve). Near the minimum though the SCF curve cannot be 2p like since the lower C $^1\Sigma_g^+$ state has all the 2p character. As a result the $^1\Sigma_g^+$ (2p) SCF curve obtains 3p character

from the only other attractive g FO curve shown in Fig. 5. This is clearly shown in the left-hand column of Fig. 14 where we see that the 2p orbital begins to change for R < 4.2 Bohr to a 3p orbital. The minimum in the v = 3p $^1\Sigma_g^+$ (FO) curve falls above the separated atom v = 2p limit and as a result the well for $^1\Sigma_g^+$ (2p) is not as deep as that for the A state. In fact, the minimum of the $^1\Sigma_g^+$ (2p) SCF curve is 0.00564 a.u. above the separated atom limit.

There are no experimental results reported for this state.

It is interesting to note here that in his experimental study of the excited states of He_2 Ginter[35] did not correlate the separated atom $^1\Sigma_g^+$ (2p) state with any molecular state. Nevertheless he speculated that it might correlate with a state denoted as $4p\sigma\ ^1\Sigma_g^+$ which is the next molecular state above those which correlate with all the other n = 2 separated atom levels. This state would have its v = 0 level at several hundred cm^{-1} below the $1s^2$ + (1s, 2p) ^1P limit.

Considering our error of about 25% (see the discussion of A $^1\Sigma_u^+$) in D_0 this would be a very reasonable description and indeed our $^1\Sigma_g^+$ (2p) state is the state which Ginter[35] refers to as 4pσ. Nevertheless we have seen that the Rydberg orbital is 3pσ-like (see Fig. 13b) and not 4pσ-like. It is a diffuse 3pσ having maxima at ~4.1 and ~13.2 Bohr from the midpoint between the two heliums at R = 2.2 Bohr (compared to 1.75 and 10.24 Bohr for an H atom 3p orbital). The potential curve is similar in shape to that for the C state.

We have earlier mentioned a three term CI calculation on C $^1\Sigma_g^+$ by Browne.[30] For this wavefunction he plots not only the energy curve corresponding to the root appropriate to the C state but also the curve

obtained from the next root. This latter root of the CI matrix corresponds to $^1\Sigma_g^+$ (2p). But since there are no 3p orbitals in his basis (which was not meant to describe this state anyway) his energy curve does not have an attractive well. Instead the curve rises to a plateau near 4 Bohr and then (when 3p character is needed) it rises again to become totally repulsive. In the absence of 3p character the Rydberg orbital for this repulsive part of the curve will be 2s-like since this curve corresponds to the upper part of the avoided crossing which gave rise to the C state discussed earlier. This repulsive 2s character will be referred to later when we discuss the higher states.

Once again we see that a promotional effect[38] is not important here. Indeed the v = 2p FO curve shows both a high maximum (nearly equal in magnitude to that of the SCF curve) and an attractive well.

d. The $^1\Sigma_u^+$ (2p) state.

In order to understand the nature of the SCF $^1\Sigma_u^+$ (2p) state we will refer to the FO curves shown in Fig. 6. As has already been described the $^1\Sigma_u^+$ (2p) FO curve is totally repulsive. Note that near 4 Bohr this curve crosses both the attractive v = 3s and v = 3d $^1\Sigma_u^+$ FO curves. From Fig. 14 we see that the Rydberg orbital becomes predominantly 3d-like for $R < 4.2$ Bohr and does not become 3s-like until $R < 2.2$ Bohr. Thus the SCF Rydberg orbital is predominantly 3d-like at the larger distances even though the v = 2p FO curve crosses the corresponding v = 3s curve. In order to explain the avoided crossing in the SCF curve the interaction Hamiltonian and overlap matrix elements between the v = 2p and v = 3s, 3d FO wavefunctions have been calculated.

At R = 3.8 Bohr we obtain for the total FO wavefunctions:

$$\langle \Phi_{2p} | H | \Phi_{3s} \rangle = 0.01628, \quad \langle \Phi_{2p} | H | \Phi'_{3s} \rangle = 0.00158$$

$$\langle \Phi_{2p} | H | \Phi_{3d} \rangle = -0.44638, \quad \langle \Phi_{2p} | H | \Phi'_{3d} \rangle = -0.02755$$

$$\langle \Phi_{2p} | \Phi_{3s} \rangle = -0.00245, \quad \langle \Phi_{2p} | \Phi_{3d} \rangle = 0.06980 \qquad (33)$$

where Φ_{2p}, Φ_{3s} and Φ_{3d} are $^1\Sigma_u^+$(FO) wavefunctions appropriate to the $R = \infty$ ϕ_v = 2p, 3s, 3d states. Also $\Phi'_{3\ell} = N(\Phi_{3\ell} - \langle \Phi_{2p} | \Phi_{3\ell} \rangle \Phi_{2p})$, i.e., Φ_{2p} and $\Phi'_{3\ell}$ are orthonormal. In this manner the matrix elements of Φ_{2p} and $\Phi'_{3\ell}$ over H in (33) are more closely related to the energy splitting due to their interaction. They are larger by a factor of $(1-S^2)^{1/2}$, where S is their overlap, from the actual splitting. We see here that the Hamiltonian matrix element for the interaction of the ϕ_v = 2p $^1\Sigma_u^+$(FO) with ϕ_v = 3d $^1\Sigma_u^+$(FO) is about 29 times larger than that for interaction with the $\phi_v = 3s_u$ state. The overlaps differ by a factor of 28. This confirms our observation of the 3d nature of the Rydberg orbital in Fig. 14. We now look further at the overlaps in (33) in order to understand this interaction. We will separate our FO wavefunctions into two parts and consider each part separately. Due to the spatial projection operator we write $\Phi_v = \Phi_v^A - \Phi_v^B$ where Φ_v^A is the result of operating on the G1 wavefunction with the identity operator part of the projection operator shown in section B.1. Φ_v^B results from operating with the inversion operators. We first consider the unprojected part of the overlaps in (33) and we find that at R = 3.8 Bohr they differ by a factor of about 2:

$$\langle \Phi^A_{2p} | \Phi^A_{3d} \rangle = 0.04930$$
$$\langle \Phi^A_{2p} | \Phi^A_{3s} \rangle = -0.02644 \quad . \tag{34}$$

Upon expanding the O_{11} operator and examining the terms contributing to (34) we find that the factor of 2 arises from the difference in the overlap of the $\phi_v = 3d_u$ and $\phi_v = 3s_u$ orbitals with the ϕ_c and $\phi_{c'}$ orbitals on the opposite center. For example at R = 3.8, we have (keeping the phases shown in Fig. 3)

$$\langle \phi_{c'_L} | \phi_{3d_R} \rangle = 0.17182, \qquad \langle \phi_{c'_L} | \phi_{3s_R} \rangle = -0.09448 \quad . \tag{35}$$

This is understood by considering that the amplitudes of the $\phi_v = 3d_u$ and $3s_u$ orbitals at 3.8 Bohr from their centers also differ by a factor of 2 and are 0.02567 and -0.01317 a.u., respectively. From the projected contribution to the overlaps we obtain

$$\langle \Phi^A_{2p} | \Phi^B_{3d} \rangle = -0.02050$$
$$\langle \Phi^A_{2p} | \Phi^B_{3s} \rangle = -0.02399 \quad . \tag{36}$$

The important terms contributing to (36) involve overlaps between $\phi_v = 2p_L$ and $\phi_v = 3d_R, 3s_R$. These overlaps are nearly equal in magnitude and have the same sign

$$\langle \phi_{2p_L} | \phi_{3d_R} \rangle = 0.35992, \qquad \langle \phi_{2p_L} | \phi_{3s_R} \rangle = 0.39873 \tag{37}$$

leading to the nearly equal overlaps in (36). Subtracting the results in

(36) from those in (34) we obtain the results in (33). Thus at distances near the FO curve crossings the signs of the overlaps between the 3d orbital on one center and the cores and 2p orbitals on the other center are the same while they are opposite for the 3s orbital.

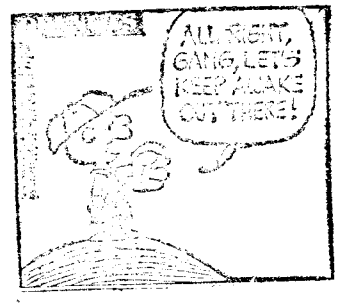

This mathematical explanation accounts for the difference in overlaps shown in (33) and helps explain why $^1\Sigma_u^+$ (2p) becomes 3d-like and not 3s-like for ~ 2.2 Bohr $< R < \sim 4.2$ Bohr. Note though from Fig. 14 that for $R < 2.2$ Bohr, ϕ_v becomes 3s-like. This is explained by the avoided crossing near their minima of the $^1\Sigma_u^+$ (3s) and $^1\Sigma_u^+$ (2p) curves. From his experimental data Ginter [35] has commented on the "crossing" of these states. Our $^1\Sigma_u^+$ (2p) and $^1\Sigma_u^+$ (3s) states are denoted at large R as his F and D states, respectively. At large R his F state has a large hump and in fact crosses the D state near 2.5 Å. Thus the minimum of the experimental [40] D state falls about 676 cm^{-1} below the minimum in the F state (our calculated $^1\Sigma_u^+$ (2p) lies 410 cm^{-1} below $^1\Sigma_u^+$ (3s) at the minimum). Although our SCF curves

cannot cross they show that both states only weakly avoid each other for $R < \sim 2.6$ Bohr and may come even closer than shown in Fig. 6 if we had calculated more points on our potential curve in this region. Indeed we see from Figs. 14 and 15 that the $^1\Sigma_u^+$ (2p) and $^1\Sigma_u^+$ (3s) Rydberg orbitals switch character near 2.2 Bohr offering additional evidence of the avoided crossing in these calculated curves. Our calculated R_{MIN} (or R_e) is 2.17 Bohr and agrees favorably with the value of 2.06 Bohr given by Ginter.[41] There are no accurate experimental data for D_0 and the magnitude and position of the maximum.

As a further check on the potential curve the experimental value for the energy difference between the minima of A $^1\Sigma_u^+$ and D $^1\Sigma_u^+$ is 18695[42a] and 18711[40] cm^{-1}. The difference calculated here between the minima in the potential curves for A $^1\Sigma_u^+$ and $^1\Sigma_u^+$ (2p) is 18182 cm^{-1}, an error of about 0.002 a.u. or only about 3%.

In our discussion of the SCF A $^1\Sigma_u^+$ state we noted that a temperature of 300 °K corresponded to a distance of about 4.2 Bohr on the ground state X $^1\Sigma_g^+$ curve. Since the hump in the A state came at about 5.8 Bohr we expect to see transitions in absorption spectra between the ground state and high bound or quasibound levels of A $^1\Sigma_u^+$. But note that for $^1\Sigma_u^+$ (2p) the maximum now falls at 3.77 Bohr and thus in absorption at 300 °K we should expect to see mostly free-free or continuous spectra for this state. Indeed in their studies of the absorption spectra of He_2 at 77 °K, Tanaka and Yoshino[21a] report finding no bands near the 584.33 Å line corresponding to $1s2p\ ^1P \leftarrow 1s^2\ ^1S$. As a matter of fact they report no bands between 600 Å and 540.76 Å. (The latter has

$^1\Sigma_u^+$ (3s) as the upper state and is discussed below.) This is understood from examination of Fig. 6.

Although Mulliken[38] correctly describes this state as being 3dσ-near the equilibrium separation we see that promotional effects are unimportant in causing the maximum. 3dσ character was necessary though in order that the curve have an attractive well.

e. The $^1\Sigma_u^+$ (3s) state.

From Fig. 6 and the right-hand column of Fig. 15[42b] we see that this state is analogous to the A state. The FO wavefunction provides a good qualitative description of this state. In the SCF wavefunction the Rydberg orbital remains 3s-like until about 2.2 Bohr when the near degeneracy with $^1\Sigma_u^+$ (2p) mixes in 3d character. This has been discussed above. Thus the curve is quite similar in shape to the A state and has a calculated D_e = 0.06916 a.u. compared to 0.06920 a.u. for the A state. The calculated R_e for this state is 2.19 a.u. compared to the experimental value of 2.02 a.u.[40] Also we find that there is a small maximum of 0.00015 a.u. in the spline fitted potential curve for this state (see Table XVI) at R = 11.38 - 11.54 Bohr. This maximum is much larger in the FO curve and is due to the unfavorable overlap of the outer maximum of ϕ_v = 3s with the cores on the opposite center.

Tanaka and Yoshino[4,21a] have reported a band in absorption at 540.77 Å. This comes at an energy slightly greater than the atomic line at 540.94 Å corresponding to $1s3s\ ^1S \rightarrow 1s^2\ ^1S$. They also report that this band was quite similar in appearance to the band at 600 Å which

arose from transitions to quasibound levels of the A state. Thus they propose that the $^1\Sigma_u^+$ (3s) (D $^1\Sigma_u^+$) state has a hump of about 60 cm^{-1} or 0.00027 a.u. Their predicted hump is larger than our calculated maximum and may be due in part to the limited number of points used in our spline fit near the maximum.

f. The $^1\Sigma_g^+$ (3s) state.

At large R this state is degenerate with $^1\Sigma_u^+$ (3s) and as a result shows the same maximum near 11.50 Bohr (see Table XVI). The potential curve falls (see Table XIV) as R decreases to less than the distance to the outer maximum in ϕ_v = 3s. We see from Fig. 5 that as R is decreased the repulsive core v = 3s $^1\Sigma_g^+$ (FO) curve rises and crosses the attractive curve resulting from v = 3p $^1\Sigma_g^+$ near 5 Bohr. This results in an avoided crossing of the SCF curves causing a maximum for $^1\Sigma_g^+$ (3s) and a small dip for $^1\Sigma_g^+$ (3d). Figure 15[42b] shows this 3p character mixing into the 3s orbital at R = 4.2 and R = 3.4 Bohr. For smaller R there is apparently a strong interaction with the repulsive core FO state arising from ϕ_v = 2s. This leads to another maximum in the curve near 3 Bohr. Now in order for $^1\Sigma_g^+$ (3s) to be attractive near R_e it must have an avoided crossing with a higher state in order to obtain favorable $^3\Sigma_u^+$ core. Since there are no remaining favorable FO curves shown in Fig. 5 we must go to the n = 4 levels. The ϕ_v = 4f, 4p $^1\Sigma_g^+$ (FO) states would both provide favorable core. These states[13] are separated by only 39 cm^{-1} at R = ∞ with ϕ_v = 4f being

the lower of the two. (ϕ_v = 5f, 5p are about 2200 cm^{-1} above these states and could also mix although our basis set will not provide a good description of these orbitals.) From Fig. 15 we see that $^1\Sigma_g^+$ (3s) becomes 4f-like near R_e. Note though that our basis set does not contain any 4f basis functions and that the 4f orbital shown in Fig. 15 is somewhat tighter than a hydrogenic 4f which has its maximum near R = 12.0 Bohr. The inclusion of n = 4 basis functions could improve the potential curve in this region.

g. The $^1\Sigma_g^+$ (3d) state.

In the calculations here (see section B3) we find the (1s, 3d) ^{1}D atom state to be 0.00059 a.u. lower than (1s, 3p) ^{1}P. Experiment[13] shows the ^{1}D state to be 0.00047 a.u. lower than ^{1}P. In the discussion of the FO curves we noted that the v = 3d curves rise steadily until R reaches the distance corresponding to the maximum in the 3d orbital near 6 Bohr. After this point the core-core interactions became important. For ϕ_v = 3p the unfavorable Rydberg-core interaction had a maximum near 11 Bohr corresponding to the distance to the maximum in the outer lobe of this orbital. For R $<$ 11 Bohr ϕ_v = 3p falls until about 6 Bohr corresponding to the outer node in the orbital. At this point the energy is near the R = ∞ value. Naturally we expect this to lead to an avoided crossing of the SCF curves. From Fig. 2d we see that the amplitudes of the ϕ_v = 3p and ϕ_v = 3d orbitals cross at 12.22 Bohr. Thus we would expect the FO energy curves to cross near this distance and indeed the crossing comes at 12.15 Bohr. Note that the amplitude

plot for the ϕ_v = 3d orbital is steeper than ϕ_v = 3p and correspondingly the FO energy curve is steeper in the region. Surprisingly though the maximum in the SCF $^1\Sigma_g^+$ (3d) curve does not come until R = 8.2 Bohr.

This can be explained by the near degeneracy of the states for ϕ_v = 3p and ϕ_v = 3d at R = ∞. Because of this the orbitals for very large R (15 Bohr $\leq$ R $<$ ∞) are represented by approximately orthogonal linear combinations of ϕ_v = 3d, 3p. The orbitals shown at R = 15 Bohr for $^1\Sigma_g^+$ (3d) and $^1\Sigma_g^+$ (3p) in Figs. 16 and 17 are virtual orbitals taken from $^1\Sigma_g^+$ (3s). The orbitals shown are good approximations to the appropriate SCF orbitals. The orbital for the lowest energy combination is shown at R = 15 Bohr in Fig. 16a. We see that this orbital is significantly polarized away from the opposite He and causes the maximum in the SCF curve to come at much smaller R than that which would be predicted from the crossing of the FO curves. For the higher $^1\Sigma_g^+$ (3p) state the orbital is just as in Fig. 16a except that it is polarized toward the opposite He (see Fig. 17). Thus for the latter state this energy curve is more repulsive in this region. Note that this did not occur at very large R for ϕ_v = 2s, 2p because of their large energy separation. In Fig. 16a we see that the 3p character begins to become dominant in the Rydberg orbital near 10 Bohr. The FO curves now separate considerably and are no longer nearly degenerate. The orbital now remains 3p-like until 4.2 Bohr. From Fig. 5 we see that between 8.0 and 4.2 Bohr the potential curve falls as it follows that for FO ϕ_v = 3p $^1\Sigma_g^+$. Near 5 Bohr there is a crossing of ϕ_v = 3s, 3p $^1\Sigma_g^+$. This results in an avoided crossing of the SCF curves and leads to a small well at R = 5.2

Bohr of 0.00210 a.u. The avoided crossing causes 3s character to mix into $^1\Sigma_g^+$ (3d) as is seen at R = 4.2 in Fig. 16b. Note that the orbital is now roughly g-like necessitating unfavorable $^2\Sigma_g^+$ core. Thus the potential curve rises. In order to fall to a minimum at R_e it must mix in favorable character from an n = 4 FO state. We see from Fig. 16b that 4f character mixes into ϕ_v between 3.8 and 3.0 Bohr causing it to fall from a maximum at 3.8 Bohr. At 3.0 Bohr $^1\Sigma_g^+$ (3d) becomes nearly degenerate with the rising $^1\Sigma_g^+$ (3s). The 4f character is then transferred to $^1\Sigma_g^+$ (3s) and it becomes attractive. Now $^1\Sigma_g^+$ (3d) mixes in favorable 4p character and falls to a minimum at 2.17 Bohr. Once again the inclusion of n = 4 basis functions in this region could improve our description.

h. The $^1\Sigma_g^+$ (3p) state.

Some of the orbitals for this state are shown in Fig. 17. The polarization of the Rydberg orbital toward the incoming He has been discussed in the previous section. At R = 6.2 Bohr the FO curves are no longer nearly degenerate as they were for very large R and ϕ_v is dominated by 3d character. Near R = 4.2 Bohr ϕ_v mixes in some 4f character (compare R = 3.0 for $^1\Sigma_g^+$ (3s) in Fig. 15). At R = 3.4 Bohr 4p character, as expected, becomes evident. For smaller R this character is lost to the lower states and we must resort to the states resulting from ϕ_v = 5f, 5p (or higher states) in order that the $^1\Sigma_g^+$ (3p) have an attractive core and thus fall below the curve for $^2\Sigma_u^+$. Our basis set though does not contain any functions appropriate for the

n = 4 or n = 5 separated atoms and hence we would expect it to give a very poor description of such an orbital. Although the Rydberg orbital eventually becomes 5p-like at R = 1.8 (see Fig. 17) it becomes approximately g-like at R = 2.6 due to the unfavorable interaction with the repulsive curve arising from v = 2s $^1\Sigma_g^+$ (FO). Thus our basis set is unable to build in 5p character near R = 3.4 Bohr. Instead near R = 2.2 Bohr 5p character begins to become evident and the slope of the potential curve decreases. Finally the curve follows the inner wall of the poorly described ϕ_v = 5p $^1\Sigma_g^+$ (FO) potential well. In summary then it appears that one would at least need atomic basis functions appropriate to n = 4 and 5 in order to obtain a good description of this state. Because of the great crowding of 4 electron states just below the He_2^+ $^2\Sigma_u^+$ minimum one may even need basis functions appropriate for n > 5.

i. The $^1\Sigma_u^+$ (3d) state.

For R > 6.2 Bohr this state is degenerate with $^1\Sigma_g^+$ (3d) and the reader is referred to section g for a discussion of the latter state at these distances. For R < 6.2 Bohr the SCF curve for $^1\Sigma_u^+$ (3d) begins to follow the repulsive v = 3p $^1\Sigma_u^+$ (FO) curve. The latter curve crosses for the second time that for v = 3d $^1\Sigma_u^+$ (FO). The effect on the SCF curve is shown at R = 4.2 and 3.8 Bohr of Fig. 16b where 3d character becomes evident in the Rydberg orbital. At these distances though 3d character, as we have already seen, becomes important in $^1\Sigma_u^+$ (2p). As a result $^1\Sigma_u^+$ (3d) must mix with states having n = 4 Rydberg orbitals in order to have an attractive potential well near R_e. Figure 16b shows

that near R = 3.8-3.4 Bohr 4d character becomes important. The absence of 4s character here may be due to the same factors used to explain the absence of 3s character in $^1\Sigma_u^+$ (2p) at large distances.

j. The $^1\Sigma_u^+$ (3p) state.

For R > 6.2 Bohr the description of this state is the same as that for $^1\Sigma_g^+$ (3p) and is found in section h. Near R = 4.2 Bohr (see Figs. 6 and 17) this curve begins to rise as it obtains unfavorable core from v = 3p $^1\Sigma_u^+$ (FO). At smaller R it approaches the repulsive curve for v = 2p $^1\Sigma_u^+$ (FO) and rises even further. The mixing of 2p character into the Rydberg orbital is shown at R = 3.4 Bohr in Fig. 17. At R = 2.6 Bohr favorable 4s-like character becomes evident in the Rydberg orbital and the potential curve begins to drop. Our basis set though is not adequate for this state and as for $^1\Sigma_g^+$ (3p) the inclusion of basis functions appropriate for atomic orbitals with $n \geq 4$ is necessary for a good description.

4. Summary

In conclusion we see that because of the independent particle nature of the projected G1 wavefunctions we have been able to provide a highly interpretable and meaningful description of the excited states of He_2. Two types of interactions have been shown to be important in

understanding the shapes of the potential energy curves. Interaction between core orbitals on opposite centers is dominant at small R whereas at large R the significant interaction is between Rydberg and core orbitals on opposite centers. The former interaction leads to repulsive and attractive FO potential energy curves which in turn leads to avoided crossings of SCF curves. The FO curves are therefore essential to understanding the SCF curves at small R. At large R where spatial projection is not important we have found that the unfavorable Rydberg-core interactions can be understood through examination of the exchange part of the kinetic energy. Through partitioning of the exchange kinetic energy into pairwise contributions we find that the unfavorable Rydberg-core interactions can be described in terms of Rydberg-core overlaps. Furthermore we found that this interaction can be understood from simply a knowledge of the shape of the Rydberg orbital. Indeed for the n = 3 states where the maxima occurred at large enough R where core-core interactions can be neglected we find that the maxima and shape of the FO potential energy curves correlate well with the amplitudes of the Rydberg orbitals. The same approach is used to explain the origin of the maxima in the SCF curves (with slight variations due to the SCF readjustment of the orbitals).

The only available experimental estimate of a maximum in a He_2^* potential energy curve is that for the A state. We have seen that the value calculated here is quite close to the experimental result. We expect the calculated maximum in the C state to be equally reliable

while those in the states arising from a ϕ_v = 2p separated atom orbital may be slightly less quantitatively reliable. For most of the n = 3 states our description for R < ~ 6.2 Bohr could be improved through the (financially obliterating) inclusion of basis functions appropriate for n ≥ 4 atomic orbitals.

D. APPLICATION TO OTHER SYSTEMS

The ideas presented here concerning FO curves and Rydberg-core interactions can be used to qualitatively describe and predict shapes of excited state potential curves of other systems. Here we will consider H_2 and HeH.

1. Excited States of H_2

As in He_2 the excited orbitals of H_2 are diffuse compared to the core orbitals. In addition the ion core has both an attractive and repulsive state arising from the lowest state at R = ∞. Thus H_2 provides for an ideal application of the ideas discussed here.

Nevertheless though there are some significant differences. First we note that the total T^X for this system is simply the single pairwise term shown in Eq. (22). In addition, for the singlet excited states $D_1^2 = S_{12}$ and $N = 1 + S_{12}^2$. Thus at large enough distances where we can ignore the projection operator we have

$$T_{12}^X = -(1/(1+S_{12}^2))S_{12}^2\tau_{12} \quad . \tag{38}$$

Before proceeding further we remind the reader of the work of Wilson

and Goddard[19] where it was shown that Eq. (38) dominated the energy and was the important term in determining bonding for the ground state of H_2. We see that as R decreases and S_{12} increases, T^X will decrease. This should cause the total energy to decrease. Thus as opposed to He_2 we should not expect to find any Rydberg-core type maxima in the singlet excited states of H_2. In He_2 we encountered maxima arising from the unfavorable interaction between two singlet coupled pairs of electrons whereas in H_2 we consider the favorable interaction in a single singlet coupled pair. These ideas have been discussed for H_2 by Goddard and Ladner.[43]

Now consider FO potential curves arising from H(1s) + H(2s or 2p). Taking the excited H atom orbitals to be either 2s or 2p at R = ∞ (unhybridized) we find that the FO curve arising from ϕ_v = 2p should fall more rapidly than that due to ϕ_v = 2s in view of Eq. (38) and the greater overlap of ϕ_v = 2p with the opposite core orbital. This effect is enhanced further by the fact that projected GI calculations on H_2[10a,b] show these orbitals to be hybridized. As a result the upper curve remains relatively flat at large R while the lower curve is attractive.

A further more quantitative consideration is that in H_2 the splitting of the ion core into $^2\Sigma_u^+$ and $^2\Sigma_g^+$ occurs at larger R than in He_2. For example, at R ≈ 7.7 Bohr these states are already split by 0.005 a.u.[44] whereas this does not occur until approximately R = 6.0 Bohr in He_2. The core orbital in H_2[10a] is more diffuse than those in He_2. In addition as opposed to He_2 $^2\Sigma_g^+$ is now the attractive core whereas $^2\Sigma_u^+$ is totally repulsive. Now for the FO curves corresponding to ϕ_v = 2p we expect both $^1\Sigma_g^+$ and $^1\Sigma_u^+$ curves to fall at

large R due to Eq. (38). At small R the core-core interactions become important. At small R, just as for He_2, $S_{\ell r}$ (as in Eq. (16)) becomes negative. This occurs for R $\approx$ 5.5 Bohr (see Table IV) in He_2 and should occur at about the same distance for H_2. Now using Eq.s (12) and (13) for H_2 with

$$\Phi_g^+ = (\phi_{c\ell} + \phi_{cr}), \qquad \Phi_u^+ = (\phi_{c\ell} - \phi_{cr})$$

we see that for R $< \sim$5.0 Bohr we have $C_2^2 > C_1^2$ (in Eq. (16)) and therefore for $^1\Sigma_g^+$ we have unfavorable core in the wavefunction while for $^1\Sigma_u^+$ we have favorable core. Thus $^1\Sigma_u^+$ should continue to be attractive at smaller distances while $^1\Sigma_g^+$ will become repulsive. This is shown in the rough qualitative sketch in Fig. 18. For 5.5 < R < 7.7 there are roughly equal amounts of favorable and unfavorable core in the wavefunction (see Table IV) and thus for ϕ_v = 2p, core-core interactions as in He_2 will not be important at these distances.

For ϕ_v = 2s, Eq. (38) should add attractive character to the FO curve for $^1\Sigma_g^+$ and $^1\Sigma_u^+$. In addition since $S_{\ell r}$ remains positive at all distances we should obtain increasingly favorable core for $^1\Sigma_g^+$ and unfavorable core for $^1\Sigma_u^+$ as R is decreased. These curves are sketched roughly in Fig. 18. Also based in the results in Ref. 10a we have added the curves for v = 3d $^1\Sigma_g^+$ (FO) and v = 3p $^1\Sigma_u^+$ (FO). The shapes of these curves also follow from the qualitative considerations given above. In Fig. 18 we have also roughly sketched the SCF curves with the avoided crossings based on the crossings of the FO curves. We see that we reproduce the double minima in the E, F $^1\Sigma_g^+$ and H $^1\Sigma_g^+$ states.

In addition there is a maximum in the SCF curve for $B'\,^1\Sigma_u^+$ state while $B\,^1\Sigma_u^+$ is smooth without a maximum. These shapes are verified by projected G1 calculations on H_2.[10a,b] The reader is referred to Refs. 10a and 10b for a detailed discussion of the excited states of H_2.

2. Two Excited States of HeH

For HeH the molecular symmetry is now $C_{\infty v}$ and as a result the spatial projection operator which we have considered for He_2 and H_2 is no longer of any importance. Nevertheless a similar approach can be used. Here we discuss the lowest two singlet excited states of HeH.

Wilson and Goddard[19] have discussed the repulsive ground state of HeH. The term in T^X representing the pairwise interaction between the orbital on H and an orbital on He is given to a good approximation by:

$$T_{i1}^X \approx (1/N)S_{i1}^2\tau_{i1} \quad . \tag{39}$$

Thus we see that, unlike Eq. (38), T_{i1}^X now increases as S_{i1} increases (N and τ_{i1} vary only slowly with R). For the excited states of HeH Eq. (39) also applies and as a result we expect to find energy maxima at large R just as in the excited states of He_2.

Before proceeding further it is necessary to consider the ion core since it will provide the major contribution to the energy at small distances. From the ground state of the separated atoms $(He(1s)^2 + H^+)$ we obtain only one molecular state, $^2\Sigma$. We expect this state to be attractive and to have a dissociation energy in the same ballpark as He_2^+. The calculated values for HeH^+ are 2.04 eV,[45a] 1.93 eV,[45b] and

2.28 eV[45c] compared to 2.50 eV[28,34,35] for He_2^+. The lowest excited states[46] of HeH^+ arise from the separated atom limit $He^+(1s) + H(1s)$. These have only shallow minima (< 0.1 eV) and lie about 0.38 a.u. above the ground state. Therefore we can neglect these core states in discussing the low lying states of HeH. At small R we expect the HeH excited states considered here to have minima of about 2 eV.

Now at R_e once again most of the amplitude of the Rydberg orbital will enclose the nuclei and the core. But since we have no inversion symmetry here the Rydberg orbital is not required to be g or u at R_e as it was in He_2. As a result in the molecular states arising from $He(1s)^2 + H(2s \text{ or } 2p)$ the orbitals are allowed to be hybrids at R_e. Since $\phi_v = 2s, 2p$ on H are degenerate at $R = \infty$ we will take the FO orbitals to be hybrids with one state having an orbital pointing toward the incoming He while the other is polarized in the opposite direction (as for $\phi_v = 3p$, 3d in He_2 and $\phi_v = 2s, 2p$ in H_2). According to Eq. (39) the orbital pointing away from the incoming He will have the lower potential curve at large R. At smaller R this curve will be attractive with $D_e \approx 2$ eV (assuming only a small unfavorable Rydberg core interaction for this state).

The upper state will show a much larger hump due to its greater overlap with the cores on the opposite He. At small R it should also have a potential well except that we must add the attractive core interaction to the repulsive Rydberg-core interaction to determine the well depth. Full CI calculations have been reported[47] for these two states, confirming the qualitative description given here. The lower state has

D_e = 2.5 eV with no hump indicating that the orbital is polarized considerably away from the opposite He with the core being dominant in determining the shape of the potential curve. For the upper state there is a large hump of 0.85 eV at 3.8 Bohr. This hump is comparable in magnitude and position to that obtained for $\phi_v = 2p\ ^1\Sigma_g^+$ in He_2 (1.03 eV at 3.5 Bohr)! In addition the curve has a well depth (below E(∞)) of 0.63 eV at 1.6 Bohr compared to 0.70 eV at 2.05 Bohr for the same He_2 state.

E.1. Dissociative Recombination

In order to explain large atmospheric and experimentally observed[48] electron-ion recombination coefficients Bates[49] proposed the process of dissociative recombination

$$AB^+ + e^- \rightarrow AB' \rightarrow A^* + B \qquad (40)$$

and described it in terms of the intersection of an attractive ion potential curve and a repulsive neutral curve.[50] The latter curve necessarily has an excited ion core in order to cross the potential curve for the ground state ion, AB^+. In the mechanism for generating AB^+ in Eq. (40) via a radiationless transition the incoming electron excites an electron of the ion to a high lying level while it is captured in a previously unoccupied level. From a knowledge of the location of the crossing of the potential curves for AB^+ and AB^-, the electron energy, and the shapes of the curves one can then consider the relevant Franck-Condon factors and discuss the likelihood of dissociative

recombination (DR). What makes DR attractive in explaining large recombination coefficients is the fact that it can provide a very efficient means of removing electrons. Namely, once the state AB′ is formed it can be expected to move past the crossing point in a time which is of the order of 10^{-16} to 10^{-15} sec.[50] Once past the point where the diabatic curve is lower in energy than the ion curve autoionization (with lifetimes of about 10^{-14} sec[50]) would be impossible and dissociation, without other complicating effects, is assured.

Now we ask: Do our potential curves provide a route for dissociative recombination (DR) in He_2? All of the SCF curves (see Fig. 11) involve, of course, single excitations and have the favorable $^2\Sigma_u^+$ core at R_e. As a result all of the properly described adiabatic curves are lower in energy at R_e than the ion. In addition, at $R = \infty$ the lowest doubly occupied neutral state lies about 16 eV above $He + He^+$ and it is unlikely that these states can provide a mechanism for DR in He_2. The possibility of doubly excited separated atom ionic states being of some importance has been discussed by Mulliken[38a] although with more recent reservations.[51] This will be discussed in section E. 2.

At this point we will take a short sidetrack. Returning to the adiabatic states discussed previously we can view these qualitatively in terms of a CI wavefunction in which each of the configurations is composed of frozen orbitals. For some of the states one need only consider two FO configurations in order to get a reasonable qualitative description of the adiabatic state. For example, for C $^1\Sigma_g^+$ these are the v = 2p and v = 2s $^1\Sigma_g^+$ (FO) states already discussed. In the adiabatic description the nuclei move along the SCF potential curve infinitely slowly and as a result the orbitals can readjust considerably in the neighborhood of crossings of FO potential curves. By the non-crossing rule the adiabatic states of the same symmetry must avoid each other leading to changes in orbital character as one moves along an adiabatic curve. It is well-known though that such adiabatic curves are not always relevant to real life. An example of this has already been discussed concerning the spectral results for $^1\Sigma_u^+$(3s) on p. 45. Further examples are discussed by O'Malley[52] and Lichten.[53] The infinitely slow change in orbital character found in the adiabatic description may not occur (see conditions below) and as a result the wavefunction may not be able to rearrange from one FO wavefunction or mixture of FO wavefunctions to another mixture. Thus only one FO wavefunction or mixture may be appropriate throughout. We will now refer to our FO wavefunctions as diabatic wavefunctions. The conditions under which a diatomic molecule may remain on one diabatic curve instead of transferring to another in the vicinity of the crossing of these curves has been discussed by O'Malley[52] based on the early work of Zener.[54] We can expect that near their crossing there is a greater chance of remaining in one of the diabatic states if the nuclei are

moving rapidly, if the slopes of both curves are quite different, and if there is a small electronic matrix element between the two states, i.e., when the orbitals have a lot of readjusting to do. Since all these factors are interrelated and much further work is needed before one can discuss this quantitatively, the analysis below is only qualitative. The reader is referred to Ref's. 52-55 and references therein for a further discussion of similarly defined diabatic curves.

From the preceding discussion it is therefore natural to inquire as to whether these FO curves may be the diabatic states which can offer a route for dissociative recombination in He_2. We note from Figs. 5 and 6 that half of the FO curves are repulsive and intersect the outer wall of the He_2^+ potential well. These FO curves can therefore be represented by the state AB′ in Eq. (40). These states can be loosely[56] thought of as being doubly excited at small R since they involve an excited Rydberg orbital and mostly an excited unfavorable $^2\Sigma_g^+$ core. Nevertheless these FO repulsive states dissociate to singly excited states at $R = \infty$.

In order to have dissociative recombination to the n = 2 levels it is necessary to employ the repulsive curves arising from v = 2s $^{1,3}\Sigma_g^+$ (FO) and v = 2p $^{1,3}\Sigma_u^+$ (FO). Although these curves can in themselves provide a route for DR strong interactions amongst the v = 2s and v = 2p states could result in DR via a g curve to give v = 2p excited atoms. In order to check this and in addition to see if such an interaction altered appreciably the location of the intersection of the diabatic and ion curves we performed a full CI on the $^{1,3}\Sigma_g^+$ states using only n = 2 basis functions. The 1s, 1s′, 2s, and $2p_z$ basis functions of Tables I and II were used on

each center. Thus character from n = 3 states could not interfere adiabatically and the CI could only reproduce the avoided crossing of the n = 2 FO curves shown in Fig. 5. The result is shown in Fig. 19. It is seen that the crossing is quite effectively avoided providing a route for these g diabatic states to give rise to v = 2p excited atoms upon DR. Of equal importance is the fact that the intersection of the diabatic curves for $^3\Sigma_g^+$ and $^1\Sigma_g^+$ with the ion in Fig. 19 comes at roughly the same location as the intersection of the v = 2s $^1\Sigma_g^+$ (FO) curve with the ion (see Fig. 20). Important experimental evidence for this process will be discussed below.

It is well-known that the DR coefficient for He_2 is at least two orders of magnitude less than the values for the molecular ions of the other rare gases.[57] In addition it has been reported[57, 58] that the visible atomic lines coming from a He afterglow have their origin in radiative and collisional recombination of He^+ and may not be related to He_2^+. These processes are described by

$$\begin{aligned} He^+ + e^- &\rightarrow He^* + h\nu \\ He^+ + 2e^- &\rightarrow He^* + e^- \quad . \end{aligned} \tag{41}$$

Also the molecular bands apparently arise from collisional radiative recombination of He_2^+ [57-59] (i.e., replace He^+ and He^* with He_2^+ and He_2^* in (41)) and dissociative recombination plays only a small role although there are some exceptions to this (e.g., compare Ref. 60 and see below). The experimental results obtained from He discharges are quite conflicting. The state of the art is discussed by Stevefelt and Robben[61] who point out that "useful experiments are very difficult to

perform, and that as a corollary there are numerous errors in the published papers."

From our potential curves we see that if virtually all the He_2^+ in these experiments is in the ground vibrational level we would not expect DR to be important in He_2 since our FO curves intersect the ion curve above v = 1 (see Fig. 20) and the Franck-Condon factors are small. This has been a popular explanation for the small DR coefficient in He_2 and our potential curves offer the first verification of this. Mulliken[38a] has remarked that since most of the excited states of He_2 arise from collisional radiative recombination of He_2^+ and since most of the spectra observed involve v = 0 levels, most of the He_2^+ may very well be in this vibrational level. This would also confirm the lack of dissociative curves crossing the He_2^+ curve near the bottom of the well.

Since the DR coefficient is proportional to the Franck-Condon factor connecting the ion and the diabatic state, let us look at the variation of the DR coefficient with the location of the crossing between these states (taking the electronic matrix element to be constant) in order to see if this is a viable explanation of the small DR coefficient. Assuming only the v = 0 level to be populated and taking a delta function to represent the nuclear wavefunction the Franck-Condon factor falls off as $e^{-(R - R_0)^2/d^2}$. Here we take a harmonic oscillator wavefunction for the v = 0 level. R_0 is the position of the minimum in the ion curve, R is the position on the diabatic curve corresponding to the energy of the v = 0 ion plus the electron and d is the amplitude of vibration of the v = 0 level. For R very close to R_0 this factor is about 1. For the

$v = 2s\ ^3\Sigma_g^+$ (FO) curve shown in Fig. 20 and electrons at room temperature this factor is about .0008 while for $v = 2s\ ^1\Sigma_g^+$ (FO) it is .000002. Thus with these assumptions and assuming other factors to be equal the position of the crossing of ion and diabatic curves as shown in Fig. 20 could easily account for the small DR coefficient in He_2 compared to other molecules where the crossing may be more favorable. Indeed from the curves shown in Fig. 20 we estimate that electron temperatures near 25000°K would be necessary in order to have a favorable Franck-Condon factor (with the v = 0 level) for dissociation on the $v = 2s\ ^3\Sigma_g^+$ (FO) curve. Such electron temperatures in He glow discharges have not yet been reported. Note that we have neglected the effect of the electronic matrix element here and this would also have to be considered.

Results reported by W. W. Robertson[62] with more recent confirmation by C. B. Collins and W. B. Hurt[63] has shown that there is a strong correlation between the time decay of the intensity of the 10,830 Å line ($2^3P \rightarrow 2^3S$) and the molecular light emanating from a flowing He afterglow. These workers also report that apparently there is no similar correlation between the molecular light and lines in the visible region (transitions between n = 3 and n = 2 He atom states). Thus these workers were able to show a definite dependence of the concentration of the 2^3P atoms on the concentration of He_2^+ although with a very small DR coefficient. Additional results describing DR into the n = 2 levels has also been recently reported by Johnson and Gerardo.[60] The repulsive diabatic curves reported here can offer a direct route for these processes.

The curves shown in Figs. 19 and 20 for the g states and the v = $2p\ ^{1,3}\Sigma_u^+$ curves in Figs. 6 and 20 provide such routes. The experimental results do not distinguish between a direct DR process as discussed here and one in which an intermediate Rydberg state is formed by collisional and/or radiative recombination with He_2^+ which then dissociates to the atoms via the diabatic curves. Compared to the ion such a Rydberg state may have a more favorable Franck-Condon factor with the repulsive diabatic state. A serious problem with the Rydberg state is that the transition to the diabatic state will have to compete with autoionization. There is an obvious need for further work here. An example of one of the many additional possibilities is dissociative recombination to v = 3s via the v = $2s\ ^1\Sigma_g^+$ (FO) curve and the $^1\Sigma_g^+$ (3s) adiabatic curve shown in Fig. 5. The calculation of electronic and nuclear interaction matrix elements between the adiabatic and diabatic states is imperative before anything more definitive can be said.

E.2. Associative Ionization

The reverse of dissociative recombination, associative ionization

$$He + He^* \rightarrow He_2^+ + e^- \qquad (42)$$

has been shown[64,65] to account for the formation of He_2^+ at low pressures in discharges and electron impact experiments where three body processes

$$He^+ + 2He \rightarrow He_2^+ + He \qquad (43)$$

are not important. The formation of He^* precedes Eq. (42) and has been shown[66] to result from

$$He + e^- \rightarrow He^* + e^- \quad . \tag{44}$$

Several electron impact-mass spectrometer experiments have been reported in which the appearance potential of He_2^+ has been measured. Several values are 23.18 (+0.2 - 0.7) eV,[66] 23.1 ± 0.1 eV,[67] and 23.1 ± 0.05 eV.[68] The excitation energies[13] of several excited He atom states are 20.61 eV (2^1S), 19.81 eV (2^3S), 21.22 eV (2^1P), 20.96 eV (2^3P), 22.72 eV (3^3S), 22.92 eV (3^1S), 23.00 eV (3^3P), 23.08 eV (3^1P), 23.07 eV (3^3D and 3^1D). Thus based on the appearance potential of He_2^+ experimentalists have proposed that the n = 2 excited states and the 3s level are not important in associative ionization (AI). But due to the lack of potential curves for these states, only one mechanism, that of Mulliken[38a] (discussed at the end of this section) has been proposed to describe this process. The potential curves calculated here provide an alternate mechanism to that proposed by Mulliken. For reasons discussed in section E. 1 the discussion below is only qualitative.

A look at our n = 3 repulsive FO potential curves shows that they rise considerably with respect to R = ∞ before crossing the attractive $^2\Sigma_u^+$ ion curve. Considering the experimental evidence for AI it is therefore doubtful that these are the relevant curves for this process. We can think of an additional mechanism that may explain AI in He_2. The nuclei may follow the adiabatic curves at large R and then at small R the potential curve may be somewhat diabatic, i.e., the orbitals do not

readjust in the optimum adiabatic manner. Instead of favorable character mixing in from upper states the curve may suffer an avoided crossing with a repulsive lower diabatic state. An example of this is the SCF potential curve which we have calculated for $^1\Sigma^+_{g,u}$ (3p). Here the basis set description was not good at small R. The orbitals were not allowed to relax favorably and obtain character from upper states (only character from n = 3 basis functions was allowed). As a result the four electron curve actually crosses the ion curve. For $^1\Sigma^+_g$ (3p) this was due to repulsive character from v = 2s $^1\Sigma^+_g$ (FO) while for $^1\Sigma^+_u$ (3p) it was due to v = 2p $^1\Sigma^+_u$ (FO). These 3p SCF curves are mentioned here as examples of the presence of repulsive core character at these distances and energies in the n = 3 states. Such repulsive character could be important in other n = 3 states. Consider first the u states. The repulsive ϕ_v = 2p $^1\Sigma^+_u$ (FO) curve crosses the ion curve at E = -4.919 a.u. This is about 0.014 a.u. (0.38 eV) above the separated atom limit for ϕ_v = 3d, 3p and about 0.018 a.u. (0.49 eV) above the limit for ϕ_v = 3s. For the g states the repulsive curve for ϕ_v = 2s $^1\Sigma^+_g$ (FO) crosses the ion curve at E = -4.93242 a.u. or about 0.00006 a.u. (0.0016 eV) below the separated atom limit for ϕ_v = 3p, 0.00053 a.u. (0.014 eV) above the limit for ϕ_v = 3d and 0.00488 a.u. (0.133 eV) above the limit for ϕ_v = 3s. Therefore with electron impact energies in the neighborhood of 30 eV or more one would not expect more than about 0.02 eV to be transferred to the kinetic energy of the nuclei.[69] Assuming that the repulsive FO curves arising from the n = 2 levels are indeed the correct diabatic curves for the n = 3 states this would rule out the 3s

level and any of the $^1\Sigma_u^+$ molecular states as being important in AI. (The n = 2 levels are, of course, also ruled out.) For the 3s levels this is apparently in agreement with experimental results,[65, 68] as already mentioned. Wellenstein and Robertson[65] report that changes in the $3\,^1S$ population produced no observable change in molecular ion concentration. The 3s level is additionally unlikely to participate in associative ionization because of its low excitation cross section compared to, e.g., $3\,^1P$.[69, 70] This leaves the ϕ_v = 3p, 3d levels as contributors to AI. Although the $3\,^1P$ level would be favored we note from Fig. 5 that this level is repulsive at large distances. Although our description of this state is not good at smaller R the rise at large R should be a real effect based on the overlap arguments presented in section C.2. At R = 10 Bohr, $\phi_v = 3p\,^1\Sigma_g^+$ has risen by about 0.005 a.u. (0.14 eV) above the energy at R = ∞. As a result tunneling would be necessary here in order that ϕ_v = 3p contribute to associative ionization. The curve for ϕ_v = 3d is much flatter at larger R (see Table XIV) but has a maximum at R = 3.8 Bohr of 0.0044 a.u. (0.12 eV). It is possible that a better basis set with n = 4 functions could reduce the size of this maximum. It is difficult though to estimate just how much of a reduction is to be expected. Nevertheless the barrier for this state is narrower than for $\phi_v = 3p\,^1\Sigma_g^+$ and this could favor ϕ_v = 3d over ϕ_v = 3p for associative ionization once these excited states are generated by electron impact (and assuming other factors are equal). Recent experimental results[65] show the cross section for AI for $3\,^1D$ to be the largest for the n = 3 levels and about a factor of 7 greater than that for $3\,^1P$. In addition triplets have lower

cross sections than the corresponding singlets. This is reasonable since their energies are lower than the corresponding singlets. In light of the above discussion it is surprising that dissociative recombination has not been observed to yield 3 ^{1}D atoms. This may be due to the fact that in real life the energy of the R = ∞ limit and that for the intersection of the diabatic 2s curve with the ion may differ so as to favor AI and not DR. Further work is needed here.

The mechanism proposed by Mulliken[38a] for AI in He_2 involves 4 electron states with unfavorable core $(1\sigma_g\ 1\sigma_u^2)$ at small R. In order to describe the dissociation of states with favorable or unfavorable core Mulliken uses expressions analogous to Eqs. (12) and (13) with

$$\Phi_g^+ = 1\sigma_u^2 1\sigma_g$$

and

$$\Phi_u^+ = 1\sigma_g^2 1\sigma_u$$

where $1\sigma_g$ and $1\sigma_u$ are the usual symmetry molecular orbitals. From our orbitals (or Mulliken's) we can obtain at R = ∞ Eqs. (12) and (13) with $C_1 = C_2 = 1/\sqrt{2}$ or we can obtain

$$\Phi'_g = \frac{1}{\sqrt{2}} (\Phi_g^+ \phi_{vg} - \Phi_u^+ \phi_{vu}) \qquad (12a)$$

$$\Phi'_u = \frac{1}{\sqrt{2}} (\Phi_u^+ \phi_{vg} - \Phi_g^+ \phi_{vu}) \quad . \qquad (13a)$$

Equations (12) and (13) correspond to dissociating to neutral separated atoms while Eqs. (12a) and (13a) describe the ionic state ($He^+ + He^-$) at R = ∞. The latter state is derived by replacing ϕ_{vr} with $\phi_{v\ell}$ and vice versa in Eq. (10). Now since Eqs. (12) and (13) represent the

lowest state at R = ∞ Mulliken argues that they should connect with the lowest states at R_e, namely those with favorable core, Φ_u^+. Further he incorrectly argues that all those states with unfavorable core at R_e, Φ_g^+ should dissociate to the ionic states, Eqs. (12a) and (13a) at R = ∞. We have seen though that a calculation of the coefficients C_1 and C_2 on page 14 shows that states with a repulsive core do originate from neutral separated atom states. Thus a particular neutral state at R = ∞ will lead to a repulsive and an attractive state while the same will happen for a particular ionic state. Thus for $\phi = 2s\ ^3\Sigma_g^+$ Mulliken correctly describes an ionic state which arises at the He + He^+ limit since He^- is unstable. This state falls rapidly crossing n = 4 and n = 3 states of the same symmetry that arise from neutrals. Because of the unfavorable core in these states the state becomes repulsive, crossing the n = 4 and n = 3 states again in addition to the ion curve. This then offers a mechanism for AI if the outer crossing is allowed and the inner crossing is avoided. The mechanism proposed here differs in that here we discussed a repulsive curve which crosses the ion curve and arises from a lower neutral state and not an ionic state. Such non-adiabatic states can provide a mechanism for AI and DR to lower n = 2 atom states. Mulliken's ionic curve cannot provide this latter route. Indeed we have found that the repulsive FO curves were necessary for an understanding of the shapes of the SCF curves. It is interesting to note that while they originate at different separated atomic limits both Mulliken's curve for $\phi = 2s\ ^1\Sigma_g^+$ and the FO curve calculated here cross the ion curve at roughly the same energy. Mulliken reports that recent calculations[51] show that his ionic curves may cross the ion curve at too large an internuclear distance to provide an effective mechanism for DR or AI.

REFERENCES

1. (a) See for example, W. A. Goddard, J. Amer. Chem. Soc., 94, 793 (1972); W. A. Goddard, Accts. Chem. Res., to be submitted and papers referenced below; (b) See the Class Notes for Chemistry 226a, Winter, 1968; (c) The variational principle leads to equations for the orbitals of the form $H_i\varphi_i = \epsilon_i\varphi_i$ and thus provides an independent particle interpretation of the orbitals.
2. The major pioneering contribution was provided here by R. S. Mulliken, Phys. Rev. 40, 55 (1932); 41, 49 (1932); Rev. Mod. Phys., 4, 1 (1932), etc.
3. T. H. Lyman, Astrophys. J., 60, 1 (1924).
4. Y. Tanaka and K. Yoshino, J. Chem. Phys., 39, 3081 (1963).
5. (a) H. B. Dorgelo and J. H. Abbink, Z. Physik., 37, 667 (1926); K. T. Compton and J. C. Boyce, J. Frank. Inst., 205, 497 (1928); (b) L. A. Sommer, Proc. Nat. Acad. Sci., 13, 213 (1927); (c) P. G. Kruger, Phys. Rev., 36, 855 (1930).
6. J. L. Nickerson, Phys. Rev., 47, 707 (1935).
7. (a) J. J. Hopfield, Phys. Rev., 35, 1133 (1930), Astrophys. J., 72, 133 (1930); (b) R. A. Buckingham, Trans. Faraday Soc., 54, 453 (1958).
8. For portions of this study already published see S. L. Guberman and W. A. Goddard, Chem. Phys. Lett., 14, 460 (1972).
9. (a) For a discussion of the G1 method and the G_i^γ operator see Phys. Rev., 157, 73 (1967); ibid., 157, 81 (1967). Here we use

a spatial projection operator in addition to the G_i^γ operator. We optimize the orbitals after projection. (b) Similar approaches have been discussed by G. A. Gallup, J. Chem. Phys., 48, 1752 (1968); ibid., 50, 1206 (1969); R. C. Morrison and G. A. Gallup, ibid., 50, 1214 (1969); D. Kunik and U. Kaldor, ibid., 56, 1741 (1972); (c) R. C. Ladner, Ph.D. Thesis, California Institute of Technology, 1972.

10. (a) D. L. Huestis, Ph.D. Thesis, California Institute of Technology, 1973; (b) D. L. Huestis and W. A. Goddard III, Chem. Phys. Lett., 16, 157 (1972).

11. E. A. Hylleraas and B. Undheim, Z. Physik., 65, 759 (1930); J. K. L. McDonald, Phys. Rev., 43, 830 (1933). For example, when we solve for a Rydberg orbital we obtain a diagonal CI matrix. Each of the diagonal elements are upper bounds to the pertinent excited states.

12. S. Huzinaga, J. Chem. Phys., 42, 1293 (1965).

13. C. E. Moore, Atomic Energy Levels (Washington, 1949), Vol. I.

14. (a) The absence of orthogonality between orbitals on the same center leads to certain terms (e.g., $\pm \langle \phi_{c\ell}\phi_{c'\ell}\phi_{\bar{c}r}\phi_{vr} |H| \phi_{\bar{c}\ell}\phi_{v\ell}\phi_{cr}\phi_{c'r} \rangle$) remaining in the energy at R = ∞ for v = 2s, 3s, and 3d. For v = 2s this causes $^1\Sigma_g^+$ to be 0.00076 a.u. (0.02 eV) higher than $^1\Sigma_u^+$ at R = ∞. This separation is shown in Figs. 4 and 21. This splitting does not occur for v = 2p, 3p since by symmetry the 2p orbital is orthogonal to the core orbitals on the same He at R = ∞. For v = 3s or 3d the overlap between this Rydberg orbital and the core orbitals on the same center is small enough

so that the splitting cannot be seen in Figs. 4 and 11. The curves drawn in Fig. 4 are from wavefunctions in which the orbitals are taken from separate $^1\Sigma_g^+$ and $^1\Sigma_u^+$ calculations at R = ∞. For v = 2p, 3p $^1\Sigma_g^+$, $^1\Sigma_u^+$ and $^1\Sigma^+$ calculations at R = ∞ all give identical orbitals. Where the splitting is non-zero it is small enough so as to not interfere with the ideas presented here. (b) The difference in the nodal structure of the Rydberg orbitals for $^1\Sigma_g^+$ and $^1\Sigma_u^+$ can be accounted for by recalling from section B.2. that upon solving Eq. (8) the virtual (vrt) and occupied solutions are orthogonal, i.e., $\langle \phi_{c\ell}\phi_{c'\ell}\phi_{\bar{c}r}\phi_{vr}^{vrt} | PO_{11}\phi_{c\ell}\phi_{c'\ell}\phi_{\bar{c}r}\phi_{v'r}\rangle = \delta_{vv'}$. Expanding, we find that for $v \neq v'$ this implies that $\langle \phi_{vr}^{vrt} | \phi_{v'r}\rangle \approx 0$ or since the core orbitals do not change significantly from state to state $\langle \phi_{vr} | \phi_{v'r}\rangle \approx 0$. Thus for $^1\Sigma_u^+(2s)$ the Rydberg orbital is the lowest solution for this state and need not have any nodes while for $^1\Sigma_g^+(2s)$ the Rydberg orbital is approximately orthogonal to the ground state orbital and has one radial node. Similar considerations follow for $^1\Sigma_{g,u}^+(3s)$. I thank Dave Huestis for a discussion of some of these points.

15. B. K. Gupta and F. A. Matsen, J. Chem. Phys., 50, 3797 (1969).

16. J. C. Browne, Phys. Rev., 138, A9 (1965).

17. M. L. Ginter, J. Chem. Phys., 42, 561 (1965).

18. B. K. Gupta et al., Bull. Am. Phys. Soc., 12, 182 (1967).

19. C. W. Wilson and W. A. Goddard III, Theoretica Chim. Acta, in press; C. W. Wilson and W. A. Goddard III, Chem. Phys. Lett., 5, 45 (1970).

20. More than 92% of ϕ_c is within r = 0.4 Bohr and about 83% of $\phi_{c'}$ is within r = 1.0 Bohr of its center (see Fig. 2a).

21. (a) Y. Tanaka and K. Yoshino, J. Chem. Phys., 50, 3087 (1969); (b) F. R. Innes, K. Yoshino, and Y. Tanaka, Sixth International Conference on Electronic and Atomic Collisions, 891 (1969).

22. M. G. Waggoner, K. W. Chow, and A. L. Smith, Chem. Phys. Lett., 3, 151 (1969).

23. Y. Tanaka, A. S. Jursa, and F. J. LeBlanc, J. Opt. Soc. Am., 48, 304 (1958).

24. R. E. Huffman, Y. Tanaka, and J. C. Larrabee, App. Opt., 2, 617 (1963).

25. K. M. Sando and A. Dalgarno, Mol. Phys., 20, 103 (1971).

26. A. L. Smith and K. W. Chow, J. Chem. Phys., 52, 1010 (1970).

27. A. L. Smith, J. Chem. Phys., 49, 4817 (1968).

28. K. M. Sando, Mol. Phys., 21, 439 (1971).

29. R. A. Buckingham and A. Dalgarno, Proc. Roy. Soc., A213, 329 (1952).

30. J. C. Browne, J. Chem. Phys., 42, 2826 (1965).

31. D. C. Allison, J. C. Browne, and A. Dalgarno, Proc. Phys. Soc., 89, 41 (1966).

32. D. R. Scott, E. M. Greenawalt, J. C. Browne, and F. A. Matsen, J. Chem. Phys., 44, 2981 (1966).

33. S. Mukamel and U. Kaldor, Mol. Phys., 22, 1107 (1971).

34. M. L. Ginter and C. M. Brown, J. Chem. Phys., 56, 672 (1972); K. M. Sando, Mol. Phys., 23, 413 (1972).

35. M. L. Ginter and R. Battino, J. Chem. Phys., 52, 4469 (1970).

36. M. L. Ginter, J. Chem. Phys., 42, 561 (1965).

37. M. L. Ginter and D. S. Ginter, J. Chem. Phys., 48, 2284 (1968).

38. R. S. Mulliken, Phys. Rev., 136, A962 (1964); R. S. Mulliken, J. Amer. Chem. Soc., 88, 1849 (1966).

39. From the molecular symmetry orbitals of Mulliken one would predict the 2p character to be in the ground state. From Fig. 3b we can see that this is not the case. If it were true the ground state would have attractive u core character in order to have total g symmetry. But the ground state is repulsive. It has equal amounts of g and u core (replace ϕ_v with a core orbital in Eqs. (10)-(12)) at the distances of interest here and becomes appreciably repulsive for $R < 4.2$ Bohr. At this distance the splitting of $^2\Sigma_g^+$ from $E(\infty)$ becomes much greater than $^2\Sigma_u^+$ (see Table XIII). Thus the 2p character comes into the next highest $^1\Sigma_g^+$ state, namely the C state. This 2p-like orbital has maxima at R = 4.4 and 4.6 Bohr from the midpoint between the two centers at 1.8 Bohr separation and is quite diffuse compared to a hydrogenic 2p which has its maxima at 2.0 Bohr.

40. Données Spectroscopiques Relatives aux Molécules Diatomiques, B. Rosen (Ed.), (Pergamon Press, Oxford, 1970).

41. M. L. Ginter, J. Chem. Phys., 45, 248 (1966).

42. (a) G. Herzberg, Spectra of Diatomic Molecules (D. Van Nostrand Co., Inc., New York, 1950), p. 536; (b) The unsymmetrical nature of the 3s orbital at $R = \infty$ in Fig. 15 is due to the nature of the 3d function used here. See section B.3.

43. W. A. Goddard III and R. C. Ladner, J. Amer. Chem. Soc., 93, 6750 (1971).

44. This is obtained from a spline fit of the exact H_2^+ energies given by D. R. Bates, K. Ledsham, and A. S. Stewart, Phil. Trans. Roy. Soc. London, 246, 215 (1953).

45. (a) L. Wolniewicz, J. Chem. Phys., 43, 1087 (1965); (b) B. G. Anex, J. Chem. Phys., 38, 1651 (1963); (c) H. Conroy, J. Chem. Phys., 41, 1341 (1964).

46. H. H. Michels, J. Chem. Phys., 44, 3834 (1966).

47. C. A. Slocomb, W. H. Miller, and H. F. Schaefer, J. Chem. Phys., 55, 926 (1971).

48. M. A. Biondi and S. C. Brown, Phys. Rev., 75, 1700 (1949).

49. D. R. Bates, Phys. Rev., 77, 718 (1950); 78, 492 (1950).

50. J. N. Bardsley and M. A. Biondi, in Advances in Atomic and Molecular Physics, D. R. Bates (Ed.) (Academic Press, New York, 1970), Vol. 6, pp. 1-57.

51. R. S. Mulliken, J. Chem. Phys., 52, 5170 (1970).

52. T. F. O'Malley, in Advances in Atomic and Molecular Physics, D. R. Bates and I. Estermann (Eds.) (Academic Press, New York, 1971), Vol. 7, pp. 223-249.

53. W. Lichten, Phys. Rev., 131, 229 (1963).

54. C. Zener, Proc. Roy. Soc. Ser. A, 137, 696 (1932).

55. T. F. O'Malley, J. Chem. Phys., 51, 322 (1969).

56. Note that even at small R the repulsive FO states do have some $^2\Sigma_u^+$ favorable core (see Table IV). In addition, 50% of the core at $R = \infty$ is described as $^2\Sigma_u^+$ even though the states are only singly excited.

57. E. E. Ferguson, F. C. Fehsenfeld, and A. L. Schmeltekopf, Phys. Rev., 138, A381 (1965).

58. R. A. Gerber, G. F. Sauter, and H. J. Oskam, Physica, 32, 2173 (1966).

59. C. B. Collins and W. W. Robertson, J. Chem. Phys., 40, 2208 (1964).

60. A. Wayne Johnson and J. B. Gerardo, Phys. Rev. Lett., 28, 1096 (1972).

61. J. Stevefelt and F. Robben, Phys. Rev. A, 5, 1502 (1972).

62. W. W. Robertson, J. Chem. Phys., 42, 2064 (1965).

63. C. B. Collins and W. B. Hurt, Phys. Rev., 179, 203 (1969).

64. J. A. Hornbeck, Phys. Rev., 84, 615 (1951). Here it is reported that He_2^+ ions were formed within one microsecond after the passage of a pulse of electrons through He gas. In addition the molecular ion concentration varied linearly with the electron beam current.

65. H. F. Wellenstein and W. W. Robertson, J. Chem. Phys., 56, 1077 (1972).

66. J. A. Hornbeck and J. P. Molnar, Phys. Rev., 84, 621 (1951). Associative ionization in He_2 is known as the Hornbeck-Molnar process.

67. M. S. B. Munson, J. L. Franklin, and F. H. Field, J. Phys. Chem., 67, 1541 (1963).

68. R. K. Curran, J. Chem. Phys., 38, 2974 (1963).

69. S. Trajmar, J. K. Rice, and A. Kuppermann, Advan. Chem. Phys., 18, 15 (1970).

70. R. M. St. John, F. J. Miller, and C. C. Lin, Phys. Rev., 134, A888 (1964).

Table I. Contractions for the Primitive s Gaussian Basis Functions

Type	Exponents[a]	Contraction Coefficients[b]					
		1s	1s′	$\overline{1s}$	2s	3s	s″
1s	3293.694	0.00012887	0.00005759	0.00011387	-0.00001730	0.00000511	-
1s	488.8941	0.00103003	0.00044813	0.00090289	-0.00013719	0.00003793	-
1s	108.7723	0.00553555	0.00245992	0.00489181	-0.00074142	0.00022531	-
1s	30.17990	0.02390381	0.00955277	0.02057741	-0.00308267	0.00082306	-
1s	9.789053	0.08349549	0.02790154	0.06987433	-0.00996341	0.00317718	-
1s	3.522261	0.2573553	0.03552042	0.1932941	-0.02411251	0.00580818	-
1s	1.352436	0.4211109	0.1254567	0.3812743	-0.04772558	0.01826489	-
1s	0.552610	0.2486744	0.4345431	0.3746710	-0.1154706	0.02091972	-
1s	0.240920	0.1003354	0.3901162	0.09825736	-0.2053583	0.1066267	-
1s	0.107951	0.02090514	0.09275031	0.00208112	-0.1110785	-0.06168577	-
1s	0.048370	0.00060967	-0.00144919	-0.00058942	0.4942509	-0.00537152	-
1s	0.021674	0.00022920	0.00121299	0.00004699	0.6987543	-1.0019850	-
1s	0.009712	- - - -	- - - -	- - - -	- - - -	- - - -	1.0

[a]The first ten exponents are taken from Ref. 12. See the text, Section B. 3. for the others.

[b]See text, Section B. 3.

Table II. Contractions for the Primitive p and d Gaussian Basis Functions

Type	Exponents[a]	Contraction Coefficients[b]		
		$2p_z$	$2p'_z$	$3d_{z^2}$
$2p_z$	1.553506	0.0055170	- -	- - - -
$2p_z$	0.368859	0.0444838	- -	- - - -
$2p_z$	0.119213	0.2346465	- -	- - - -
$2p_z$	0.044914	0.5242484	- -	- - - -
$2p_z$	0.018133	0.3378460	- -	- - - -
$2p_z$	0.0073207	- - - -	1.0	- - - -
$3d_{z^2}$	0.185990	- - - -	- -	0.0307214
$3d_{z^2}$	0.050033	- - - -	- -	0.1468541
$3d_{z^2}$	0.017912	- - - -	- -	0.6334969
$3d_{z^2}$	0.0072191	- - - -	- -	0.3418591

[a]The first five p exponents and the d exponents are scaled from Ref. 12. See section B. 3. of the text for a discussion.

[b]See text, section B. 3.

Table III. $\langle z^2 \rangle^{\frac{1}{2}}$ for the He Atom Orbitals

Orbital	$\langle z^2 \rangle^{\frac{1}{2}}$
2s	3.30
2s[b]	3.30
2s[c]	3.17
$2p_z$	4.35
3s	7.70
$3p_z$	10.70
$3d_{z^2}$	7.43
1s[d]	0.46
1s'[d]	0.80

[a]Except as indicated all orbitals are taken from (1s, nℓ) singlet He atom calculations in the ⟨621⟩ basis. Distances are in Bohr.

[b]This orbital is from C $^1\Sigma_g^+$ at R = ∞.

[c]This orbital is from A $^1\Sigma_u^+$ at R = ∞.

[d]These are the two split orbitals from 1 ^{1}S He.

Table IV. Occupation Numbers for the Three Electron Core[a]

R	$S_{\ell r}$	C_1^2	C_2^2
		v = 2s, $^1\Sigma_g^+$ (FO)	
1.8	0.916	0.958	0.042
2.2	0.888	0.944	0.056
3.0	0.831	0.916	0.085
4.2	0.748	0.874	0.126
5.4	0.662	0.831	0.169
5.8	0.632	0.816	0.184
6.2	0.602 0.602[b]	0.801, 0.801[b]	0.199, 0.199[b]
10.0	0.309, 0.309[b]	0.655, 0.655[b]	0.346, 0.346[b]
		v = 2s, $^1\Sigma_u^+$ (FO)	
1.8	0.957	0.979	0.022
2.2	0.937	0.967	0.032
3.0	0.889	0.945	0.056
4.2	0.798	0.899	0.101
5.0	0.729	0.865	0.136
5.4	0.692	0.846	0.154
5.8	0.655	0.828	0.173
6.2	0.618, 0.602[b]	0.809, 0.801[b]	0.191, 0.199[b]
10.0	0.295, 0.309[b]	0.648, 0.655[b]	0.353, 0.346
		v = 2s, $C^1\Sigma_g^+$ SCF	
1.8	-0.968	0.016	0.984
2.6	-0.919	0.041	0.960
3.4	-0.567	0.217	0.784
4.2	0.015	0.507	0.493
6.2	0.328	0.664	0.336

Table IV. (Continued)

R	$S_{\ell r}$	C_1^2	C_2^2
		v = 2s, $A^1\Sigma_u^+$ SCF	
1.8	0.992	0.996	0.004
2.6	0.963	0.982	0.019
3.8	0.748	0.874	0.126
4.6	0.518	0.759	0.241
5.8	0.382	0.691	0.309
6.2	0.369	0.685	0.316
8.0	0.340	0.670	0.330
		v = 2p, $^1\Sigma_{g,u}^+$ (FO)	
1.8	-0.794	0.103	0.897
2.2	-0.704	0.148	0.852
3.0	-0.506	0.247	0.753
4.2	-0.204	0.398	0.602
5.0	-0.030	0.485	0.515
5.8	0.111	0.556	0.446
6.2	0.168	0.584	0.416
10.0	0.327	0.664	0.337
		v = 3s, $^1\Sigma_g^+$ (FO)	
3.0	0.848	0.924	0.076
4.2	0.743	0.872	0.129
5.8	0.594	0.797	0.203
8.0	0.413	0.707	0.294

Table IV. (Continued)

R	$S_{\ell r}$	C_1^2	C_2^2
		v = 3s, $^1\Sigma_u^+$ (FO)	
3.0	0.856	0.928	0.072
4.2	0.741	0.871	0.130
5.8	0.574	0.787	0.213
8.0	0.378	0.689	0.311
		v = 3p, $^1\Sigma_{g,u}^+$ (FO)	
1.8	-0.916	0.042	0.958
2.2	-0.880	0.060	0.940
3.0	-0.796	0.102	0.898
4.2	-0.661	0.170	0.831
5.0	-0.576	0.212	0.788
5.8	-0.497	0.252	0.749
8.0	-0.322	0.339	0.661
15.0	0.129	0.565	0.436
		v = 3d, $^1\Sigma_g^+$ (FO)	
3.0	0.790	0.895	0.105
5.0	0.522	0.761	0.239
5.8	0.414	0.707	0.293
8.0	0.172	0.586	0.414
		v = 3d, $^1\Sigma_u^+$ (FO)	
3.0	0.795	0.898	0.103
5.0	0.528	0.764	0.236
5.8	0.421	0.710	0.290
8.0	0.177	0.589	0.412

Table IV. (Continued)

[a] See Eqs. (12) and (13) of the text for the definition of C_1 and C_2. $S_{\ell r}$ is the overlap of excited orbitals on opposite centers. All FO calculations reported here use orbitals from spatially projected wavefunctions at R = ∞ except as noted. See Ref. 14. Distances are in Bohr.

[b] These are calculated from orbitals obtained from spatially unprojected G1 FO wavefunctions (i.e., for the separated atoms) and are included for comparison.

Table V. Partition of the Energy for Frozen Orbital Unprojected G1, v = 2s [a, b]

R	15.0	10.0	8.0	6.2
T	5.021407	5.022747	5.027635	5.041550
$2_{e\ell}$	1.504650	1.636955	1.732064	1.857046
$2^{c\ell}_{e\ell}$	1.450799	1.583456	1.680013	1.809815
V	-11.814170	-12.080827	-12.279554	-12.559629
$V^{c\ell}$	-11.809264	-12.075345	-12.272277	-12.548486
Z^2/R	0.266667	0.400000	0.500000	0.645161
E	- 5.021446	- 5.021126	- 5.019855	- 5.015872
$E^{c\ell}$	- 4.834852	- 4.834944	- 4.835319	- 4.836564
T^X	- 0.235538	- 0.234199	- 0.229310	- 0.215395
$2e\ell^X$	0.053851	0.053499	0.052051	0.047231
V^X	- 0.004906	- 0.005483	- 0.007277	- 0.011143
ΔE	0.000004	0.000324	0.001595	0.005578
ΔT^X	0.000018	0.001357	0.006246	0.0201610
ΔV^X	- 0.000008	- 0.000585	- 0.002379	- 0.006245
$\Delta 2e\ell^X$	- 0.000004	- 0.000356	- 0.001804	- 0.006624
ΔE^X	0.000006	0.000416	0.002063	0.007292
$\Delta V^{c\ell}$	- 0.533327	- 0.799408	- 0.996340	- 1.272549
$\Delta 2^{c\ell}_{e\ell}$	0.266659	0.399316	0.495874	0.625676
$\Delta E^{c\ell}$	- 0.000000	- 0.000092	- 0.000467	- 0.001712

Table V. (Continued)

---

[a] The energies here are for a spatially unprojected wavefunction the orbitals of which were obtained from unprojected G1 calculations on the separated atoms. Distances are in Bohr.

[b] The symbols in the first column are defined as follows: T = total kinetic energy; $2_{e\ell}$ = total two electron repulsion energy; $2_{e\ell}^{c\ell}$ = the classical or coulomb two electron energy, i.e., $2_{e\ell}^{c\ell} = \sum_{i>j}^{N} \langle ij|\frac{1}{r_{ij}}|ij\rangle$; V = total electron nuclear attraction energy; $V^{c\ell} = \sum_{i=1}^{N} \langle i|\frac{1}{r_{iA}} + \frac{1}{r_{iB}}|i\rangle$ where A and B are He nuclei; Z^2/R = nuclear repulsion energy; E = total energy with the bare nuclei and the electrons at infinity as the energy zero; $E^{c\ell} = T^{c\ell} + V^{c\ell} + 2_{e\ell}^{c\ell}$ where $T^{c\ell} = \frac{-\hbar^2}{2m} \sum_i \langle i|\nabla^2|i\rangle$; $T^X = T - T^{c\ell}$; $2_{e\ell}^X = 2_{e\ell} - 2_{e\ell}^{c\ell}$; $V^X = V - V^{c\ell}$; $\Delta E = E(R) - E(\infty)$; $\Delta T^X = T^X(R) - T^X(\infty)$ and similarly for other Δ quantities.

Table VI. Partition of the Energy for Frozen Orbital

Unprojected G1, v = 2p [a]

R	15.0	10.0	6.2	4.2
T	5.000369	5.004193	5.046743	5.111709
$2_{e\ell}$	1.506198	1.653447	1.901630	2.119894
$2_{e\ell}^{c\ell}$	1.466923	1.615267	1.878281	2.131487
V	-11.773645	-12.057064	-12.580052	-13.146016
$V^{c\ell}$	-11.823159	-12.105121	-12.617356	-13.186527
Z^2/R	0.266667	0.400000	0.645161	0.952381
E	- 5.000411	- 4.999424	- 4.986517	- 4.962032
$E^{c\ell}$	- 4.809960	- 4.810244	- 4.814304	- 4.823049
T^X	- 0.279240	- 0.275417	- 0.232867	- 0.167901
$2_{e\ell}^X$	0.039275	0.038180	0.023349	- 0.011593
V^X	0.049514	0.048053	0.037304	0.040511
ΔE	0.000018	0.001005	0.013912	0.038397
ΔT^X	0.000078	0.003902	0.046452	0.111418
ΔV^X	- 0.000035	- 0.001496	- 0.012245	- 0.009038
$\Delta 2_{e\ell}^X$	- 0.000021	- 0.001116	- 0.015947	- 0.050889
ΔE^X	0.000022	0.001290	0.018260	0.051491
$\Delta V^{c\ell}$	- 0.540795	- 0.822758	- 1.334993	- 1.904164
$\Delta 2_{e\ell}^{c\ell}$	0.274125	0.422469	0.685483	0.938689
$\Delta E^{c\ell}$	- 0.000005	- 0.000289	- 0.004349	- 0.013094

[a] See the Footnotes to Table V for a description of the wavefunction and the definition of the symbols in the first column.

Table VII. Partition of the Energy for SCF Wavefunctions at R = 6.2 Bohr[a]

	$C\ ^1\Sigma_g^+$ (2s)	$A\ ^1\Sigma_u^+$ (2s)	$^1\Sigma_g^+$ (2p)	$^1\Sigma_u^+$ (2p)
T	5.028	5.022	5.036	5.026
$2e\ell$	1.812	1.812	1.904	1.906
$2_{e\ell}^{c\ell}$	1.757	1.794	1.867	1.874
V	-12.504	-12.500	-12.574	-12.570
$V^{c\ell}$	-12.492	-12.587	-12.617	-12.616
Z^2/R	0.64516	0.64516	0.64516	0.64516
E	- 5.01852	- 5.02009	- 4.98882	- 4.99245
$E^{c\ell}$	- 4.833	- 4.866	- 4.808	- 4.811
E^X	- 0.185	- 0.154	- 0.181	- 0.181
T^X	- 0.228	- 0.260	- 0.260	- 0.260
$2e\ell^X$	0.055	0.019	0.036	0.032
V^X	- 0.012	0.087	0.043	0.047
ΔE	0.00293	0.00213	0.01161	0.00798
ΔT^X	0.006	0.003	0.019	0.019
ΔV^X	- 0.006	0.003	- 0.007	- 0.003
$\Delta 2e\ell^X$	0.001	- 0.005	- 0.003	- 0.007
ΔE^X	0.001	0.001	0.009	0.009
$\Delta V^{c\ell}$	- 1.217	- 1.221	- 1.335	- 1.334
$\Delta 2_{e\ell}^{c\ell}$	0.573	0.579	0.675	0.682
$\Delta T^{c\ell}$	0.000	- 0.002	0.017	0.007
$\Delta E^{c\ell}$	0.001	0.001	0.002	- 0.001

Table VII. (Continued)

[a] See Table V for the definition of the symbols in the first column.

Table VIII. Partition of the Energy for Frozen Orbital Unprojected G1, v = 3s [a]

R	15.0	10.0	8.0
T	4.954142	4.960435	4.957603
$2e\ell$	1.382684	1.487751	1.547244
$2_{e\ell}^{c\ell}$	1.341866	1.450293	1.508422
V	-11.540085	-11.782833	-11.940350
$V^{c\ell}$	-11.571892	-11.814274	-11.972178
Z^2/R	0.266667	0.400000	0.500000
E	- 4.936593	- 4.934647	- 4.935503
$E^{c\ell}$	- 4.746278	- 4.746900	- 4.746675
T^x	- 0.262940	- 0.256646	- 0.259478
$2_{e\ell}^{x}$	0.040818	0.037458	0.038822
V^x	0.031807	0.031441	0.031828
ΔE	0.000702	0.002648	0.001792
ΔT^x	0.002473	0.008767	0.005935
ΔV^x	- 0.000432	- 0.000798	- 0.000411
$\Delta 2_{e\ell}^{x}$	- 0.001138	- 0.004498	- 0.003134
ΔE^x	0.000903	0.003471	0.002390
$\Delta V^{c\ell}$	- 0.540596	- 0.782978	- 0.940882
$\Delta 2_{e\ell}^{c\ell}$	0.273727	0.382154	0.440283
$\Delta E^{c\ell}$	- 0.000202	- 0.000824	- 0.000599

[a] See the Footnotes to Table V for a description of the wavefunction and the definition of the symbols in the first column.

Table IX. Partition of the Energy for Frozen Orbital Unprojected G1, v = 3p[a]

R	15.0	10.0	8.0
T	4.932155	4.935350	4.930198
$2e\ell$	1.379819	1.471830	1.523920
$2^{c\ell}_{e\ell}$	1.345633	1.439640	1.489090
V	-11.509266	-11.736699	-11.885324
$V^{c\ell}$	-11.558024	-11.785720	-11.934717
Z^2/R	0.266667	0.400000	0.500000
E	- 4.930624	- 4.929519	- 4.931206
$E^{c\ell}$	- 4.740152	- 4.750508	- 4.740055
T^x	- 0.273417	- 0.270222	- 0.275374
$2^x_{e\ell}$	0.034186	0.032190	0.034830
V^x	0.048758	0.049021	0.049393
ΔE	0.001740	0.002845	0.001158
ΔT^x	0.005902	0.009097	0.003945
ΔV^x	- 0.000790	- 0.000527	- 0.000155
$\Delta 2^x_{e\ell}$	- 0.002865	- 0.004861	- 0.002221
ΔE^x	0.002247	0.003709	0.001569
$\Delta V^{c\ell}$	- 0.558850	- 0.786546	- 0.935543
$\Delta 2^{c\ell}_{e\ell}$	0.291676	0.385683	0.435133
$\Delta E^{c\ell}$	- 0.000507	- 0.000863	- 0.000410

[a] See the Footnotes to Table V for a description of the wavefunction and the definition of the symbols in the first column.

Table X. Partition of the Energy for Frozen Orbital Unprojected G1, v = 3d[a]

R	15.0	10.0	8.0
T	4.940030	4.955376	4.964625
$2e\ell$	1.382658	1.505878	1.573875
$2^{c\ell}_{e\ell}$	1.347907	1.479320	1.553663
V	-11.521261	-11.788301	-11.962221
$V^{c\ell}$	-11.569669	-11.835947	-12.011455
Z^2/R	0.266667	0.400000	0.500000
E	- 4.931907	- 4.927048	- 4.923720
$E^{c\ell}$	- 4.739750	- 4.741282	- 4.742447
T^x	- 0.275315	- 0.259969	- 0.250720
$2^x_{e\ell}$	0.034751	0.026558	0.020212
V^x	0.048408	0.047646	0.049234
ΔE	0.001038	0.005897	0.009225
ΔT^x	0.003541	0.018887	0.028136
ΔV^x	- 0.000559	- 0.001321	0.000267
$\Delta 2^x_{e\ell}$	- 0.001648	- 0.009841	- 0.016187
ΔE^x	0.001334	0.007725	0.012216
$\Delta V^{c\ell}$	- 0.549613	- 0.815891	- 0.991399
$\Delta 2^{c\ell}_{e\ell}$	0.282652	0.414065	0.488408
$\Delta E^{c\ell}$	- 0.000294	- 0.001826	- 0.002991

[a] See the Footnotes to Table V for a description of the wavefunction and the definition of the symbols in the first column.

Table XI. Components of T^x for Unprojected Frozen Orbital G1[a]

		$v = 2s^b$		
R	15.0	10.0	8.0	6.2
T^x_{cv}	0.000010	0.000855	0.004049	0.013573
S_{cv}	0.002198	0.020493	0.045312	0.084598
$S_{cv}\bar{S}_{c,c'v}$	0.000007	0.000630	0.003033	0.010348
τ_{cv}	2.709957	2.629184	2.443208	2.503472
$T^x_{c'v}$	0.000008	0.000606	0.002682	0.008163
$S_{c'v}$	0.004558	0.041021	0.088552	0.160053
$S_{c'v}\bar{S}_{c,c',v}$	0.000015	0.001262	0.005927	0.019579
$\tau_{c'v}$	0.975567	0.892362	0.837961	0.764840
$T^x_{c\bar{c}}$	0.000000	0.000000	-0.000001	-0.000015
$T^x_{c'\bar{c}}$	0.000000	0.000000	-0.000002	-0.000041
$\Delta T^x_{cc'}$	-0.000002	-0.000148	-0.000696	-0.002176
$\Delta T^x_{\bar{c}v}$	0.000001	0.000044	0.000213	0.000803
N	1.784186	1.782418	1.775736	1.755968
		$v = 2p^c$		
T^x_{cv}	0.000049	0.002589	0.033302	0.086152
S_{cv}	0.004851	0.035921	0.132371	0.217483
$S_{cv}\bar{S}_{c,c'v}$	0.000036	0.001916	0.025014	0.064857
τ_{cv}	2.664913	2.596537	2.463818	2.310401

Table XI. (Continued)

$v = 2p^c$				
R	15.0	10.0	6.2	4.2
$T^x_{c'v}$	0.000037	0.001758	0.018831	0.038821
$S_{c'v}$	0.009875	0.070731	0.245563	0.378950
$S_{c'v}\bar{S}_{c,c'v}$	0.000073	0.003772	0.046403	0.113009
$\tau_{c'v}$	0.930979	0.858882	0.722570	0.576653
$T^x_{c\bar{c}}$	0.000000	0.000000	0.000001	0.000373
$T^x_{c'\bar{c}}$	0.000000	0.000000	0.000004	0.000884
$\Delta T^x_{cc'}$	-0.000008	-0.000445	-0.005685	-0.014811
N	1.772436	1.767160	1.705058	1.604150

$v = 3s^d$			
R	15.0	10.0	8.0
T^x_{cv}	0.001696	0.006281	0.004307
S_{cv}	0.029874	0.058887	0.049224
$S_{cv}\bar{S}_{c,c'v}$	0.001308	0.004972	0.003452
τ_{cv}	2.497045	2.416875	2.391510
$T^x_{c'v}$	0.001046	0.003480	0.002311
$S_{c'v}$	0.057702	0.109983	0.091035
$S_{c'v}\bar{S}_{cc'v}$	0.002527	0.009286	0.006384
$\tau_{c'v}$	0.765410	0.689490	0.667765

Table XI. (Continued)

$v = 3s^d$			
R	15.0	10.0	8.0
$T^x_{c\bar{c}}$	0.000000	0.000000	0.000012
$T^x_{c'\bar{c}}$	0.000000	0.000000	0.000002
$\Delta T^x_{cc'}$	-0.000297	-0.001100	-0.000755
$\Delta T^x_{\bar{c}v}$	0.000028	0.000104	0.000069
N	1.772217	1.762368	1.766547
$v = 3p^e$			
R	15.0	10.0	8.0
T^x_{cv}	0.004177	0.006620	0.002886
S_{cv}	0.047287	0.060440	0.040209
$S_{cv}\bar{S}_{c,c'v}$	0.003258	0.005251	0.002316
τ_{cv}	2.456502	2.407016	2.388466
$T^x_{c'v}$	0.002463	0.003646	0.001570
$S_{c'v}$	0.090493	0.113307	0.075007
$S_{c'v}\bar{S}_{c,c'v}$	0.006234	0.009843	0.004321
$\tau_{c'v}$	0.726882	0.680016	0.670073
$T^x_{c\bar{c}}$	0.000000	0.000000	0.000000
$T^x_{c'\bar{c}}$	0.000000	0.000000	0.000000
$\Delta T^x_{cc'}$	-0.000737	-0.001169	-0.000511
$\Delta T^x_{\bar{c}v}$	0.000000	0.000000	0.000000
N	1.763566	1.758275	1.766267

Table XI. (Continued)

	$v = 3d^f$		
R	15.0	10.0	8.0
T^X_{cv}	0.002470	0.013810	0.021202
S_{cv}	0.036108	0.087138	0.109348
$S_{cv}\bar{S}_{c,c'v}$	0.001909	0.010864	0.016873
τ_{cv}	2.485413	2.405432	2.355089
$T^X_{c'v}$	0.001504	0.007492	0.010642
$S_{c'v}$	0.069608	0.162214	0.199255
$S_{c'v}\bar{S}_{c,c'v}$	0.003679	0.020224	0.030745
$\tau_{c'v}$	0.753466	0.674323	0.624786
$T^X_{c\bar{c}}$	0.000000	0.000000	0.000000
$T^X_{c'\bar{c}}$	0.000000	0.000000	-0.000001
$\Delta T^X_{cc'}$	-0.000434	-0.002423	-0.003719
$\Delta T^X_{\bar{c}v}$	0.000001	0.000007	0.000013
N	1.767371	1.743278	1.727675

[a]Here we take $\Delta T^X = T^X(R) - T^X(\infty)$. We denote c and c′ as core orbitals on the left He and $\bar{c}$, v are the core and Rydberg orbitals on the right He. Also, $T^X_{c\bar{c}}(\infty) = T^X_{c'\bar{c}}(\infty) = T^X_{cv}(\infty) = T^X_{c'v}(\infty) = 0.0$ for all v. $T^X_{i,j} = \Delta T^X_{i,j}$ for these cases. τ_{ij} is discussed in the text and is given by $\tau_{ij} = t_{ii} + t_{jj} - 2t_{ij}/S_{ij}$. S_{ij} is the overlap between orbitals i and j. $\bar{S}_{i,j,k} = \frac{1}{2}(S_{ik} + S_{jk})$. N is the normalization constant for the total wavefunction. See Footnote a of Table V for a description of the wavefunction. Distances are in Bohr.

Table XI. (Continued)

[b] For v = 2s, $T^{X}_{cc'}(\infty) = -0.279466$, $T^{X}_{\bar{c}v}(\infty) = 0.043763$.

[c] For v = 2p, $T^{X}_{cc'}(\infty) = -0.279319$. This differs from that for v = 2s because of the term $S^{2}_{\bar{c}v}S_{cc'}$ in D^{2}_{1}. $T^{X}_{\bar{c}v}(\infty) = T^{X}_{\bar{c}v}(R) = 0.0$.

[d] For v = 3s, $T^{X}_{cc'}(\infty) = -0.279319$, $T^{X}_{\bar{c}v}(\infty) = 0.013906$.

[e] For v = 3p, $T^{X}_{cc'}(\infty) = -0.279319$, $T^{X}_{\bar{c}v}(\infty) = T^{X}_{\bar{c}v}(R) = 0.0$.

[f] For v = 3d, $T^{X}_{cc'}(\infty) = -0.279319$, $T^{X}_{\bar{c}v}(\infty) = 0.000463$.

Table XII. Total Energies for FO[a] $^1\Sigma_g^+$ and $^1\Sigma_u^+$

	v = 2s		v = 2p		v = 3s		v = 3p		v = 3d	
R	$^1\Sigma_g^+$	$^1\Sigma_u^+$	$^1\Sigma_g^+$	$^1\Sigma_u^+$	$^1\Sigma_g^+$	$^1\Sigma_u^+$	$^1\Sigma_g^+$	$^1\Sigma_u^+$	$^1\Sigma_g^+$	$^1\Sigma_u^+$
1.8	-4.64002	-5.04641	-5.01180	-4.57192	- - - -	-4.95437	-4.94669	-4.50875	- - - -	-4.94501
2.0	- - - -	-5.06891	-5.02546	-4.68835	- - - -	-4.98083	-4.97178	-4.63178	- - - -	-4.97231
2.2	-4.82260	-5.07429	-5.02305	-4.76792	- - - -	-4.98981	-4.97964	-4.71654	- - - -	-4.98183
2.6	-4.90866	-5.06324	-5.00143	-4.86121	- - - -	- - - -	-4.97336	-4.81710	- - - -	-4.97708
3.0	-4.95163	-5.04561	-4.98014	-4.90817	-4.87673	-4.97147	-4.95993	-4.86821	-4.87341	-4.96310
4.2	-4.99706	-5.01695	-4.96354	-4.96049	-4.92614	-4.94602	-4.93715	-4.92016	- - - -	-4.93313
4.6	-5.00308	-5.01487	-4.96712	-4.96858	- - - -	- - - -	- - - -	- - - -	- - - -	- - - -
5.0	-5.00747	-5.01454	-4.97183	-4.97500	- - - -	- - - -	-4.93391	-4.92894	-4.92014	-4.92574
5.4	-5.01079	-5.01514	- - - -	- - - -	- - - -	- - - -	- - - -	- - - -	- - - -	- - - -
5.8	-5.01333	-5.01613	-4.98115	-4.98451	-4.93634	-4.93883	-4.93313	-4.93193	-4.92132	-4.92299
6.2	-5.01530	-5.01722	-4.98503	-4.98800	- - - -	- - - -	- - - -	- - - -	- - - -	- - - -
8.0	-5.01982	-5.02067	-4.99541	-4.99686	-4.93545	-4.93586	-4.93110	-4.93131	-4.92369	-4.92369
10.0	-5.02113	-5.02189	-4.99906	-4.99979	-4.93465	-4.93496	-4.92959	-4.92944	-4.92704	- - - -
12.0	-5.02139	- - - -	-5.00000	-5.00042	-4.93527	-4.93558	-4.92933	-4.92942	-4.92978	-4.92975
15.0	- - - -	- - - -	-5.00030	-5.00052	-4.93659	-4.93687	-4.93060	-4.93065	-4.93191	-4.93190
∞	-5.02145	-5.02221	-5.00043	-5.00043	-4.93730	-4.93754	-4.93236	-4.93236	-4.93295	-4.93295

[a]The FO orbitals used here are from $^1\Sigma_g^+$ and $^1\Sigma_u^+$ SCF calculations at R = ∞. See Ref. 14. The energies are shown in Fig. 4. All energies are rounded off and are good to ± 0.00001. All distances are in Bohr and energies in Hartrees.

Table XIII. Total Energies[a] for FO $^2\Sigma_g^+$, $^2\Sigma_u^+$, and SCF $^2\Sigma_u^+$

R	$^2\Sigma_g^+$ (FO)	$^2\Sigma_u^+$ (FO)	$^2\Sigma_u^+$ (SCF)[b]
1.8	-4.431235	-4.898593	-4.93550
2.0	-4.559086	-4.927130	- - - -
2.2	-4.647732	-4.937633	-4.95025
2.6	-4.753864	-4.934149	-4.93965
3.0	-4.808379	-4.920709	-4.92410
3.4	- - - -	- - - -	-4.91018
4.2	-4.863754	-4.890612	-4.89203
5.0	-4.872781	-4.882937	- - - -
5.8	-4.876064	-4.879854	-4.88022
8.0	-4.877855	-4.878096	- - - -
10.0	-4.877966	-4.877985	- - - -
15.0	-4.877976	-4.877976	- - - -
∞	-4.877976	-4.877976	- - - -

[a]The energies in the first two columns were calculated from a (13s/13s) primitive basis shown in Table I. These are essentially identical to those obtained from the ⟨621/621⟩ basis. Distances are in Bohr.

[b]These energies were obtained by projecting the three core orbitals from $^1\Sigma_g^+$ (2s) SCF calculations. The minimum in the spline fitted curve comes at R_{min} = 2.18 Bohr with E_{min} = -4.950269 a.u.

Table XIV. Total Energies[a] for SCF $^1\Sigma_g^+$ States

R[b]	v = 2s	v = 2p	v = 3s	v = 3d	v = 3p
1.8	-5.02827	-4.97948	-4.94454	-4.94447	-4.85416[c]
2.0	-5.04221	-4.99262[c]	-4.95864[c]	-4.95758[c]	-4.86931[c]
2.2	-5.04506	-4.99479[c]	-4.96172[c]	-4.95974	-4.87278[c]
2.6	-5.03646	-4.98474	-4.95348	-4.94999	-4.88475[d]
3.0	-5.02422	-4.97050	-4.94180	-4.93983[d]	-4.92453[d]
3.4	-5.01616	-4.96310	-4.94945	-4.93113	-4.91988
3.8	-5.01357	-4.96637[c]	-4.94473[c]	-4.92761[c]	-4.91622[c]
4.2	-5.01394	-4.96944[c]	-4.94047	-4.93002[d]	-4.91747[d]
4.6	-5.01506	-4.97299	-4.93786[c]	-4.93293[c]	-4.91844
5.0	-5.01615	-4.97721	-4.93626[c]	-4.93486[c]	-4.92042[c]
5.4	-5.01708	-4.98157	-4.93638	-4.93490	-4.92263
5.8	-5.01786	-4.98525[c]	-4.93690[c]	-4.93391[c]	-4.92421[c]
6.2	-5.01852	-4.98882	-4.93730	-4.93338	-4.92535
8.0	-5.02047	-4.99673[c]	-4.93738	-4.93252[d]	-4.92645[d]
10.0	-5.02123	-4.99943	-4.93720	-4.93259	-4.92703
12.0	- - - -	-5.00003[d]	-4.93716	-4.93269[d]	-4.92866[d]
15.0	-5.02144	-5.00023[c]	-4.93728	-4.93279[d]	-4.93095[d]
∞	-5.02145	-5.00043	-4.93730	-4.93295	-4.93236

[a]All energies are in Hartrees and except as noted below in c are good to -0.00001. The states are denoted by v = nℓ where nℓ refers to the R = ∞ limit of the Rydberg orbital.

[b]Distances are in Bohr.

Table XIV. (Continued)

[c]This is the appropriate virtual energy from v = 2s, C $^1\Sigma_g^+$. They should differ from the SCF energy for this state by no more than -0.00020.

[d]This is appropriate virtual energy from v = 3s, $^1\Sigma_g^+$. The error estimate is the same as in b.

Table XV. Total Energies[a] for SCF $^1\Sigma_u^+$ States

R[b]	v = 2s	v = 2p	v = 3s	v = 3d	v = 3p
1.8	-5.08158	-4.99548	-4.99144	-4.96264	-4.91418
2.0	-5.09081	- - - -	- - - -	- - - -	- - - -
2.2	-5.08975	-5.00855	-5.00668	-4.97779	-4.92454
2.6	-5.07466	-4.99894	-4.99538	-4.96821	-4.91170
3.0	-5.05647	- - - -	- - - -	- - - -	- - - -
3.4	-5.04169	-4.97906	-4.96510	-4.94413	-4.92030
3.8	-5.03167	-4.97733	-4.95507	-4.93746	-4.92559
4.2	-5.02570	-4.97870	-4.94859	-4.93307	-4.92780
4.6	-5.02246	- - - -	- - - -	- - - -	- - - -
5.0	-5.02085	- - - -	- - - -	- - - -	- - - -
5.4	-5.02017	-4.98721	-4.94076	-4.93254	-4.92704
5.8	-5.01999	- - - -	- - - -	- - - -	- - - -
6.2	-5.02008	-4.99245	-4.93909	-4.93314	-4.92645
8.0	-5.02130	-4.99833[c]	-4.93777	-4.93288	-4.92642
10.0	-5.02200	-5.00017	-4.93744	-4.93272	-4.92704
12.0	- - - -	-5.00046[c]	-4.93740	-4.93277	-4.92868[c]
15.0	-5.02220	-5.00047[c]	-4.93753	-4.93282	-4.93097[c]
∞	-5.02221	-5.00043	-4.93754	-4.93295	-4.93236

[a]All energies are in Hartrees and except as noted below in c are good to -0.00001. The states are denoted by v = nℓ where nℓ refers to the R = ∞ limit of the Rydberg orbital.

[b]Distances are in Bohr.

[c]This is the appropriate virtual energy from v = 3d, $^1\Sigma_u^+$. They should differ from the SCF energy of this state by no more than -0.00015.

Table XVI. Extrema in the SCF Potential Curves[a]

State	R_{min}[b]	E_{min}[c]	R_{max}[b]	E_{max}[d]
$A\ ^1\Sigma_u^+$ (2s)	2.07	-0.06920	5.82-5.83	0.00223
$C\ ^1\Sigma_g^+$ (2s)	2.17	-0.02368	3.90	0.00796
$^1\Sigma_u^+$ (2p)	2.17	-0.00814	3.77	0.02311
$^1\Sigma_g^+$ (2p)	2.19	+0.00564	3.52	0.03769
$^1\Sigma_u^+$ (3s)	2.19	-0.06916	11.38-11.54	0.00015
$^1\Sigma_g^+$ (3s)	2.24	-0.02460	2.97	-0.00442
	3.47	-0.01246	5.14	0.00109
	6.85-7.00	-0.00021	11.50-11.52	0.00015
$^1\Sigma_u^+$ (3d)	2.19	-0.04484	4.68-4.70	0.00119
	6.47	-0.00022	9.67-9.99	0.00023
$^1\Sigma_g^+$ (3d)	2.17	-0.02684	3.81	0.00439
	5.20	-0.00210	8.16-8.23	0.00044

[a]All energies are in Hartrees. All energies and distances are obtained from a spline fit of the points shown in Tables XIV and XV.

[b]Distances are in Bohr. Where the potential curve is flat to the accuracy reported the internuclear distances bounding the region are shown. See Figs. 5, 6, and 11 for the location of the maxima and minima.

[b] $E_{min} = E(R = R_{min}) - E(R = \infty)$.

[c] $E_{max} = E(R = R_{max}) - E(R = \infty)$.

Table XVII. Orbital Coefficients[a] for C $^1\Sigma_g^+$

	R = 1.8				R = 2.2			
	ϕ_c	$\phi_{c'}$	$\phi_{\bar{c}}$	ϕ_v	ϕ_c	$\phi_{c'}$	$\phi_{\bar{c}}$	ϕ_v
$1s_L$	1.14006	-1.23316	0.15331	-0.09283	1.11337	-0.73168	0.04208	-0.04949
$1s'_L$	-0.01716	0.60220	-0.01464	-0.24750	-0.00685	0.77670	-0.01150	-0.18555
$\overline{1s}_L$	-0.11603	1.56108	-0.15434	0.04337	-0.10916	0.91139	-0.03578	-0.00900
$2s_L$	-0.00635	-0.27445	0.17838	-0.40399	-0.01880	-0.14599	0.09500	-0.32171
$3s_L$	-0.05208	-0.20808	0.09670	1.74066	-0.05862	-0.17217	0.04931	1.39085
s''_L	-0.03726	-0.13732	0.05783	-1.75075	-0.02685	-0.08477	0.02437	-1.21955
$2p_{z_L}$	0.08740	0.10935	0.00066	0.01639	0.06545	0.12308	0.00393	0.01169
$2p'_{z_L}$	0.12967	0.20633	-0.02935	-0.00466	0.08851	0.18366	-0.01457	0.01195
$3d_{z^2L}$	0.03222	0.04487	-0.00481	0.00717	0.02808	0.05416	-0.00233	-0.01325
$1s_R$	-0.26836	-0.06901	-0.07462	0.07401	-0.14021	-0.12392	-0.07585	0.10964
$1s'_R$	-0.20084	-0.22081	-0.06478	0.23782	-0.10663	-0.18922	-0.05306	0.22781
$\overline{1s}_R$	0.43876	0.28327	1.11603	-0.10050	0.23099	0.29023	1.11133	-0.15416
$2s_R$	-0.03346	0.18217	-0.14532	0.57969	-0.07382	-0.05703	-0.06726	0.60207
$3s_R$	0.02003	0.12754	-0.06536	-1.60916	-0.02685	-0.01765	-0.02284	-1.19745
s''_R	-0.02618	0.03158	-0.03975	1.75099	-0.03163	-0.03930	-0.01284	1.21340
$2p_{z_R}$	-0.06503	-0.14765	0.04138	0.17250	-0.04196	-0.10787	0.02296	0.22696
$2p'_{z_R}$	-0.13014	-0.21500	0.03389	-0.04152	-0.08828	-0.18672	0.01668	-0.04700
$3d_{z^2R}$	0.03149	0.05910	-0.01134	-0.00380	0.02596	0.05993	-0.00746	0.02253

Table XVII. (Continued)

R = 2.6				R = 3.0			
ϕ_c	$\phi_{c'}$	$\phi_{\bar{c}}$	ϕ_v	ϕ_c	$\phi_{c'}$	$\phi_{\bar{c}}$	ϕ_v
1.06171	-0.37710	0.00780	0.00828	1.02280	-0.15630	-0.00996	0.05469
-0.00773	0.88312	-0.00585	-0.11639	-0.00762	0.94973	-0.01375	-0.05392
-0.05981	0.46769	-0.00414	-0.07888	-0.02051	0.19404	0.01403	-0.12864
-0.02560	-0.10851	0.05289	-0.22885	-0.02359	-0.07255	0.00931	-0.13136
-0.05408	-0.16941	0.02681	1.15095	-0.04301	-0.14595	0.00782	0.92703
-0.02180	-0.07279	0.01360	-0.92369	-0.01739	-0.06264	0.00357	-0.68036
0.04616	0.12213	0.00711	0.00871	0.03295	0.11440	0.00397	0.00827
0.05947	0.15850	-0.00331	0.03110	0.04156	0.13383	0.00363	0.04654
0.02266	0.05928	0.00088	-0.02065	0.01853	0.06099	0.00258	-0.01723
-0.05026	-0.06078	-0.06276	0.12145	-0.01119	-0.02235	-0.03801	0.10505
-0.05366	-0.13670	-0.04249	0.20252	-0.02911	-0.10300	-0.01903	0.16183
0.09132	0.14234	-1.09109	-0.16717	0.02382	0.05913	1.05349	-0.14235
-0.06858	-0.15784	-0.03886	0.64017	-0.05619	-0.18689	-0.00877	0.70586
-0.03411	-0.08206	-0.01328	-0.90041	-0.03189	-0.09698	-0.00697	-0.64387
-0.02608	-0.05936	-0.00953	0.90196	-0.02127	-0.06493	-0.00599	0.64239
-0.02691	-0.07737	0.01107	0.27453	-0.01732	-0.05125	-0.00160	0.33109
-0.05922	-0.15957	0.00517	-0.06409	-0.04114	-0.13317	-0.00245	-0.07797
0.02022	0.05850	-0.00398	0.04487	0.01599	0.05373	0.00012	0.05945

Table XVII. (Continued)

R = 3.4				R = 3.8			
ϕ_c	$\phi_{c'}$	$\phi_{\bar{c}}$	ϕ_v	ϕ_c	$\phi_{c'}$	$\phi_{\bar{c}}$	ϕ_v
1.00789	-0.04396	-0.02134	0.06194	0.99959	0.00485	-0.02191	0.02223
-0.00333	0.98897	-0.02393	-0.01989	0.00037	1.00923	-0.02483	-0.02686
-0.00691	0.05351	0.02810	-0.12059	0.00120	-0.00759	0.02893	-0.04922
-0.01351	-0.03478	-0.02545	-0.05476	-0.00149	-0.00488	-0.03602	-0.02775
-0.02827	-0.10665	-0.00545	0.65466	-0.01645	-0.07163	-0.00843	0.37258
-0.01174	-0.04659	-0.00693	-0.42162	-0.00612	-0.02972	-0.01182	-0.18567
0.02464	0.10165	-0.00243	0.01038	0.02113	0.08760	-0.00659	0.01307
0.02923	0.10993	0.00728	0.04516	0.02240	0.08697	0.00776	0.02748
0.01526	0.05912	0.00279	-0.00741	0.01366	0.05431	0.00224	-0.00007
0.00261	-0.01369	-0.01006	0.06808	0.00244	-0.00836	0.00573	0.02815
-0.01829	-0.08197	0.00125	0.10514	-0.01491	-0.06342	0.00928	0.04842
-0.00003	0.03248	1.01564	-0.09071	-0.00158	0.01733	0.99519	-0.03620
-0.04540	-0.17805	0.01698	0.77746	-0.03946	-0.15115	0.02510	0.81224
-0.02616	-0.08866	-0.00205	-0.41306	-0.01996	-0.06596	-0.00117	-0.24751
-0.01826	-0.06696	-0.00049	0.39028	-0.01791	-0.06463	0.00239	0.19356
-0.00955	-0.02985	-0.01339	0.38459	-0.00385	-0.01234	-0.01855	0.40130
-0.02830	-0.10664	-0.00777	-0.06707	-0.02059	-0.08091	-0.00966	-0.03037
0.01223	0.04609	0.00465	0.05258	0.00939	0.03665	0.00738	0.02371

Table XVII. (Continued)

R = 4.2				R = 5.0			
ϕ_c	$\phi_{c'}$	$\phi_{\bar{c}}$	ϕ_v	ϕ_c	$\phi_{c'}$	$\phi_{\bar{c}}$	ϕ_v
0.98988	0.02249	-0.01676	-0.03218	0.99464	0.01143	-0.00778	-0.10309
0.00094	1.01384	-0.01929	-0.05607	-0.00026	1.00653	-0.00876	-0.10664
0.01208	-0.02894	0.02205	0.03612	0.00640	-0.01481	0.00999	0.14336
0.00585	0.00367	-0.03002	-0.04296	0.00059	0.00176	-0.01313	-0.11102
-0.00841	-0.05309	-0.00500	0.16739	-0.00603	-0.03180	0.00225	-0.03392
-0.00258	-0.02162	-0.01116	-0.03721	-0.00352	-0.01740	-0.00628	0.05797
0.01870	0.07299	-0.00730	0.01242	0.01103	0.04695	-0.00525	0.00690
0.01840	0.06785	0.00655	0.01021	0.01026	0.04199	0.00394	-0.00446
0.01307	0.04800	0.00166	0.00093	0.00877	0.03628	0.00104	-0.00379
-0.00144	0.00091	0.00841	0.00443	0.00025	0.00671	0.00314	-0.00553
-0.01245	-0.04305	0.00851	0.01395	-0.00350	-0.01650	0.00295	-0.00368
0.00246	0.00300	0.99158	-0.00442	-0.00103	-0.01080	0.99749	0.00830
-0.03167	-0.11217	0.02077	0.82198	-0.00965	-0.04285	0.00825	0.85252
-0.01250	-0.03633	-0.00271	-0.15916	0.00194	0.00836	-0.00540	-0.08781
-0.01732	-0.05496	0.00221	0.08931	-0.00849	-0.03287	-0.00007	0.04190
-0.00046	-0.00270	-0.01767	0.38116	0.00042	0.00279	-0.01182	0.30299
-0.01580	-0.06095	-0.00888	0.00466	-0.00870	-0.03634	-0.00576	0.03333
0.00723	0.02917	0.00778	0.00497	0.00487	0.01981	0.00616	0.03093

Table XVII. (Continued)

R = 5.4				R = 5.8			
ϕ_c	$\phi_{c'}$	$\phi_{\bar{c}}$	ϕ_v	ϕ_c	$\phi_{c'}$	$\phi_{\bar{c}}$	ϕ_v
0.99751	0.00529	-0.00502	-0.11819	0.99882	0.00268	-0.00298	-0.12195
-0.00008	1.00264	-0.00559	-0.11953	-0.00020	1.00121	-0.00336	-0.12284
0.00300	-0.00678	0.00618	0.16463	0.00153	-0.00385	0.00358	0.17140
0.00012	-0.00092	-0.00767	-0.13236	-0.00020	-0.00188	-0.00435	-0.14541
-0.00472	-0.02390	0.00381	-0.07733	-0.00277	-0.01717	0.00417	-0.09866
-0.00323	-0.01622	-0.00445	0.06158	-0.00264	-0.01404	-0.00324	0.05617
0.00866	0.03582	-0.00414	0.00365	0.00620	0.02727	-0.00317	0.00260
0.00807	0.03199	0.00291	-0.00569	0.00586	0.02440	0.00205	-0.00460
0.00745	0.03006	0.00084	-0.00546	0.00584	0.02468	0.00066	-0.00565
0.00151	0.00784	0.00173	-0.00486	0.00140	0.00740	0.00025	-0.00336
-0.00159	-0.00642	0.00142	-0.00439	-0.00038	-0.00204	0.00047	-0.00379
-0.00176	-0.01083	0.99889	0.00723	-0.00216	-0.01261	1.00036	0.00501
-0.00514	-0.01970	0.00425	0.87079	-0.00117	-0.00575	0.00180	0.88813
0.00421	0.01990	-0.00560	-0.06988	0.00539	0.02419	-0.00518	-0.05651
-0.00650	-0.02346	-0.00065	0.04589	-0.00462	-0.01723	-0.00077	0.05215
0.00046	0.00232	-0.00920	0.25986	0.00023	0.00173	-0.00705	0.21800
-0.00678	-0.02767	-0.00441	0.03419	-0.00486	-0.02101	-0.00331	0.03110
0.00412	0.01651	0.00513	-0.03313	0.00334	0.01377	0.00416	-0.03160

Table XVII. (Continued)

R = 6.2				R = 8.0			
ϕ_c	$\phi_{c'}$	$\phi_{\bar{c}}$	ϕ_v	ϕ_c	$\phi_{c'}$	$\phi_{\bar{c}}$	ϕ_v
0.99927	0.00178	-0.00154	-0.11915	0.99963	0.00076	0.00013	0.07503
-0.00018	1.00058	-0.00192	-0.12025	0.00023	1.00013	-0.00011	0.07661
0.00102	-0.00273	0.00173	0.16799	0.00031	-0.00067	-0.00043	-0.10533
0.00001	-0.00150	-0.00228	-0.14560	0.00060	0.00216	0.00033	0.08899
-0.00163	-0.01006	0.00384	-0.10514	0.00101	0.00264	0.00118	0.06551
-0.00205	-0.01090	-0.00241	0.04810	0.00014	-0.00221	-0.00048	-0.01965
0.00487	0.01942	-0.00240	0.00189	0.00126	0.00330	-0.00054	-0.00164
0.00454	0.01754	0.00132	-0.00261	0.00090	0.00215	-0.00018	-0.00299
0.00483	0.01909	0.00046	-0.00493	0.00132	0.00377	-0.00016	0.00019
0.00147	0.00664	-0.00029	-0.00228	0.00050	0.00257	0.00045	0.00037
0.00024	0.00117	0.00011	-0.00331	0.00105	0.00350	0.00041	0.00118
-0.00207	-0.01204	1.00069	0.00346	0.00083	-0.00298	0.99912	-0.00081
0.00028	0.00278	0.00040	0.90181	0.00089	0.00426	-0.00059	-0.93067
0.00546	0.02365	-0.00441	-0.04601	0.00203	0.00691	-0.00125	0.01349
-0.00368	-0.01240	-0.00061	0.05764	-0.00126	-0.00196	0.00011	-0.06992
0.00023	0.00069	-0.00529	0.17864	-0.00016	-0.00167	-0.00118	-0.05784
-0.00365	-0.01489	-0.00240	0.02647	-0.00031	-0.00182	-0.00028	-0.01036
0.00274	0.01103	0.00324	-0.02808	0.00066	0.00290	0.00061	0.01141

Table XVII. (Continued)

R = 10.0				R = ∞			
ϕ_c	$\phi_{c'}$	$\phi_{\bar{c}}$	ϕ_v	ϕ_c	$\phi_{c'}$	$\phi_{\bar{c}}$	ϕ_v
1.00037	-0.00016	-0.00003	0.03352	1.00045	-0.00053	0.0	0.0
-0.00001	1.00018	-0.00003	0.03401	-0.00008	1.00002	0.0	0.0
-0.00023	0.00001	-0.00006	-0.04793	-0.00032	0.00050	0.0	0.0
0.00072	0.00087	0.00031	0.03770	0.00026	0.00068	0.0	0.0
0.00107	0.00056	0.00034	0.02582	0.00050	0.00001	0.0	0.0
0.00011	-0.00128	0.00008	-0.00778	0.00009	-0.00025	0.0	0.0
0.00006	0.00038	-0.00007	-0.00145	0.0	0.0	0.0	0.0
-0.00016	-0.00095	-0.00007	-0.00222	0.0	0.0	0.0	0.0
-0.00008	-0.00031	-0.00010	-0.00052	0.00000	0.00004	0.0	0.0
-0.00041	-0.00102	-0.00011	-0.00056	0.0	0.0	0.00021	-0.00085
0.00058	-0.00006	0.00034	-0.00055	0.0	0.0	0.00005	-0.00095
0.00187	-0.00088	0.99976	0.00054	0.0	0.0	0.99976	0.00087
-0.00022	0.00111	-0.00029	-0.93447	0.0	0.0	-0.00001	-0.93305
-0.00020	0.00069	-0.00039	0.00282	0.0	0.0	-0.00001	-0.00009
0.00005	0.00130	-0.00013	-0.07510	0.0	0.0	-0.00013	-0.07992
0.00044	-0.00152	-0.00021	-0.01287	0.0	0.0	0.0	0.0
0.00006	-0.00008	0.00004	-0.00477	0.0	0.0	0.0	0.0
0.00012	0.00047	0.00005	0.00441	0.0	0.0	0.00000	0.00006

Table XVII. (Continued)

[a] The coefficients given here are for the basis functions shown in Tables I and II. All distances are in Bohr.

Table XVIII. Orbital Coefficients[a] for A $^1\Sigma_u^+$

	R = 1.8				R = 2.2			
	ϕ_c	$\phi_{c'}$	$\phi_{\bar{c}}$	ϕ_v	ϕ_c	$\phi_{c'}$	$\phi_{\bar{c}}$	ϕ_v
$1s_L$	1.18142	-1.32920	0.15336	-0.13976	1.15814	-0.84418	0.04533	-0.04083
$1s'_L$	0.00548	0.56832	-0.01489	-0.17958	0.01428	0.72727	-0.00879	-0.10529
$\overline{1s}_L$	-0.16691	1.69244	-0.15801	0.11539	-0.16125	1.07867	-0.04315	0.00975
$2s_L$	-0.00027	-0.35115	0.18287	-0.61406	-0.02337	-0.23974	0.10340	-0.44877
$3s_L$	-0.05726	-0.24602	0.10265	0.07060	-0.06448	-0.20892	0.05402	0.23329
s''_L	-0.02745	-0.15087	0.05664	-0.12337	-0.01921	-0.09533	0.02363	-0.16689
$2p_{zL}$	0.08637	0.12562	-0.00047	0.04124	0.06847	0.14172	0.00488	0.04307
$2p'_{zL}$	0.12253	0.23368	-0.02963	0.19241	0.08549	0.20975	-0.01287	0.19602
$3d_{z^2L}$	0.03152	0.05468	-0.00590	0.03827	0.02855	0.06503	-0.00249	0.04650
$1s_R$	-0.25965	-0.08332	-0.05243	-0.18570	-0.14227	-0.11022	-0.05198	-0.08791
$1s'_R$	-0.21720	-0.22373	-0.05812	-0.11052	-0.12347	-0.17511	-0.04137	-0.05942
$\overline{1s}_R$	0.42855	0.26887	1.08824	0.20373	0.20951	0.21115	1.07468	0.06956
$2s_R$	-0.05856	0.16997	-0.14724	-0.50508	-0.09363	-0.06633	-0.07615	-0.47571
$3s_R$	0.02149	0.15338	-0.07253	-0.27046	-0.01921	0.02228	-0.03115	-0.21830
s''_R	-0.03345	0.02616	-0.03843	-0.04774	-0.03969	-0.05442	-0.01319	-0.04912
$2p_{zR}$	-0.05479	-0.16046	0.04033	-0.16982	-0.03399	-0.12192	0.02254	-0.21554
$2p'_{zR}$	-0.12207	-0.24192	0.03381	-0.19696	-0.08391	-0.21163	0.01470	-0.20564
$3d_{z^2R}$	0.02813	0.06261	-0.01023	0.05838	0.02319	0.06463	-0.00617	0.07818

Table XVIII. (Continued)

R = 2.6				R = 3.0			
ϕ_c	$\phi_{c'}$	$\phi_{\bar{c}}$	ϕ_v	ϕ_c	$\phi_{c'}$	$\phi_{\bar{c}}$	ϕ_v
1.12037	-0.49339	0.01952	0.03826	1.05298	-0.24453	0.00739	0.09969
0.01083	0.83737	0.00434	-0.03083	-0.00099	0.91823	0.00253	0.03590
-0.12967	0.63211	-0.02282	-0.10759	-0.05602	0.32043	-0.01264	-0.18013
-0.03872	-0.19038	0.07274	-0.28215	-0.04183	-0.14063	0.04065	-0.13476
-0.06318	-0.19777	0.03463	0.35249	-0.05067	-0.17420	0.01917	0.41316
-0.01703	-0.07750	0.01679	-0.21366	-0.01564	-0.06036	0.01119	-0.25264
0.05024	0.14347	0.00877	0.03573	0.03481	0.14302	0.00787	0.02867
0.05757	0.18201	-0.00484	0.18439	0.03890	0.15634	0.00021	0.16343
0.02358	0.07063	0.00014	0.04980	0.01860	0.07401	0.00167	0.04964
-0.05075	-0.04054	-0.05052	-0.06062	-0.02511	0.01599	-0.03430	-0.07396
-0.06152	-0.12099	-0.03876	-0.05386	-0.02946	-0.09313	-0.02226	-0.07603
0.06919	0.07298	1.06999	0.02942	0.01621	-0.02331	1.04416	0.04294
-0.07801	-0.16130	-0.05570	-0.48997	-0.04512	-0.20587	-0.03398	-0.53348
-0.02343	-0.03828	-0.02045	-0.17687	-0.01081	-0.06418	-0.01368	-0.13111
-0.03271	-0.08223	-0.01129	-0.03732	-0.02317	-0.09718	-0.01004	-0.01818
-0.02100	-0.08980	0.01589	-0.24708	-0.01431	-0.05794	0.00832	-0.26989
-0.05596	-0.18091	0.00678	-0.20211	-0.03773	-0.15183	0.00177	-0.19108
0.01803	0.06337	-0.00446	0.09494	0.01415	0.05824	-0.00232	0.10644

Table XVIII. (Continued)

R = 3.4				R = 3.8			
ϕ_c	$\phi_{c'}$	$\phi_{\bar{c}}$	ϕ_v	ϕ_c	$\phi_{c'}$	$\phi_{\bar{c}}$	ϕ_v
1.07783	-0.16270	-0.00318	0.14246	1.06298	-0.09839	-0.00884	0.16574
0.01158	0.95423	-0.00457	0.08851	0.00738	0.98375	-0.00987	0.12344
-0.09246	0.21431	0.00073	-0.22744	-0.07471	0.12377	0.00975	-0.25176
-0.04188	-0.10274	0.01265	-0.01636	-0.04087	-0.09051	-0.00656	0.07443
-0.04517	-0.13415	0.00724	0.41672	-0.03443	-0.10280	0.00001	0.37841
-0.01053	-0.04354	0.00438	-0.27323	-0.00840	-0.02985	-0.00183	-0.26715
0.02780	0.13825	0.00369	0.02214	0.02268	0.12951	-0.00076	0.01449
0.02553	0.13506	0.00234	0.13380	0.01934	0.11327	0.00331	0.10000
0.01555	0.07485	0.00178	0.04566	0.01303	0.07227	0.00138	0.03862
0.00662	0.01454	-0.01158	-0.10679	0.01067	0.01941	-0.00179	-0.14690
-0.01156	-0.07864	-0.01050	-0.11477	-0.00362	-0.05868	-0.00348	-0.16040
-0.02574	-0.03871	1.01778	0.08256	-0.02340	-0.03687	1.00680	0.13319
-0.03511	-0.19345	-0.01134	-0.59751	-0.01917	-0.15901	0.00460	-0.67426
-0.00666	-0.05146	-0.00643	-0.08305	0.00064	-0.02947	-0.00211	-0.04244
-0.02052	-0.10367	-0.00585	0.00400	-0.01669	-0.10205	-0.00161	0.02002
-0.00667	-0.03359	0.00088	-0.28673	-0.00483	-0.01540	-0.00554	-0.29848
-0.02379	-0.12666	-0.00114	-0.17160	-0.01757	-0.10132	-0.00335	-0.14558
0.01043	0.05179	-0.00005	0.10947	0.00859	0.04415	0.00230	0.10323

Table XVIII. (Continued)

R = 4.2				R = 5.0			
ϕ_c	$\phi_{c'}$	$\phi_{\bar{c}}$	ϕ_v	ϕ_c	$\phi_{c'}$	$\phi_{\bar{c}}$	ϕ_v
1.03775	-0.05727	-0.01007	0.17074	1.08018	-0.09228	-0.00676	0.15664
-0.00038	0.99787	-0.01136	0.14049	0.00899	0.98700	-0.00749	0.14434
-0.04208	0.00667	0.01239	-0.25272	-0.09296	0.10729	0.00870	-0.22503
-0.03474	-0.09377	-0.01457	0.13080	-0.03755	-0.10584	-0.01100	0.16936
-0.02148	-0.08093	-0.00176	0.31918	-0.01683	-0.04422	0.00196	0.22003
-0.00812	-0.02247	-0.00532	-0.23353	-0.00593	-0.02054	-0.00519	-0.14559
0.01977	0.11449	-0.00360	0.00945	0.01544	0.08371	-0.00446	0.00557
0.01829	0.08902	0.00376	0.07038	0.00981	0.05363	0.00325	0.03311
0.01229	0.06449	0.00107	0.03182	0.00848	0.04714	0.00080	0.02185
0.00498	0.02534	0.00315	-0.18070	0.00769	0.01947	0.00668	-0.21833
-0.00189	-0.03597	-0.00024	-0.19952	0.00209	-0.00644	-0.00124	-0.24241
-0.01084	-0.03618	1.00103	0.17597	-0.01165	-0.02810	0.99735	0.22316
-0.00988	-0.11132	0.01086	-0.74094	0.00037	-0.02827	0.00757	-0.82294
0.00463	-0.00442	-0.00156	-0.01102	0.01001	0.03714	-0.00418	0.01742
-0.01513	-0.08746	0.00044	0.01777	-0.00883	-0.05272	-0.00003	-0.01549
-0.00499	-0.00352	-0.00946	-0.29904	-0.00090	0.00495	-0.00985	-0.26418
-0.01660	-0.07581	-0.00481	-0.11796	-0.00818	-0.04250	-0.00479	-0.07273
0.00866	0.03531	0.00418	0.09069	0.00489	0.02257	0.00516	0.06389

Table XVIII. (Continued)

R = 5.4				R = 5.8			
ϕ_c	$\phi_{c'}$	$\phi_{\bar{c}}$	ϕ_v	ϕ_c	$\phi_{c'}$	$\phi_{\bar{c}}$	ϕ_v
1.08327	-0.09503	-0.00466	0.14716	1.08267	-0.09293	-0.00286	0.13703
0.00986	0.98476	-0.00508	0.14011	0.00992	0.98442	-0.00317	0.13343
-0.09666	0.11077	0.00602	-0.20961	-0.09588	0.10815	0.00366	-0.19420
-0.03699	-0.11089	-0.00733	0.16995	-0.03602	-0.11470	-0.00445	0.16415
-0.01404	-0.03361	0.00347	0.18733	-0.01137	-0.02567	0.00401	0.16112
-0.00547	-0.01928	-0.00410	-0.11076	-0.00480	-0.01695	-0.00315	-0.08400
0.01315	0.06869	-0.00385	0.00456	0.01098	0.05527	-0.00313	0.00357
0.00733	0.03935	0.00263	0.02197	0.00539	0.02861	0.00195	0.01364
0.00701	0.03808	0.00071	0.01776	0.00568	0.02991	0.00057	0.01391
0.00553	0.01863	0.00771	-0.22875	0.00316	0.01873	0.00859	-0.23620
0.00249	0.00175	-0.00209	-0.25354	0.00251	0.00694	-0.00267	-0.26114
-0.00917	-0.02800	0.99609	0.23572	-0.00634	-0.02831	0.99495	0.24452
0.00371	-0.00361	0.00447	-0.84678	0.00576	0.01108	0.00214	-0.86480
0.01141	0.04587	-0.00493	0.02019	0.01177	0.04770	-0.00494	0.01868
-0.00643	-0.03805	-0.00053	-0.03064	-0.00469	-0.02735	-0.00068	-0.04158
0.00000	0.00668	-0.00841	-0.23358	0.00057	0.00735	-0.00679	-0.19924
-0.00590	-0.02981	-0.00404	-0.05622	-0.00409	-0.01988	-0.00319	-0.04299
0.00372	0.01674	0.00472	0.05258	0.00270	0.01173	0.00404	0.04259

Table XVIII. (Continued)

R = 6.2				R = 8.0			
ϕ_c	$\phi_{c'}$	$\phi_{\bar{c}}$	ϕ_v	ϕ_c	$\phi_{c'}$	$\phi_{\bar{c}}$	ϕ_v
1.08474	-0.09341	-0.00148	0.12608	1.10095	-0.11008	0.00024	0.07138
0.01028	0.98455	-0.00182	0.12464	0.01321	0.98111	0.00003	0.07282
-0.09823	0.10817	0.00187	-0.17852	-0.11754	0.12781	-0.00031	-0.10130
-0.03595	-0.11644	-0.00251	0.15481	-0.03896	-0.11952	0.00006	0.08630
-0.00994	-0.01839	0.00380	0.13857	-0.00889	-0.00042	0.00114	0.06442
-0.00423	-0.01370	-0.00243	-0.06369	-0.00275	-0.00522	-0.00053	-0.01977
0.00922	0.04347	-0.00245	0.00242	0.00364	0.01290	-0.00056	-0.00012
0.00400	0.01960	0.00129	0.00740	0.00104	0.00438	-0.00020	-0.00211
0.00459	0.02273	0.00041	0.01033	0.00155	0.00559	-0.00018	0.00166
0.00227	0.01806	0.00900	-0.24155	0.00178	0.01150	0.00991	-0.24904
0.00264	0.01020	-0.00309	-0.26648	0.00217	0.00891	-0.00325	-0.27527
-0.00469	-0.02583	0.99440	0.25083	-0.00360	-0.01638	0.99304	0.25969
0.00649	0.01847	0.00071	-0.87958	0.00476	0.01482	-0.00037	-0.91200
0.01114	0.04461	-0.00441	0.01407	0.00588	0.01778	-0.00137	-0.01546
-0.00355	-0.01999	-0.00055	-0.04903	-0.00127	-0.00789	0.00018	-0.06464
0.00084	0.00742	-0.00526	-0.16463	0.00084	0.00448	-0.00121	-0.05273
-0.00279	-0.01211	-0.00240	-0.03252	-0.00006	0.00138	-0.00029	-0.01010
0.00192	0.00744	0.00326	0.03384	0.00005	-0.00110	0.00064	0.01102

TABLE XVIII. (Continued)

R = 10.0				R = ∞			
ϕ_c	$\phi_{c'}$	$\phi_{\bar{c}}$	ϕ_v	ϕ_c	$\phi_{c'}$	$\phi_{\bar{c}}$	ϕ_v
1.10025	-0.10877	0.00001	0.03121	1.09830	-0.10578	0.0	0.0
0.01308	0.98122	0.00003	0.03190	0.01283	0.98195	0.0	0.0
-0.11668	0.12613	-0.00003	-0.04467	-0.11435	0.12250	0.0	-0.00002
-0.03828	-0.11859	0.00020	0.03432	-0.03707	-0.11592	0.0	0.00006
-0.00782	0.00222	0.00033	0.02408	-0.00729	0.00200	0.0	0.0
-0.00277	-0.00684	0.00008	-0.00755	-0.00290	-0.00971	0.0	0.0
0.00074	0.00315	-0.00007	-0.00079	0.0	0.0	0.0	0.0
0.00045	0.00220	-0.00008	-0.00179	0.0	0.0	0.0	0.0
0.00055	0.00201	-0.00010	0.00016	0.00002	0.00001	0.0	0.0
0.00092	0.00610	0.00963	-0.24950	-0.00003	0.00003	0.00997	-0.24940
0.00080	0.00417	-0.00331	-0.27627	0.0	0.00002	-0.00332	-0.27634
-0.00208	-0.00857	0.99339	0.26056	0.00003	0.00001	0.99311	0.26064
0.00176	0.00544	-0.00007	-0.91590	0.0	-0.00001	0.00016	-0.91561
0.00187	0.00483	-0.00045	-0.02672	0.00001	-0.00001	-0.00004	-0.03056
-0.00055	-0.00398	-0.00010	-0.06967	0.0	0.0	-0.00011	-0.07404
0.00051	0.00208	-0.00021	-0.01136	0.0	0.0	0.0	0.0
0.00007	0.00132	0.00004	-0.00447	0.0	0.0	0.0	0.0
-0.00006	-0.00099	0.00004	0.00415	0.0	0.0	0.0	0.00012

TABLE XVIII. (Continued)

[a] The coefficients given here are for the basis functions shown in Tables I and II. All distances are in Bohr.

Figure 1

Tableau representing the wavefunctions for (a) the two electron singlet excited state of He, (b) the four electron unprojected ground state of He_2, (c) the unprojected excited states of He_2, (d) the g projected excited states, (e) the u projected excited states, (f) the g excited states near R_e with ϕ_v = ns, nd, etc., (g) the three electron g core of He_2, (h) the three electron u core of He_2, (j) the g excited states near R_e with $\phi_v = 2p\sigma$, (k) the u excited states near R_e with $\phi_v = 2p\sigma$.

a. $\boxed{\bar{c}\quad v}$ b. $\boxed{c\mathrm{l}\quad c'\mathrm{l}\\ c\mathrm{r}\quad c'\mathrm{r}}$ c. $\boxed{c\mathrm{l}\quad c'\mathrm{l}\\ \bar{c}\mathrm{r}\quad v\mathrm{r}}$

d. $\boxed{c\mathrm{l}\quad c'\mathrm{l}\\ \bar{c}\mathrm{r}\quad v\mathrm{r}}_{g} = \boxed{c\mathrm{l}\quad c'\mathrm{l}\\ \bar{c}\mathrm{r}\quad v\mathrm{r}} + \boxed{c\mathrm{r}\quad c'\mathrm{r}\\ \bar{c}\mathrm{l}\quad v\mathrm{l}}$

e. $\boxed{c\mathrm{l}\quad c'\mathrm{l}\\ \bar{c}\mathrm{r}\quad v\mathrm{r}}_{u} = \boxed{c\mathrm{l}\quad c'\mathrm{l}\\ \bar{c}\mathrm{r}\quad v\mathrm{r}} - \boxed{c\mathrm{r}\quad c'\mathrm{r}\\ \bar{c}\mathrm{l}\quad v\mathrm{l}}$

f. $\boxed{c\mathrm{l}\quad c'\mathrm{l}\\ \bar{c}\mathrm{r}\quad v\mathrm{r}}_{g} \approx \boxed{c\mathrm{l}\quad c'\mathrm{l}\\ \bar{c}\mathrm{r}\quad v}\ + \boxed{c\mathrm{r}\quad c'\mathrm{r}\\ \bar{c}\mathrm{l}\quad v}$

g. $\boxed{c\mathrm{l}\quad c'\mathrm{l}\\ \bar{c}\mathrm{r}}_{g} = \boxed{c\mathrm{l}\quad c'\mathrm{l}\\ \bar{c}\mathrm{r}} + \boxed{c\mathrm{r}\quad c'\mathrm{r}\\ \bar{c}\mathrm{l}}$

h. $\boxed{c\mathrm{l}\quad c'\mathrm{l}\\ \bar{c}\mathrm{r}}_{u} = \boxed{c\mathrm{l}\quad c'\mathrm{l}\\ \bar{c}\mathrm{r}} - \boxed{c\mathrm{r}\quad c'\mathrm{r}\\ \bar{c}\mathrm{l}}$

j. $\boxed{c\mathrm{l}\quad c'\mathrm{l}\\ \bar{c}\mathrm{r}\quad 2p\sigma r}_{g} = \boxed{c\mathrm{l}\quad c'\mathrm{l}\\ \bar{c}\mathrm{r}\quad 2p\sigma} - \boxed{c\mathrm{r}\quad c'\mathrm{r}\\ \bar{c}\mathrm{l}\quad 2p\sigma}$

k. $\boxed{c\mathrm{l}\quad c'\mathrm{l}\\ \bar{c}\mathrm{r}\quad 2p\sigma r}_{u} = \boxed{c\mathrm{l}\quad c'\mathrm{l}\\ \bar{c}\mathrm{r}\quad 2p\sigma} + \boxed{c\mathrm{r}\quad c'\mathrm{r}\\ \bar{c}\mathrm{l}\quad 2p\sigma}$

Figure 2

(a) Core orbitals for the He atom. ϕ_c and $\phi_{c'}$ are from He 1^1S while $\phi_{\bar{c}}$ is the core orbital from He 2^1S.

(b) 2s and 2p orbitals from atomic calculations and molecular calculation at $R = \infty$. See Ref. 14 for a discussion.

(c) Same as (b) except 3s and 3p orbitals are shown.

(d) Same as (b) except 3p and 3d orbitals are shown.

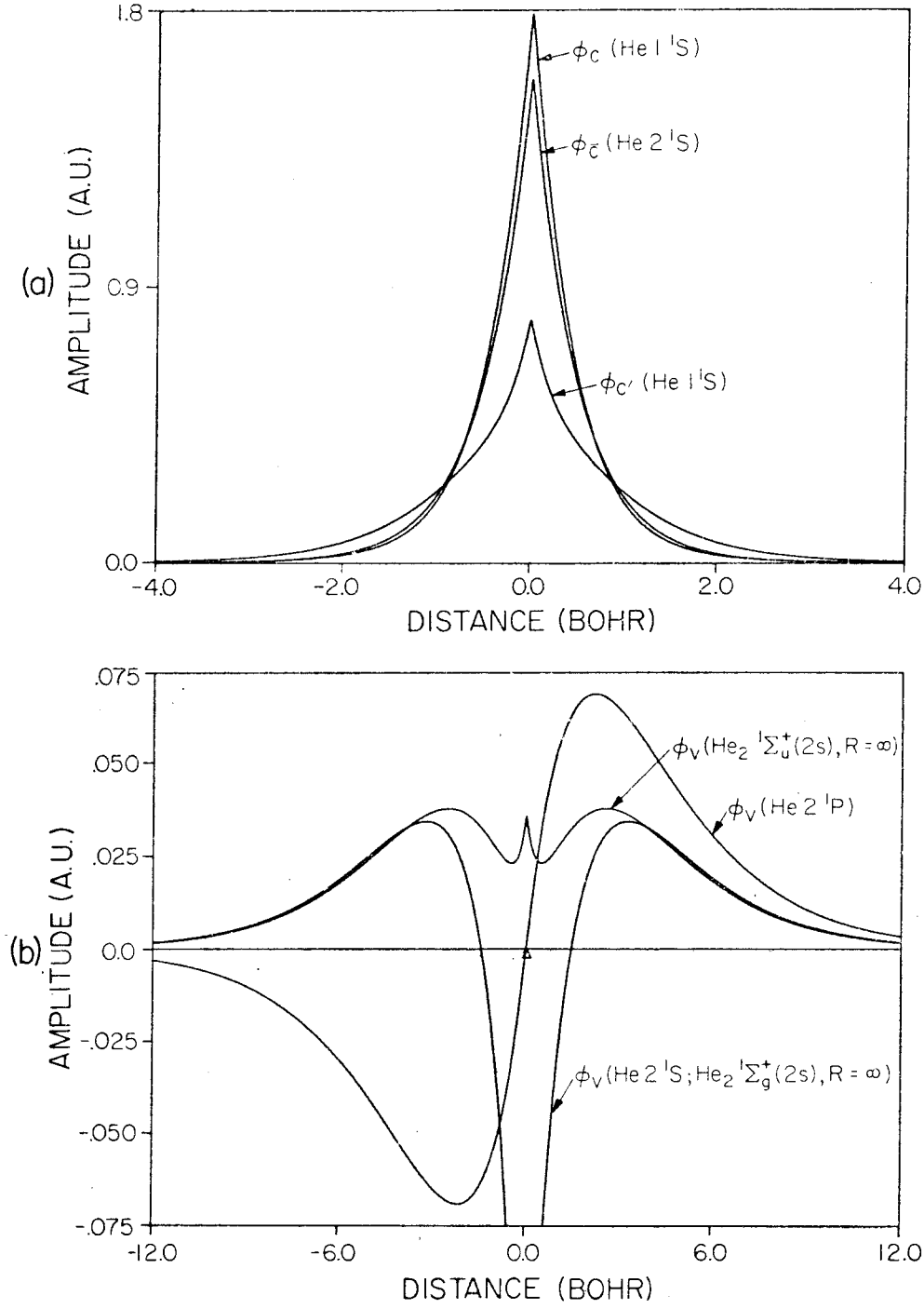
(a)
AMPLITUDE (A.U.)
1.8
0.9
0.0
-4.0
-2.0
0.0
2.0
4.0
DISTANCE (BOHR)
ϕ_C (He 1 ^{1}S)
$\phi_{\bar{C}}$ (He 2 ^{1}S)
$\phi_{C'}$ (He 1 ^{1}S)
(b)
AMPLITUDE (A.U.)
.075
.050
.025
0.0
-.025
-.050
-.075
-12.0
-6.0
0.0
6.0
12.0
DISTANCE (BOHR)
ϕ_V(He$_2$ $^1\Sigma_u^+$(2s), R = ∞)
ϕ_V(He 2 ^{1}P)
ϕ_V(He 2 ^{1}S; He$_2$ $^1\Sigma_g^+$(2s), R = ∞)

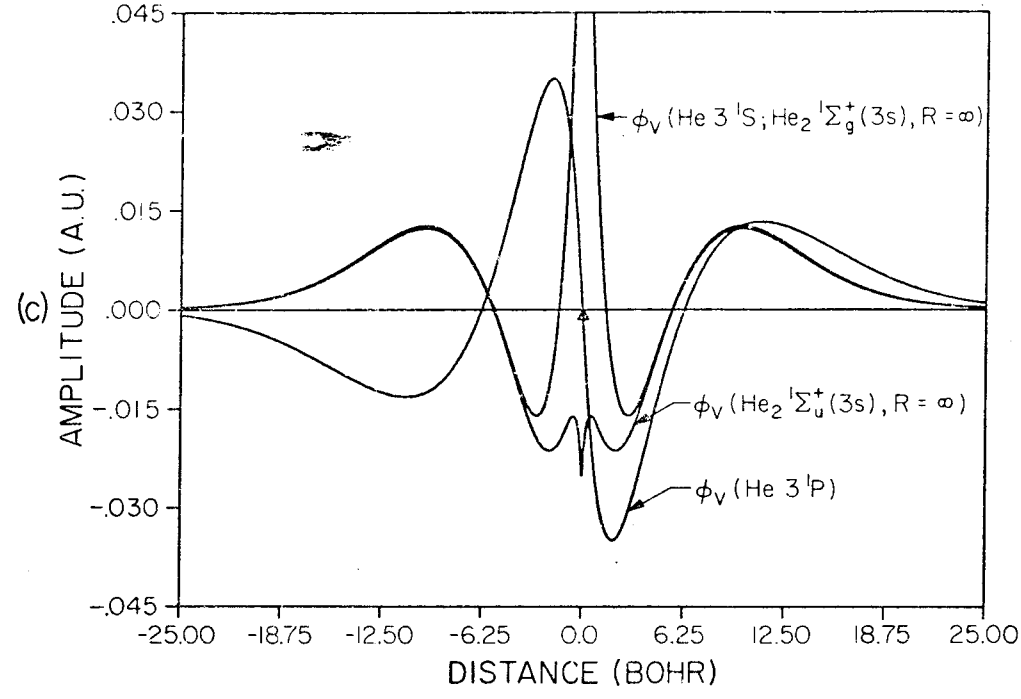
(c)
AMPLITUDE (A.U.)
.045
.030
.015
.000
-.015
-.030
-.045
-25.00
-18.75
-12.50
-6.25
0.0
6.25
12.50
18.75
25.00
DISTANCE (BOHR)
ϕ_V(He 3 ^{1}S; He$_2$ $^1\Sigma_g^+$(3s), R = ∞)
ϕ_V(He$_2$ $^1\Sigma_u^+$(3s), R = ∞)
ϕ_V(He 3 ^{1}P)

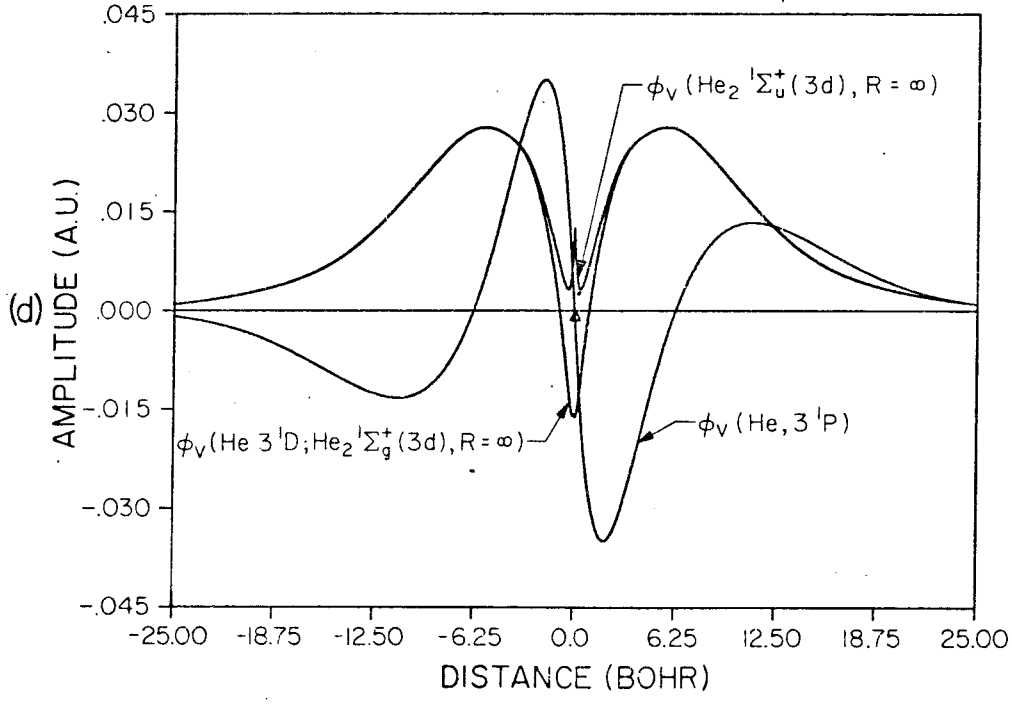
(d)
AMPLITUDE (A.U.)
.045
.030
.015
.000
-.015
-.030
-.045
-25.00
-18.75
-12.50
-6.25
0.0
6.25
12.50
18.75
25.00
DISTANCE (BOHR)
ϕ_V(He$_2$ $^1\Sigma_u^+$(3d), R = ∞)
ϕ_V(He 3 ^{1}D; He$_2$ $^1\Sigma_g^+$(3d), R = ∞)
ϕ_V(He, 3 ^{1}P)

Figure 3

(a) The core orbitals at R = 10.0 Bohr from the SCF $^1\Sigma_u^+(2s)$, $^1\Sigma_u^+(3p)$, $^1\Sigma_g^+(2s)$, $^1\Sigma_g^+(3p)$ wavefunctions. ϕ_c and $\phi_{c'}$ are the core orbitals on the unexcited He while $\phi_{\overline{c}}$ is the core orbital on the excited He. All the core orbitals are shown. The position of the He centers is denoted by the triangles. (b) The same as (a) except R = 1.8 Bohr.

(a)

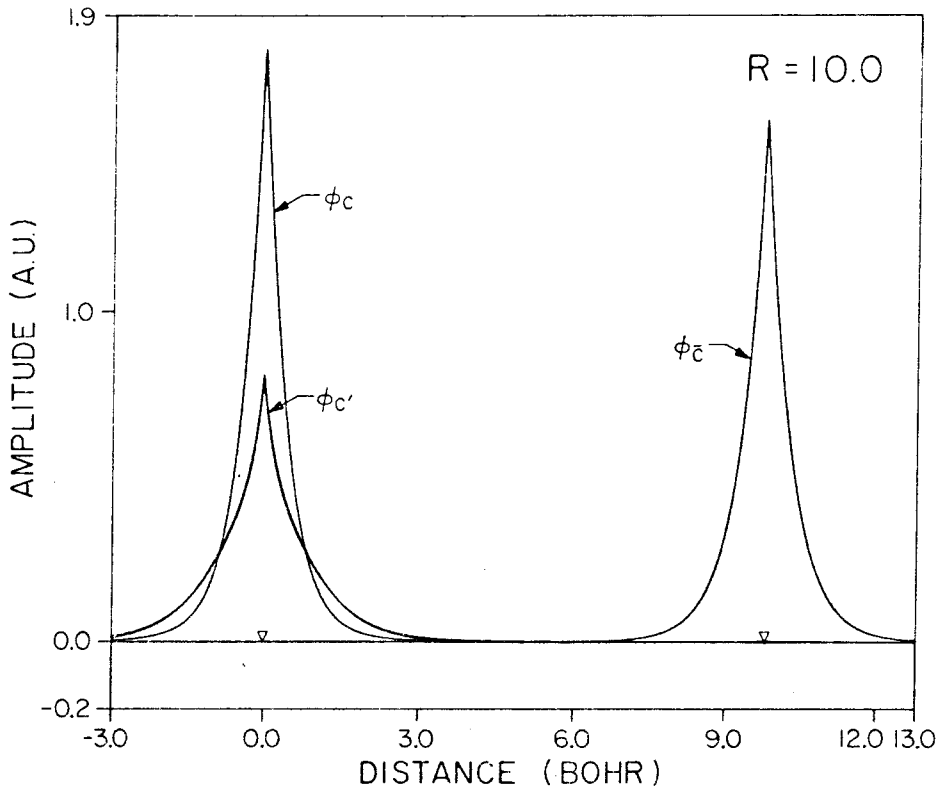
R = 10.0
ϕ_c
$\phi_{c'}$
$\phi_{\bar{c}}$
AMPLITUDE (A.U.)
1.9
1.0
0.0
-0.2
-3.0
0.0
3.0
6.0
9.0
12.0
13.0
DISTANCE (BOHR)

(b)

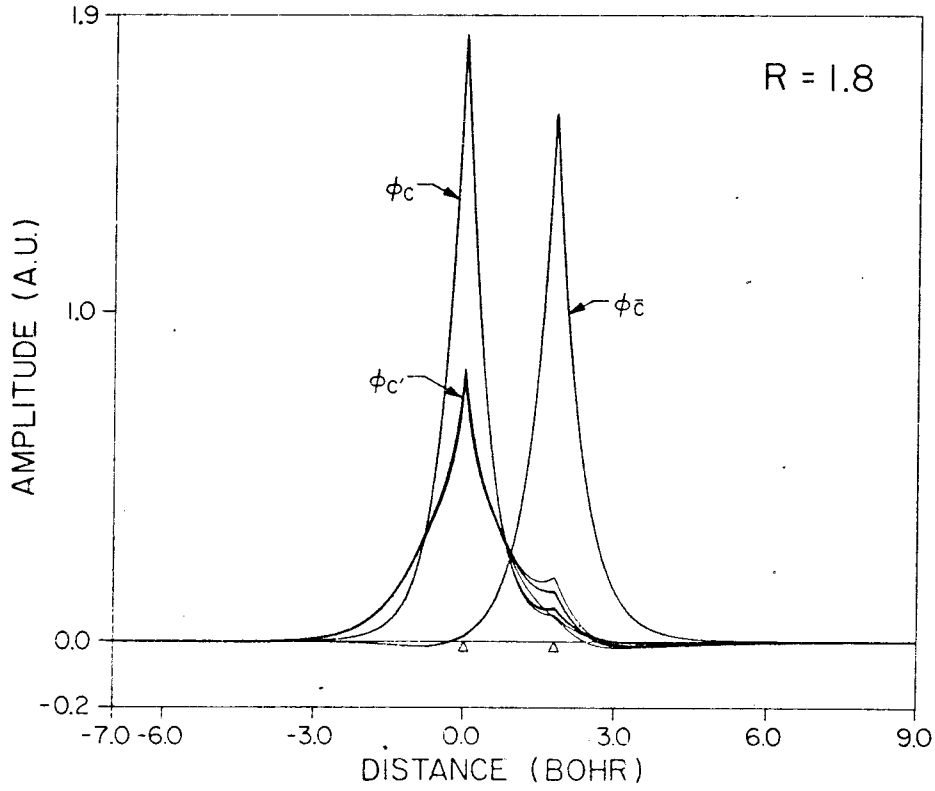
R = 1.8
ϕ_c
$\phi_{\bar{c}}$
$\phi_{c'}$
AMPLITUDE (A.U.)
1.9
1.0
0.0
-0.2
-7.0
-6.0
-3.0
0.0
3.0
6.0
9.0
DISTANCE (BOHR)

Figure 4

Potential energy curves for the $^1\Sigma_g^+$ (FO) and $^1\Sigma_u^+$ (FO) excited states of He_2. The FO wavefunctions from which these energies are calculated are composed of orbitals solved for self-consistently using projected wavefunctions at $R = \infty$.

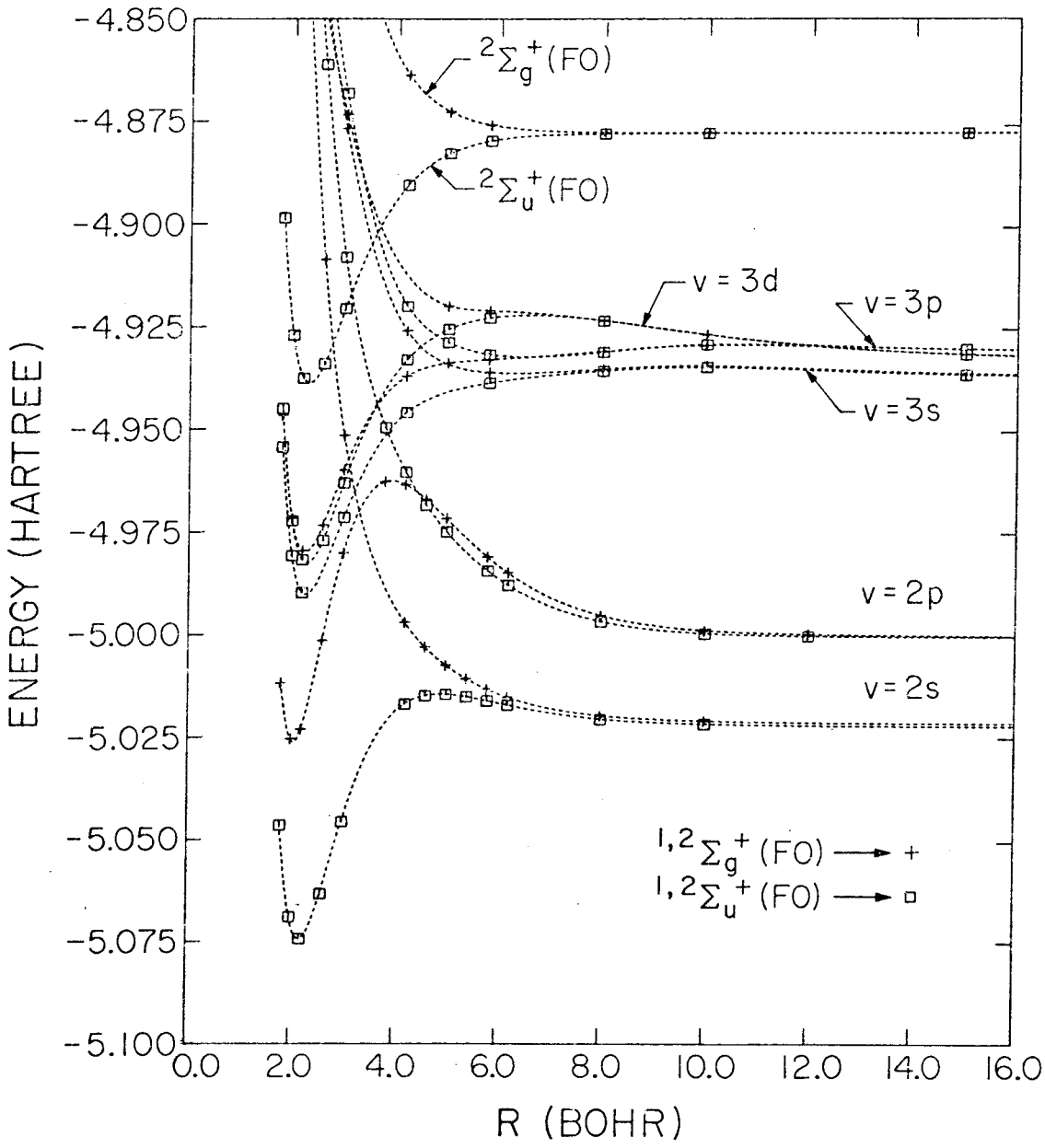
-4.850
-4.875
-4.900
-4.925
-4.950
-4.975
-5.000
-5.025
-5.050
-5.075
-5.100
ENERGY (HARTREE)
0.0
2.0
4.0
6.0
8.0
10.0
12.0
14.0
16.0
R (BOHR)
$^2\Sigma_g^+$(FO)
$^2\Sigma_u^+$(FO)
v = 3d
v = 3p
v = 3s
v = 2p
v = 2s
$^{1,2}\Sigma_g^+$(FO) → +
$^{1,2}\Sigma_u^+$(FO) → □

Figure 5

The FO (dashed) and SCF (solid) energy curves for the excited $^1\Sigma_g^+$ states of He_2. Also shown is an FO curve for $^2\Sigma_g^+$, He_2^+ and FO and SCF curves for $^2\Sigma_u^+$, He_2^+. See Table XIII for a description of the latter curve.

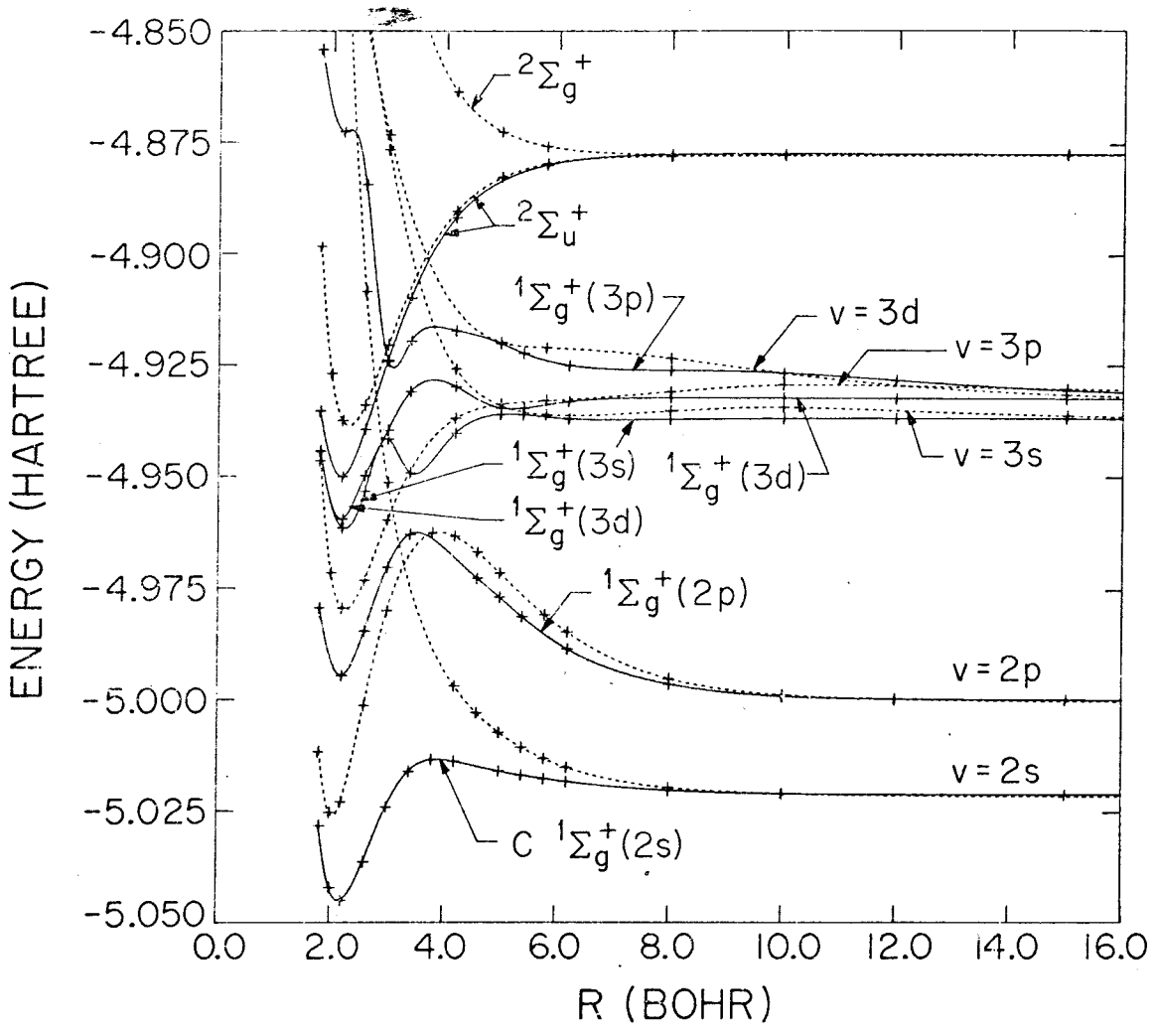
-4.850
-4.875
-4.900
-4.925
-4.950
-4.975
-5.000
-5.025
-5.050
ENERGY (HARTREE)
0.0
2.0
4.0
6.0
8.0
10.0
12.0
14.0
16.0
R (BOHR)
$^2\Sigma_g^+$
$^2\Sigma_u^+$
$^1\Sigma_g^+(3p)$
v = 3d
v = 3p
v = 3s
$^1\Sigma_g^+(3s)$
$^1\Sigma_g^+(3d)$
$^1\Sigma_g^+(3d)$
$^1\Sigma_g^+(2p)$
v = 2p
v = 2s
C $^1\Sigma_g^+(2s)$

Figure 6

The FO (dashed) and SCF (solid) energy curves for the excited $^1\Sigma_u^+$ states of He_2. Also shown is an FO curve for $^2\Sigma_g^+$, He_2^+ and FO and SCF curves for $^2\Sigma_u^+$, He_2^+. See Table XIII for a description of the latter curve.

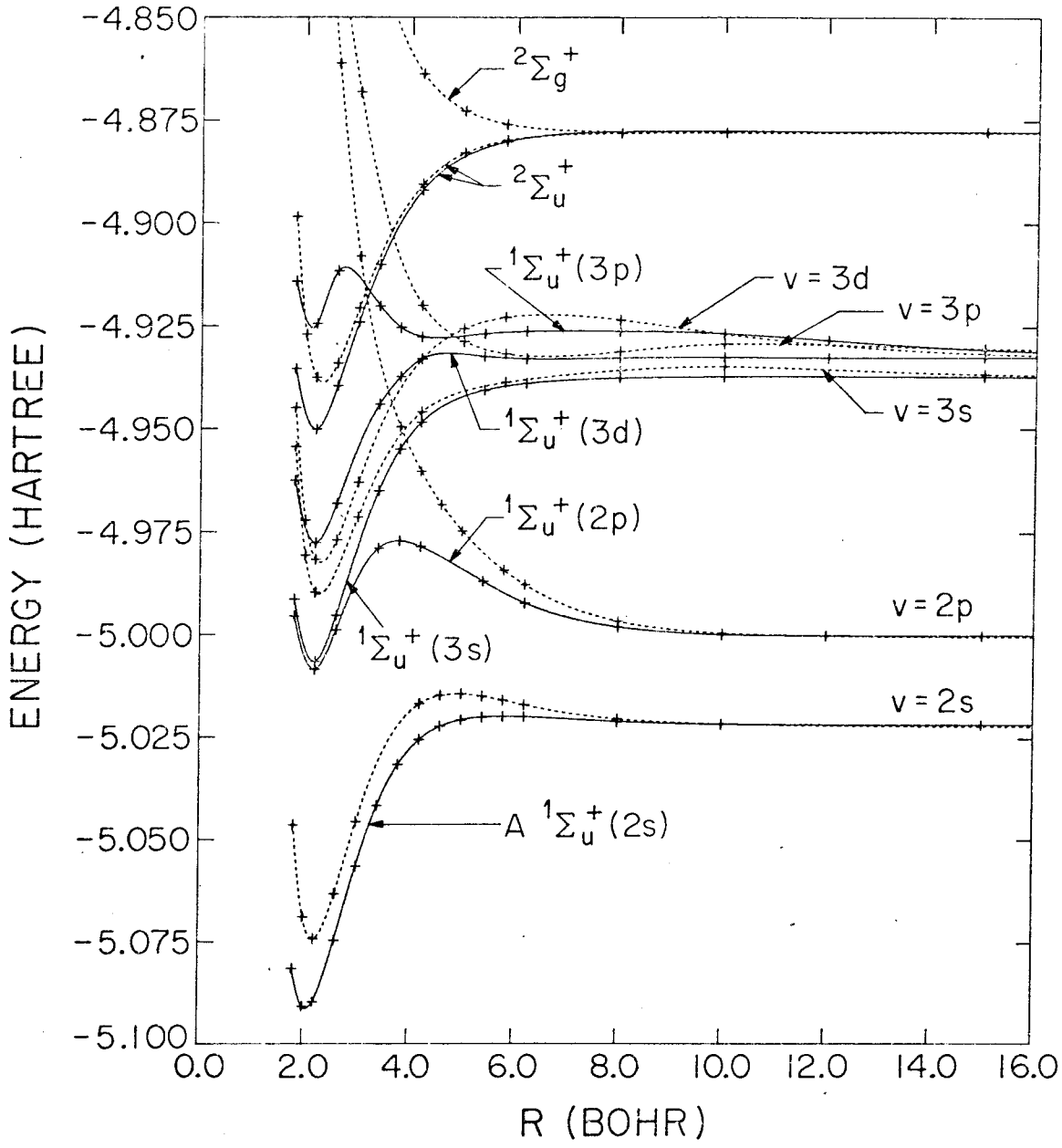
-4.850
-4.875
-4.900
-4.925
-4.950
-4.975
-5.000
-5.025
-5.050
-5.075
-5.100
ENERGY (HARTREE)
0.0
2.0
4.0
6.0
8.0
10.0
12.0
14.0
16.0
R (BOHR)
$^2\Sigma_g^+$
$^2\Sigma_u^+$
$^1\Sigma_u^+(3p)$
v = 3d
v = 3p
$^1\Sigma_u^+(3d)$
v = 3s
$^1\Sigma_u^+(2p)$
v = 2p
$^1\Sigma_u^+(3s)$
v = 2s
A $^1\Sigma_u^+(2s)$

Figure 7

The totally repulsive FO energy curves for the excited states of He_2 shown with the attractive $^2\Sigma_u^+$ state and the repulsive (solid line) $^2\Sigma_g^+$ state of He_2^+. The latter curve has been plotted to have the same asymptotic limit as the four electron excited states.

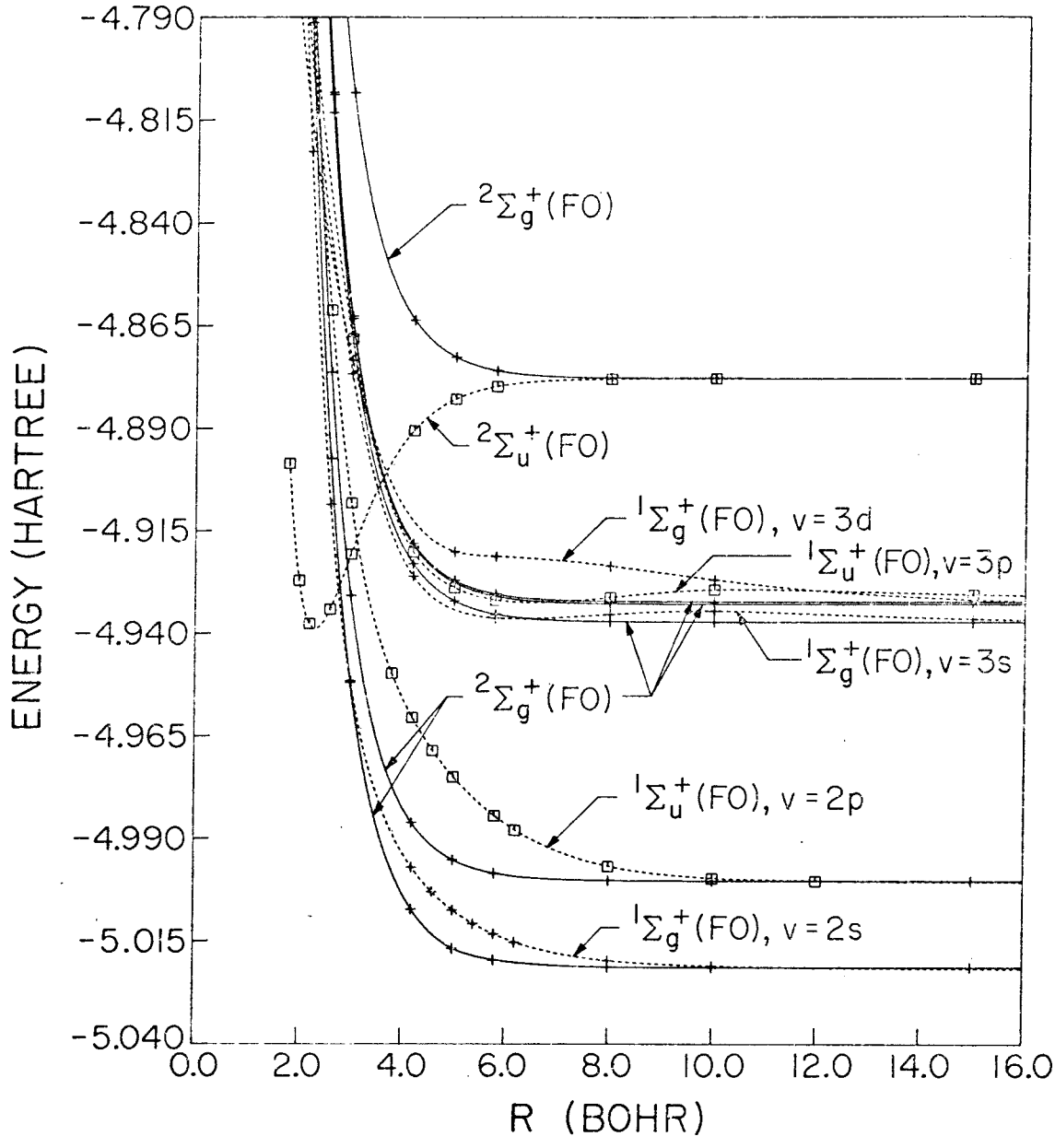
-4.790
-4.815
-4.840
-4.865
-4.890
-4.915
-4.940
-4.965
-4.990
-5.015
-5.040
ENERGY (HARTREE)
0.0
2.0
4.0
6.0
8.0
10.0
12.0
14.0
16.0
R (BOHR)
$^2\Sigma_g^+$(FO)
$^2\Sigma_u^+$(FO)
$^1\Sigma_g^+$(FO), v=3d
$^1\Sigma_u^+$(FO), v=3p
$^1\Sigma_g^+$(FO), v=3s
$^2\Sigma_g^+$(FO)
$^1\Sigma_u^+$(FO), v=2p
$^1\Sigma_g^+$(FO), v=2s

Figure 8

The total energy (solid lines) and the total exchange kinetic energy (dashed lines), T^X, for the $^1\Sigma_g^+$ (FO) excited states. The T^X curves are plotted so as to have the same asymptotic limits as the energy curves.

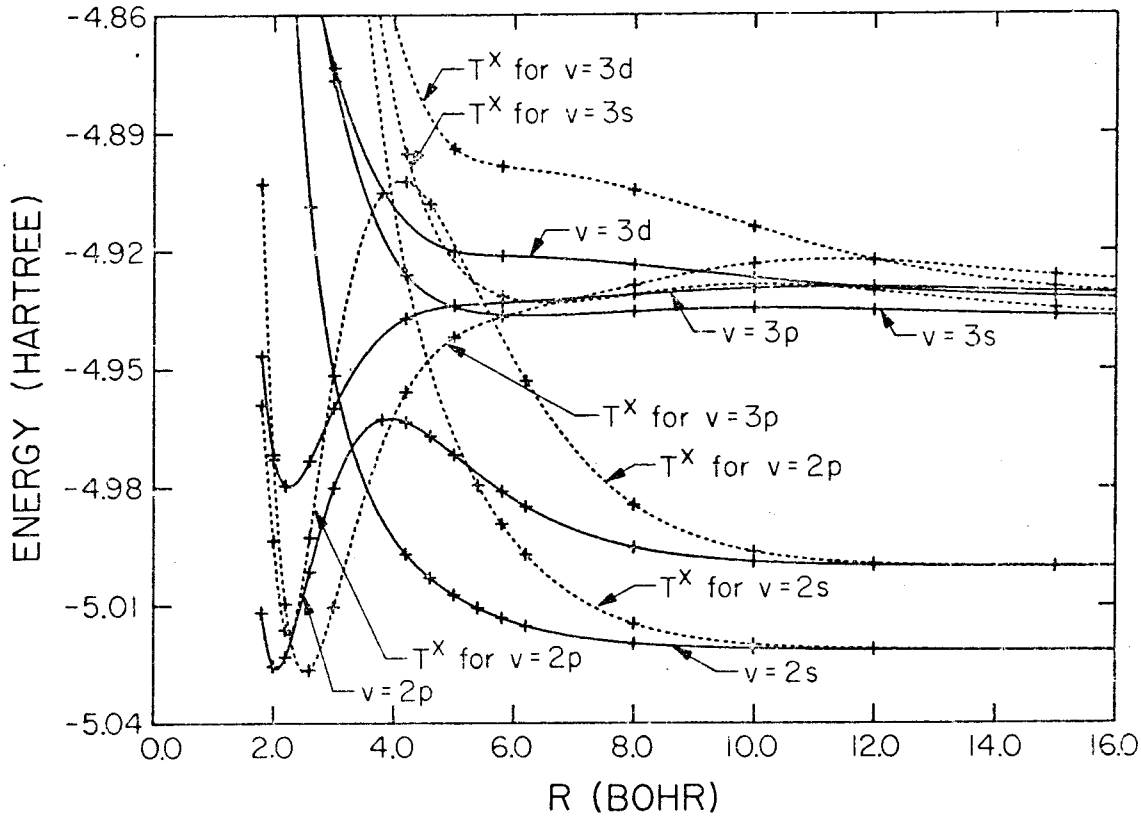
-4.86
-4.89
-4.92
-4.95
-4.98
-5.01
-5.04
ENERGY (HARTREE)
0.0
2.0
4.0
6.0
8.0
10.0
12.0
14.0
16.0
R (BOHR)
T^X for v=3d
T^X for v=3s
v=3d
v=3p
v=3s
T^X for v=3p
T^X for v=2p
T^X for v=2s
v=2s
T^X for v=2p
v=2p

Figure 9

The total energy (solid lines) and the total exchange kinetic energy (dashed lines), T^X, for the $^1\Sigma_u^+$ (FO) states. The T^X curves are plotted so as to have the same asymptotic limits as the energy curves.

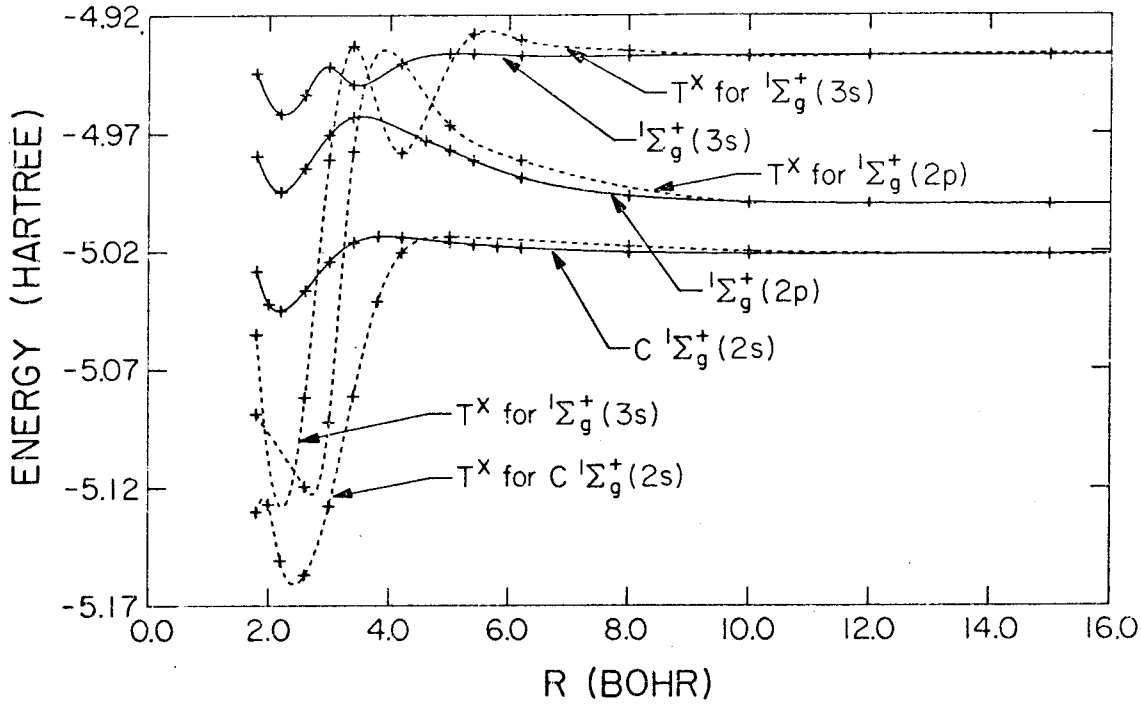
-4.92
-4.97
-5.02
-5.07
-5.12
-5.17
ENERGY (HARTREE)
0.0
2.0
4.0
6.0
8.0
10.0
12.0
14.0
16.0
R (BOHR)
T^X for ¹Σg⁺(3s)
¹Σg⁺(3s)
T^X for ¹Σg⁺(2p)
¹Σg⁺(2p)
C ¹Σg⁺(2s)
T^X for ¹Σg⁺(3s)
T^X for C ¹Σg⁺(2s)

Figure 10

The total energy (solid lines) and the total exchange kinetic energy (dashed lines), T^X, for the SCF v = 2s, 2p, 3s $^1\Sigma_g^+$ states. The T^X curves are plotted so as to have the same asymptotic limits as the energy curves.

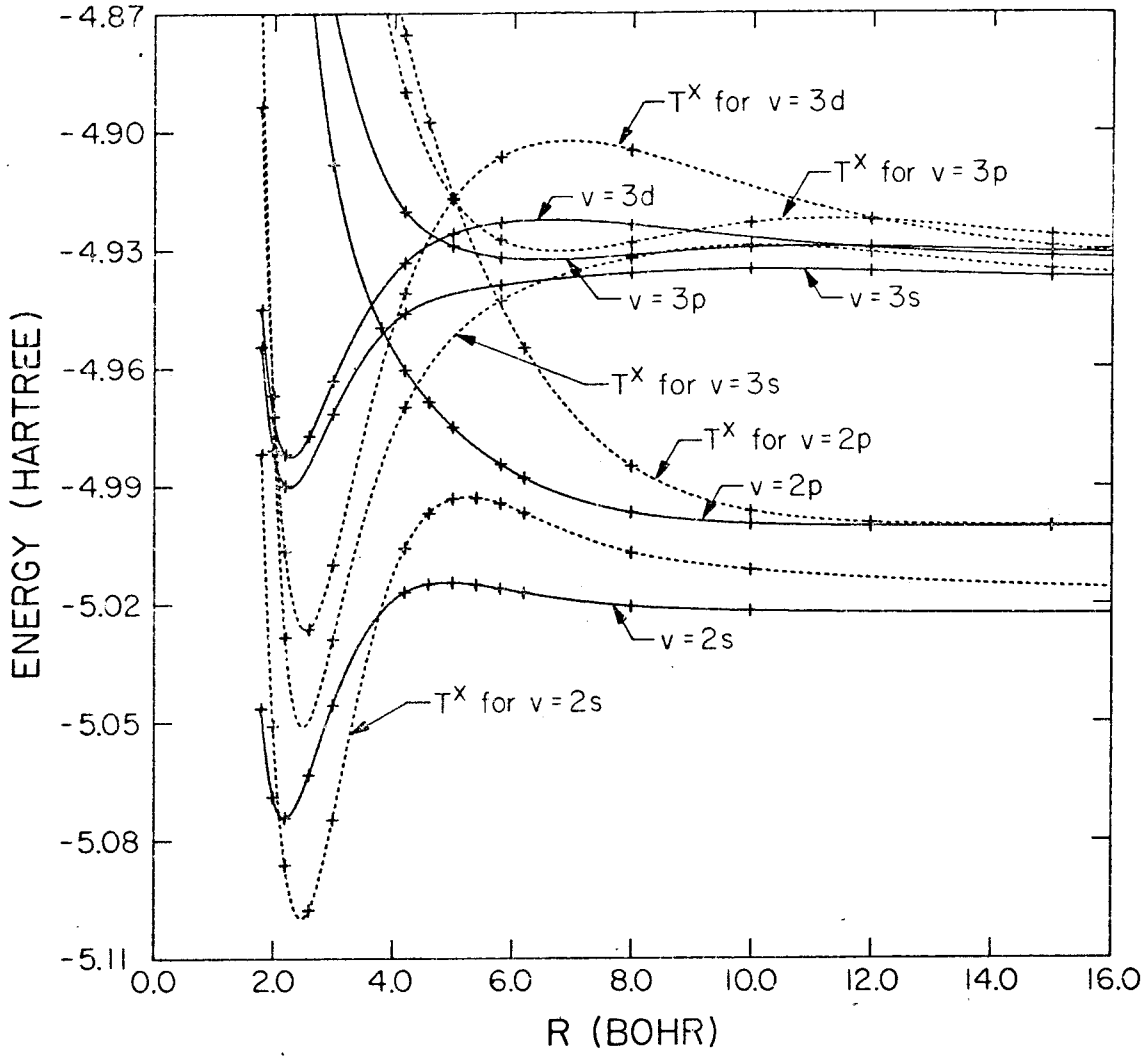
-4.87
-4.90
-4.93
-4.96
-4.99
-5.02
-5.05
-5.08
-5.11
ENERGY (HARTREE)
0.0
2.0
4.0
6.0
8.0
10.0
12.0
14.0
16.0
R (BOHR)
T^X for v = 3d
T^X for v = 3p
v = 3d
v = 3p
v = 3s
T^X for v = 3s
T^X for v = 2p
v = 2p
v = 2s
T^X for v = 2s

Figure 11

The SCF energy curves for the excited $^1\Sigma_g^+$ and $^1\Sigma_u^+$ states of He_2. Also shown are SCF projected curves for X $^1\Sigma_g^+$ and X $^2\Sigma_u^+$ of He_2^+. See Table XIII for a description of the latter curve.

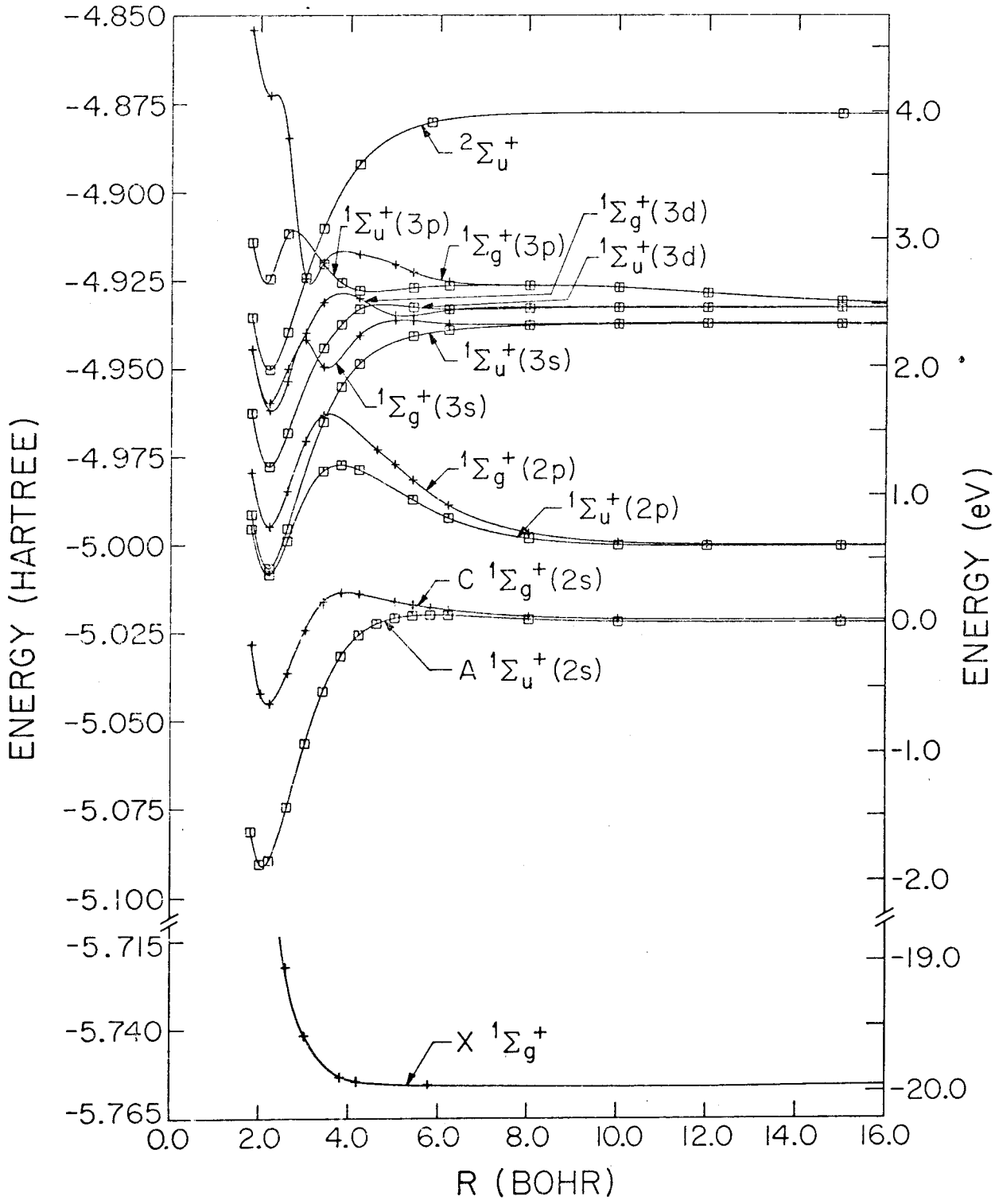
-4.850
-4.875
-4.900
-4.925
-4.950
-4.975
-5.000
-5.025
-5.050
-5.075
-5.100
-5.715
-5.740
-5.765
ENERGY (HARTREE)
4.0
3.0
2.0
1.0
0.0
-1.0
-2.0
-19.0
-20.0
ENERGY (eV)
0.0
2.0
4.0
6.0
8.0
10.0
12.0
14.0
16.0
R (BOHR)
$^2\Sigma_u^+$
$^1\Sigma_u^+(3p)$
$^1\Sigma_g^+(3p)$
$^1\Sigma_g^+(3d)$
$^1\Sigma_u^+(3d)$
$^1\Sigma_u^+(3s)$
$^1\Sigma_g^+(3s)$
$^1\Sigma_g^+(2p)$
$^1\Sigma_u^+(2p)$
C $^1\Sigma_g^+(2s)$
A $^1\Sigma_u^+(2s)$
X $^1\Sigma_g^+$

Figure 12

Contour plots of the Rydberg orbital at several internuclear distances for A $^1\Sigma_u^+$ and C $^1\Sigma_g^+$. The contours are plotted in a plane containing the internuclear axis with the two centers shown by small asterisks. The node is the contour with long dashes. The positive contours are solid lines while the negative contours are dotted. The contour interval is 0.005. Contours more negative than -.050 are not shown. Distances are in Bohr.

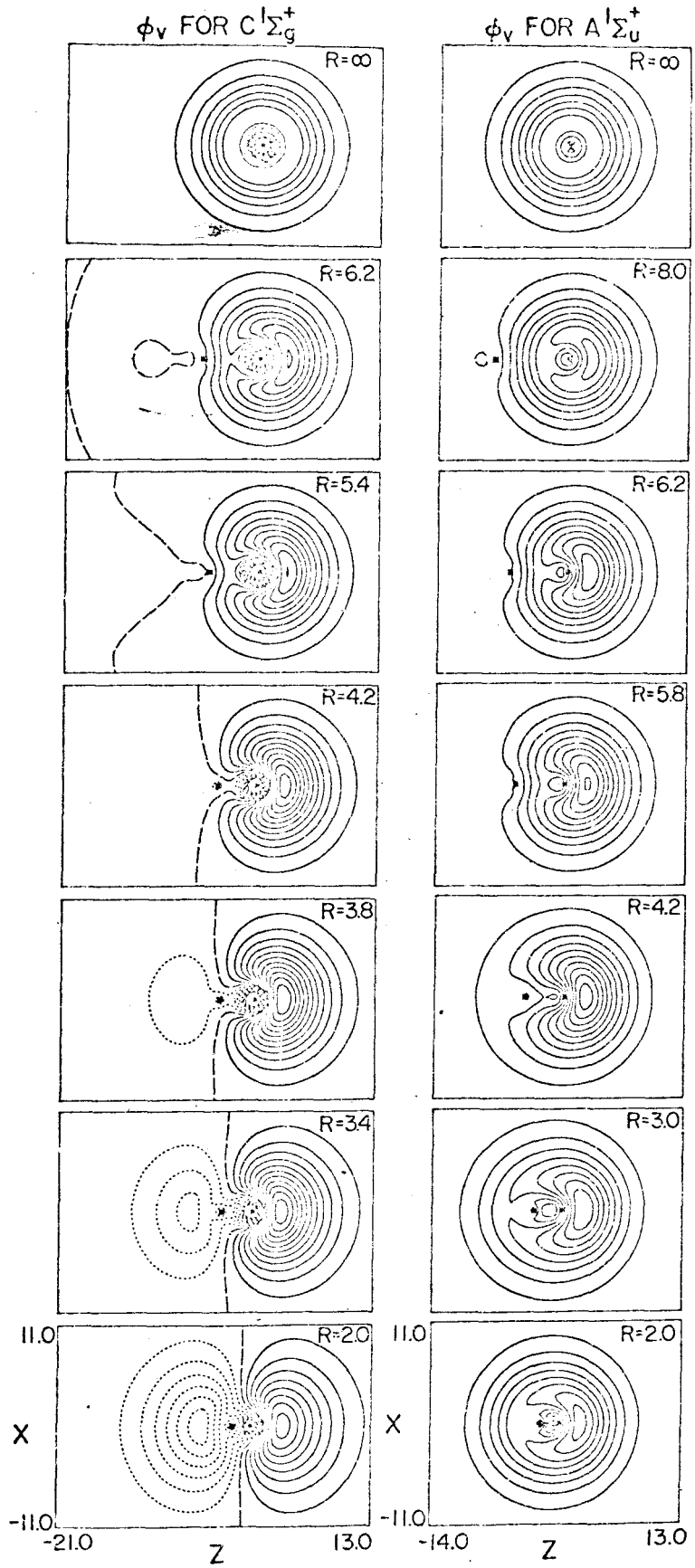
ϕ_v FOR $C\,^1\Sigma_g^+$
ϕ_v FOR $A\,^1\Sigma_u^+$
R=∞
R=6.2
R=5.4
R=4.2
R=3.8
R=3.4
R=2.0
R=8.0
R=6.2
R=5.8
R=4.2
R=3.0
R=2.0
11.0
X
-11.0
-21.0
Z
13.0
11.0
X
-11.0
-14.0
Z
13.0

Figure 13

Amplitude plot of ϕ_v at R = 1.8 Bohr for (a) C $^1\Sigma_g^+(2s)$ and (b) $^1\Sigma_g^+(2p)$.

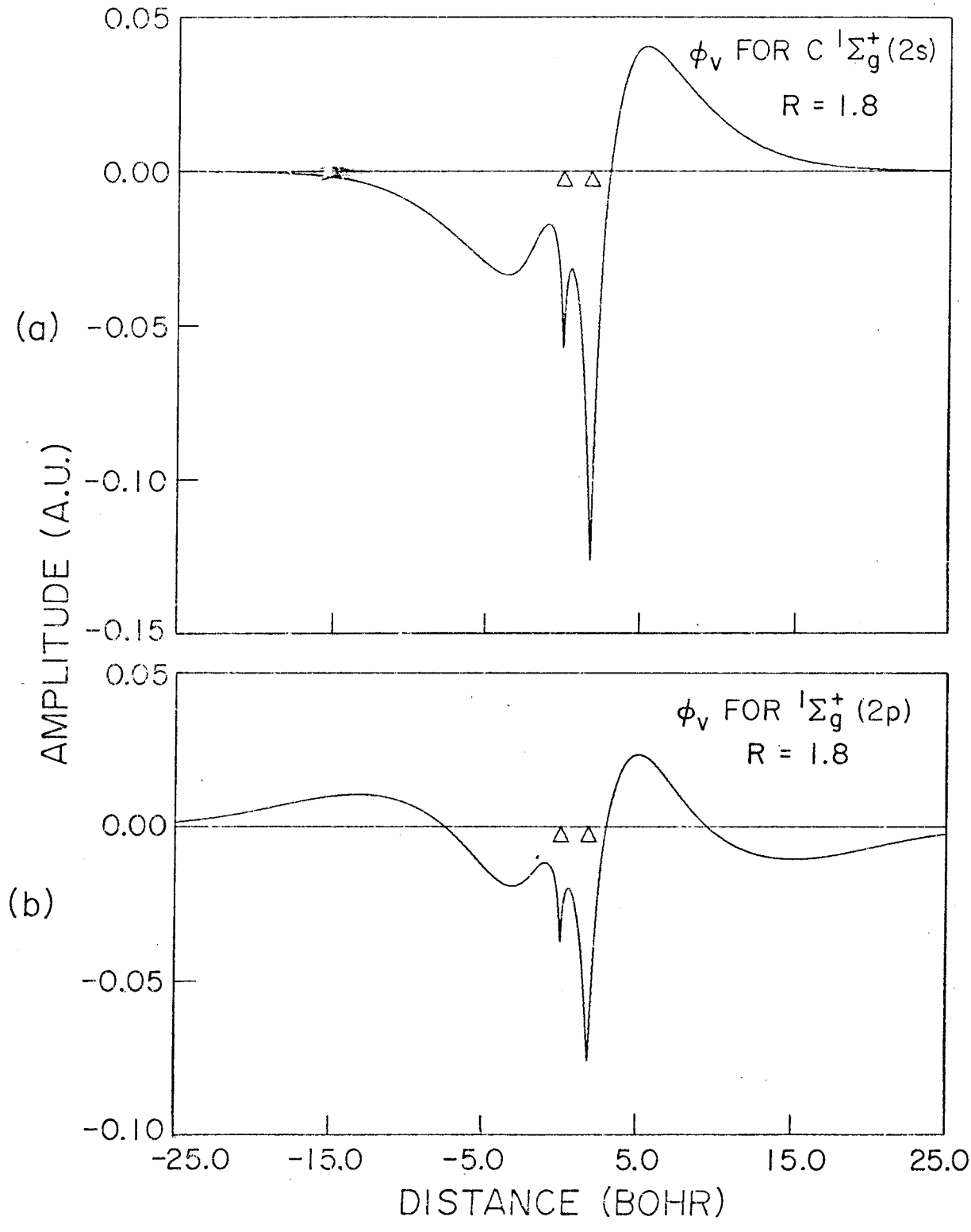
0.05
0.00
-0.05
-0.10
-0.15
(a)
ϕ_v FOR C $^1\Sigma_g^+$(2s)
R = 1.8
AMPLITUDE (A.U.)
0.05
0.00
-0.05
-0.10
(b)
ϕ_v FOR $^1\Sigma_g^+$ (2p)
R = 1.8
-25.0
-15.0
-5.0
5.0
15.0
25.0
DISTANCE (BOHR)

Figure 14

Contour plots of the Rydberg orbital at several internuclear distances for $^1\Sigma_g^+$ (2p) and $^1\Sigma_u^+$ (2p). The contours are plotted in a plane containing the internuclear axis with the two centers shown by small asterisks. The node is the contour with long dashes. The positive contours are solid lines while the negative contours are dotted. The contours plotted are of absolute value 0.0, 0.0025, 0.0050, 0.0100, 0.0200, and 0.0400. Distances are in Bohr.

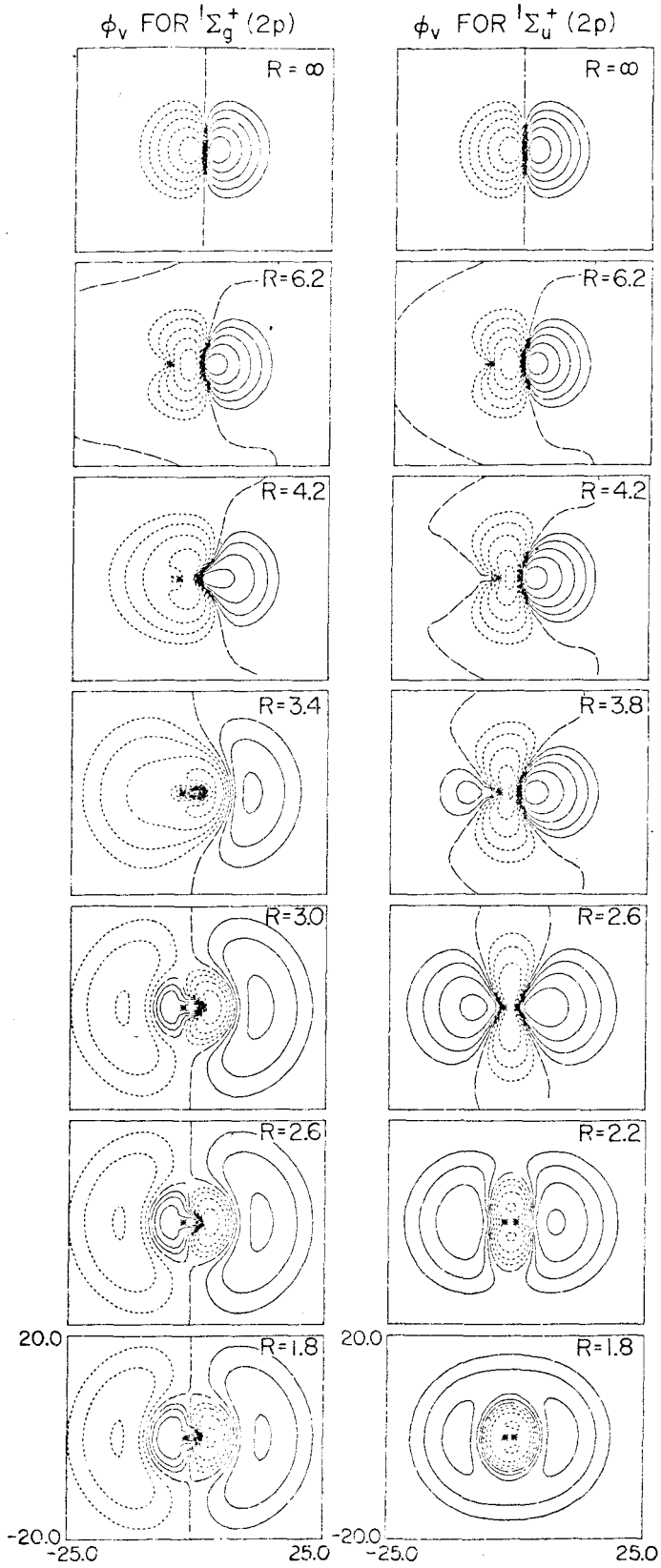
ϕ_v FOR $^1\Sigma_g^+(2p)$
ϕ_v FOR $^1\Sigma_u^+(2p)$
R = ∞
R=6.2
R=4.2
R=3.4
R=3.0
R=2.6
R=1.8
R=3.8
R=2.6
R=2.2
R=1.8
20.0
-20.0
-25.0
25.0

Figure 15

Contour plots of the Rydberg orbital at several internuclear distances for $^1\Sigma_g^+$ (3s) and $^1\Sigma_u^+$ (3s). See the caption to Fig. 14 for further details.

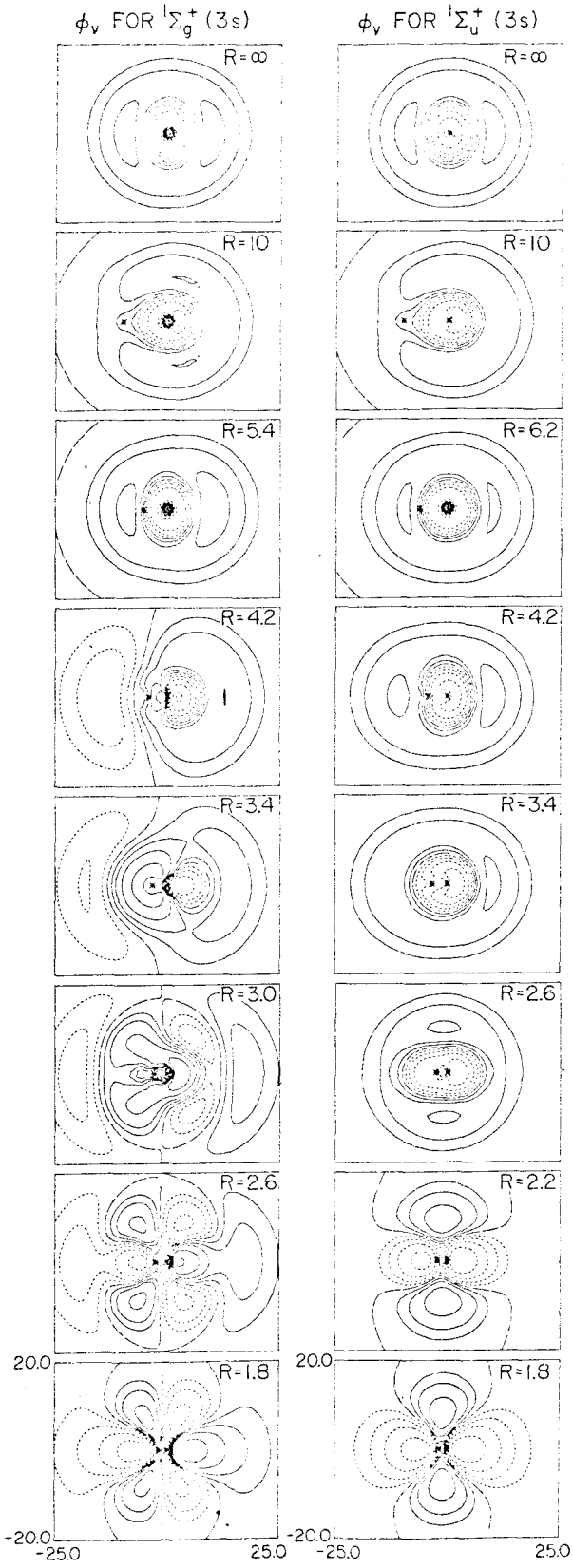
ϕ_v FOR $^1\Sigma_g^+$ (3s)
ϕ_v FOR $^1\Sigma_u^+$ (3s)
R=∞
R=10
R=5.4
R=4.2
R=3.4
R=3.0
R=2.6
R=1.8
R=∞
R=10
R=6.2
R=4.2
R=3.4
R=2.6
R=2.2
R=1.8
20.0
-20.0
-25.0
25.0
20.0
-20.0
-25.0
25.0

Figure 16

(a) Contour plots of the Rydberg orbital for R = ∞ to R = 5.4 for $^1\Sigma_g^+$ (3d) and $^1\Sigma_u^+$ (3d). See the caption to Fig. 14 for further details.

(b) Same as (a) except for R = 4.2 to R = 1.8.

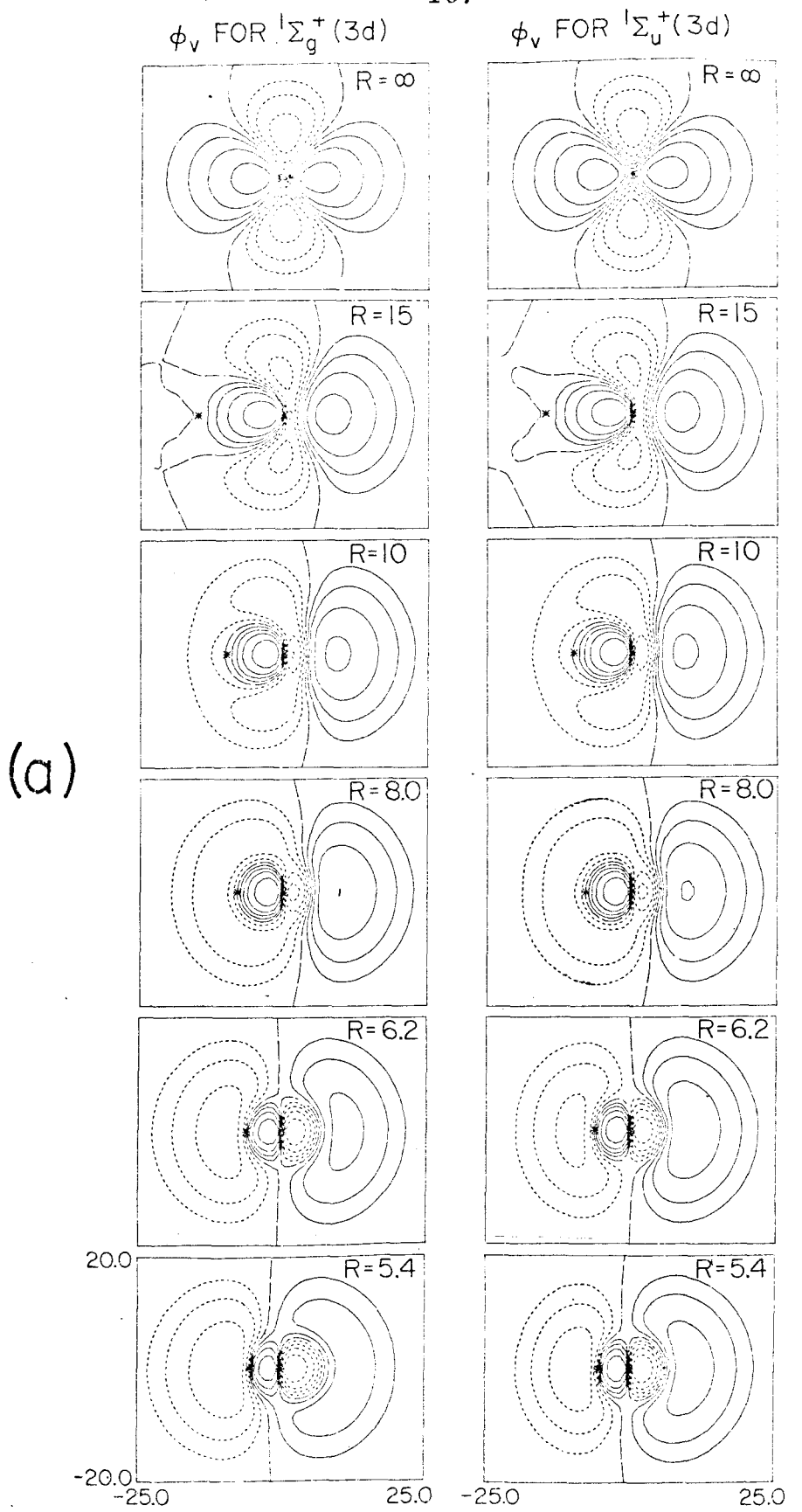
ϕ_v FOR $^1\Sigma_g^+(3d)$
ϕ_v FOR $^1\Sigma_u^+(3d)$
R = ∞
R = 15
R = 10
R = 8.0
R = 6.2
R = 5.4
(a)
20.0
-20.0
-25.0
25.0
-25.0
25.0

(b)

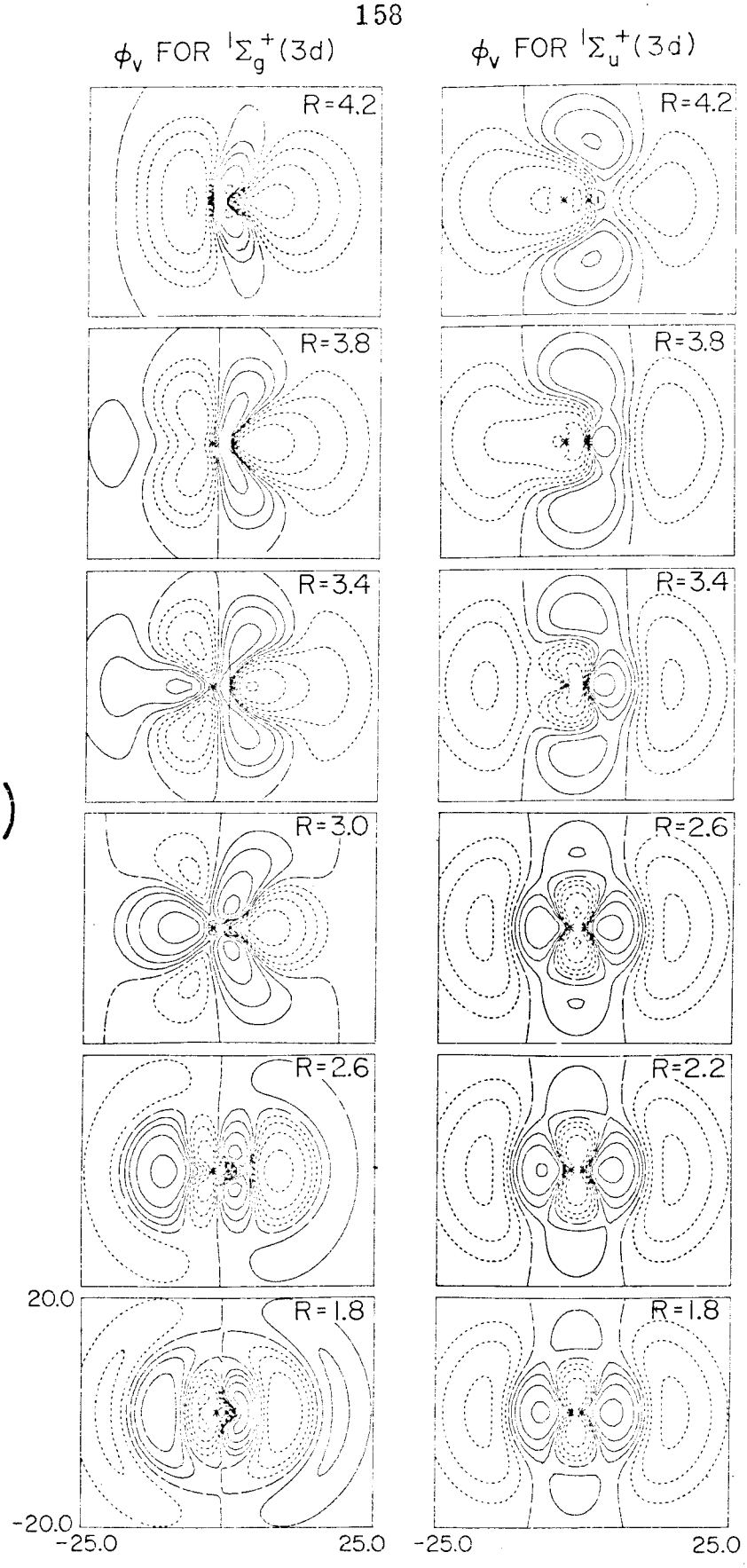
ϕ_v FOR $^1\Sigma_g^+(3d)$
ϕ_v FOR $^1\Sigma_u^+(3d)$
R=4.2
R=3.8
R=3.4
R=3.0
R=2.6
R=1.8
R=4.2
R=3.8
R=3.4
R=2.6
R=2.2
R=1.8
20.0
-20.0
-25.0
25.0
-25.0
25.0

Figure 17

(a) Contour plots of the Rydberg orbital for R = ∞ to R = 4.2 for $^1\Sigma_g^+(3p)$ and $^1\Sigma_u^+(3p)$. See the caption to Fig. 14 for further details.

(b) Same as (a) except for R = 3.8 to R = 1.8.

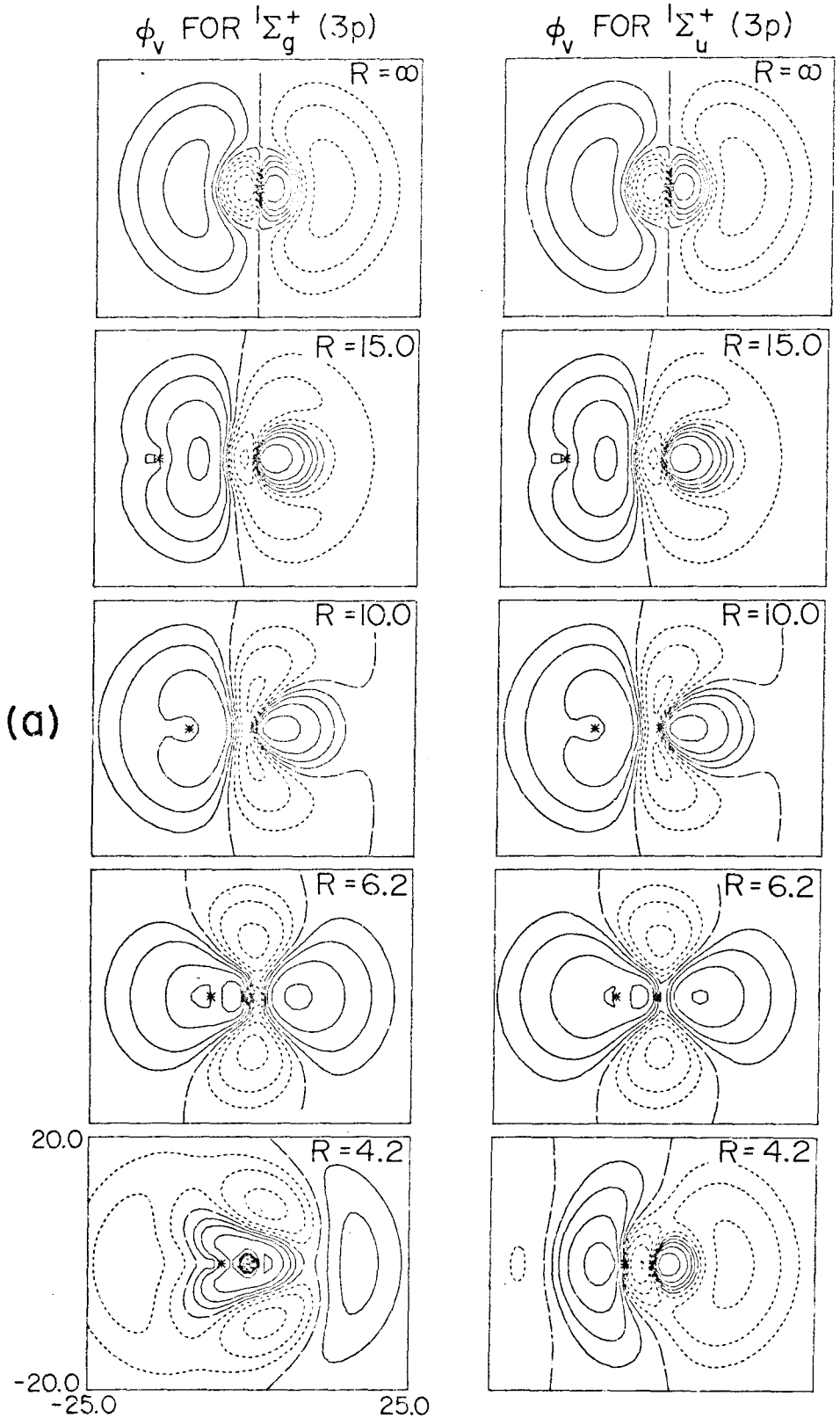
ϕ_v FOR $^1\Sigma_g^+$ (3p)
ϕ_v FOR $^1\Sigma_u^+$ (3p)
R = ∞
R = 15.0
R = 10.0
R = 6.2
R = 4.2
(a)
20.0
-20.0
-25.0
25.0

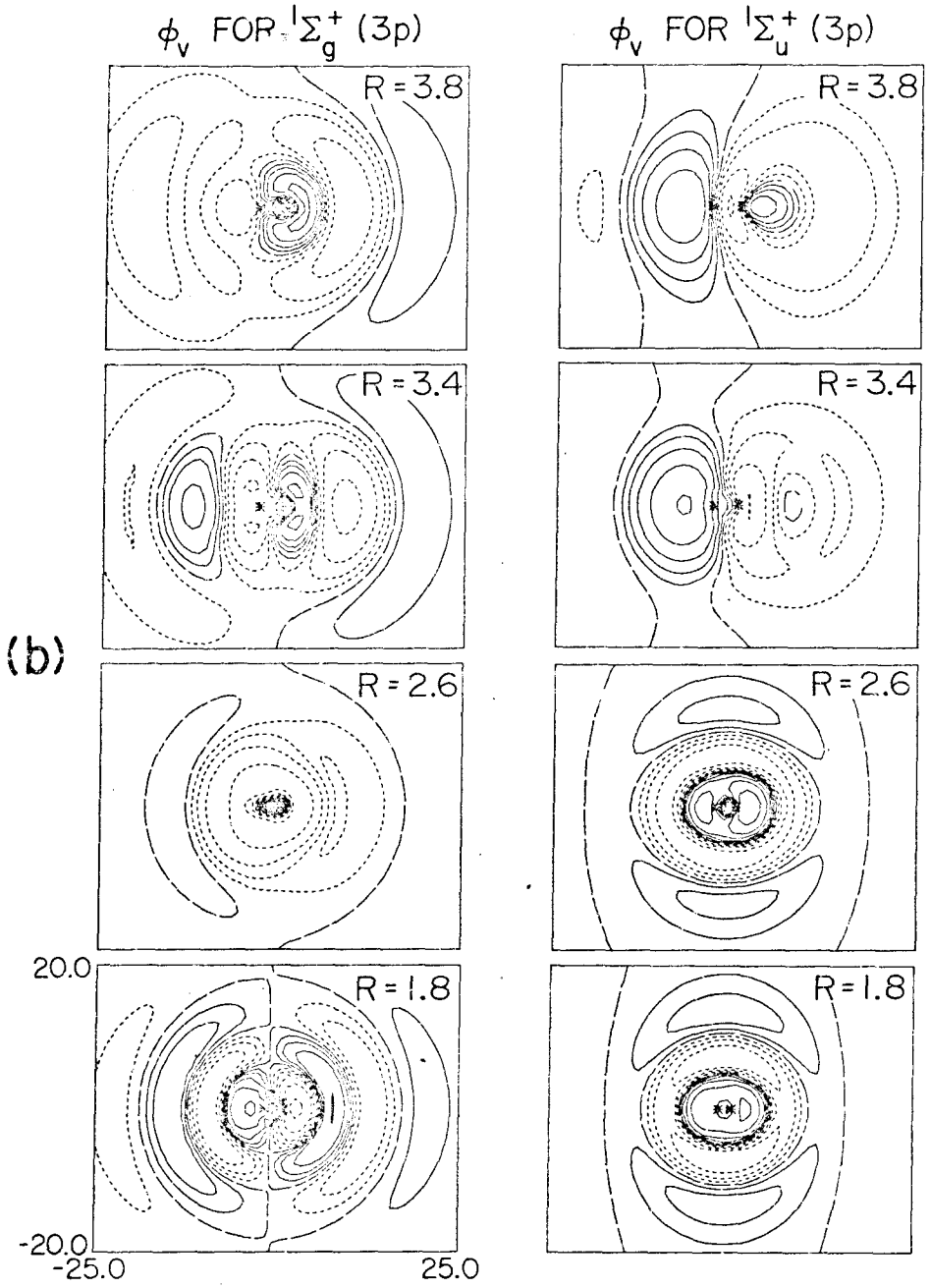
ϕ_v FOR $^1\Sigma_g^+$ (3p)
ϕ_v FOR $^1\Sigma_u^+$ (3p)
R = 3.8
R = 3.4
R = 2.6
R = 1.8
(b)
20.0
-20.0
-25.0
25.0

Figure 18

(a) Qualitative sketch of the FO (dashed) and SCF (solid) curves for two $^1\Sigma_g^+$ excited states of H_2. (b) Qualitative sketch of the FO (dashed) and SCF (solid) curves for two $^1\Sigma_u^+$ excited states of H_2.

a)

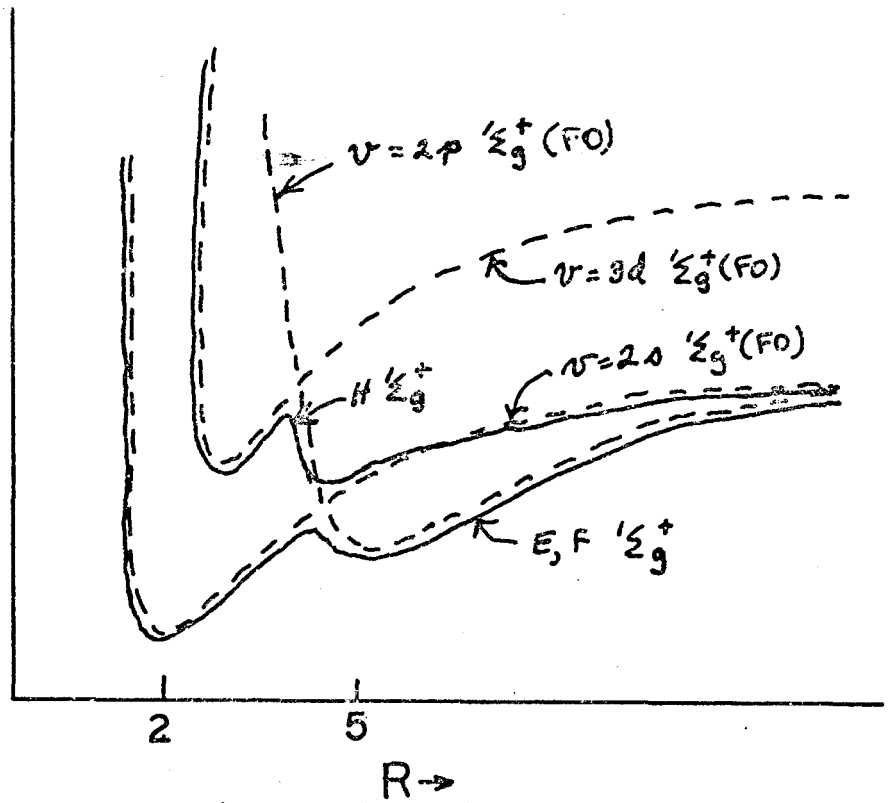
E
v=2p ¹Σg⁺(FO)
v=3d ¹Σg⁺(FO)
H ¹Σg⁺
v=2s ¹Σg⁺(FO)
E, F ¹Σg⁺
2
5
R→

b)

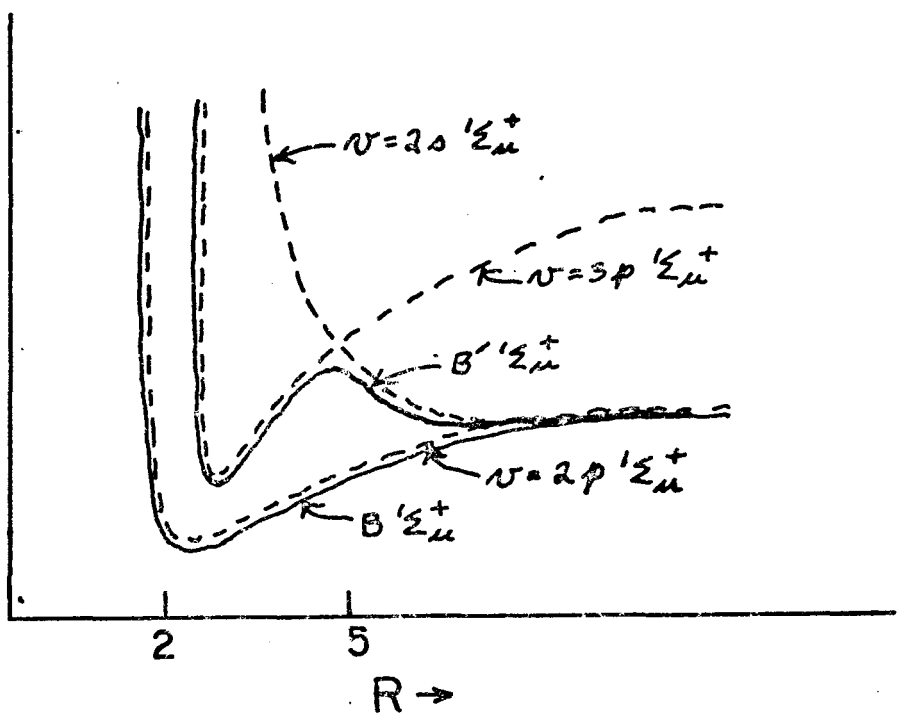
E
v=2s ¹Σu⁺
v=3p ¹Σu⁺
B' ¹Σu⁺
v=2p ¹Σu⁺
B ¹Σu⁺
2
5
R→

Figure 19

CI results for the $^{1,3}\Sigma_g^+$ states of He_2 using only basis functions appropriate for n = 2 atom states from Tables I and II.

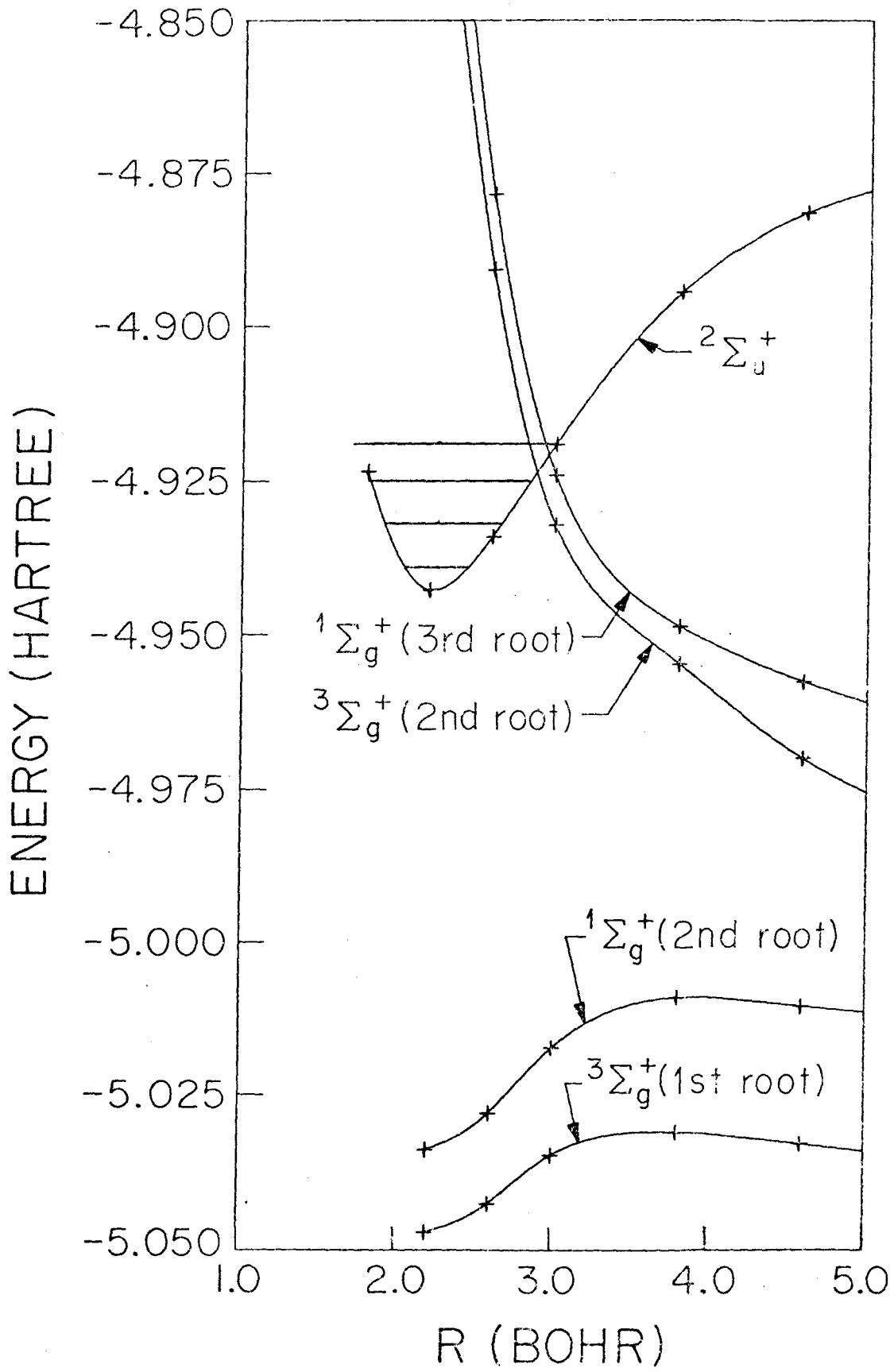
-4.850
-4.875
-4.900
-4.925
-4.950
-4.975
-5.000
-5.025
-5.050
ENERGY (HARTREE)
1.0
2.0
3.0
4.0
5.0
R (BOHR)
$^2\Sigma_u^+$
$^1\Sigma_g^+$(3rd root)
$^3\Sigma_g^+$(2nd root)
$^1\Sigma_g^+$(2nd root)
$^3\Sigma_g^+$(1st root)

Figure 20

Potential curves for the repulsive FO diabatic states and the $^2\Sigma_u^+$ SCF ion state (see Table XIII for a description of the latter state). Curves for the π states are curves for $^2\Sigma_g^+$ (FO) He_2^+ which have been adjusted so as to have the same R = ∞ limit as the four electron state.

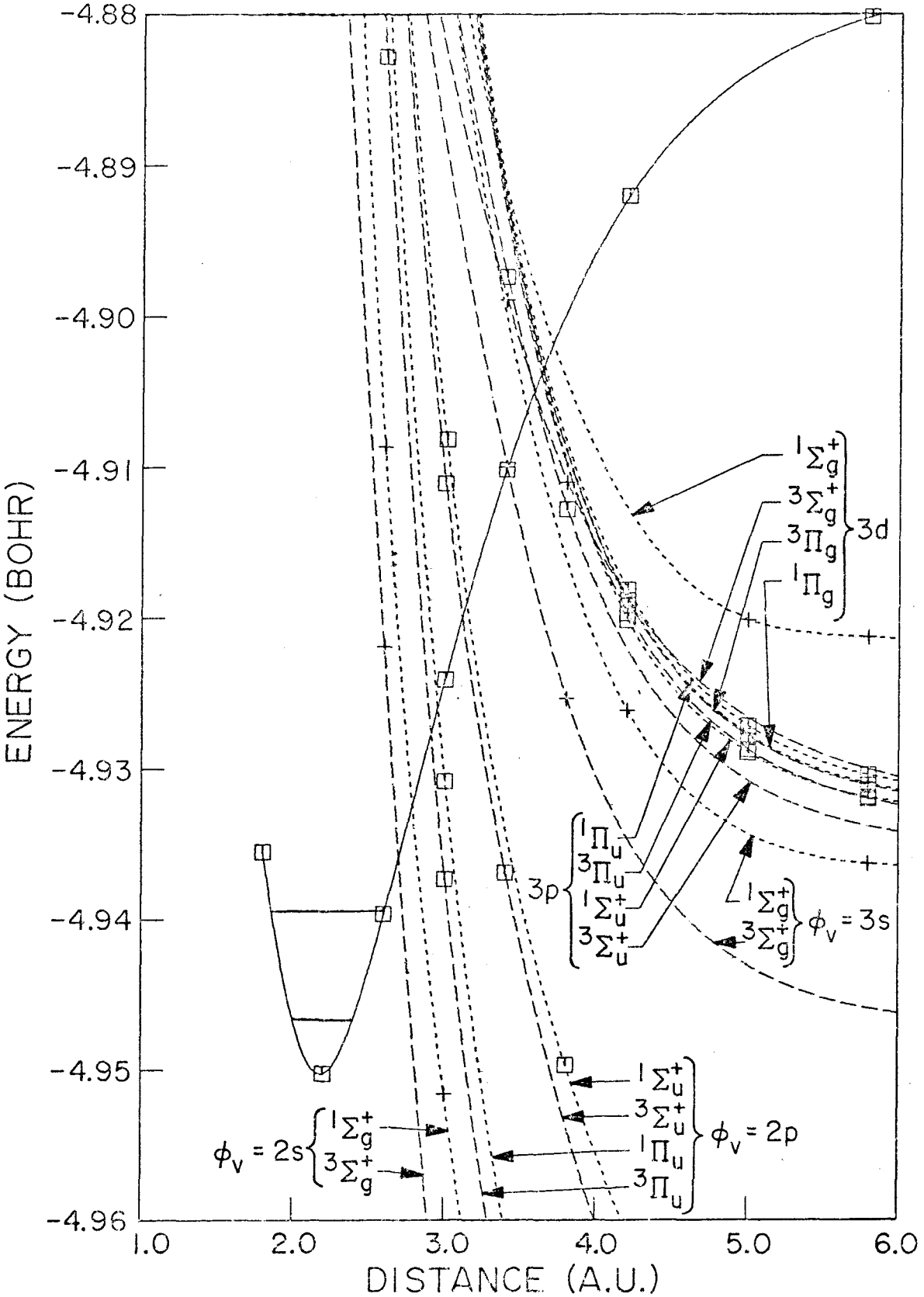
-4.88
-4.89
-4.90
-4.91
-4.92
-4.93
-4.94
-4.95
-4.96
ENERGY (BOHR)
1.0
2.0
3.0
4.0
5.0
6.0
DISTANCE (A.U.)
$^1\Sigma_g^+$
$^3\Sigma_g^+$
$^3\Pi_g$
$^1\Pi_g$
3d
$^1\Pi_u$
$^3\Pi_u$
$^1\Sigma_u^+$
$^3\Sigma_u^+$
3p
$^1\Sigma_g^+$
$^3\Sigma_g^+$
$\phi_v = 3s$
$^1\Sigma_u^+$
$^3\Sigma_u^+$
$^1\Pi_u$
$^3\Pi_u$
$\phi_v = 2p$
$\phi_v = 2s$
$^1\Sigma_g^+$
$^3\Sigma_g^+$

PART II

LOCALIZED WAVEFUNCTIONS FOR H_2O, OH, AND O

INTRODUCTION

The study reported in this section was completed approximately $2\frac{1}{2}$ years ago. Here we are not concerned with spatial projection of the type discussed in Part I since its use in systems of the size discussed here would make the computing inordinately expensive. As a result we want to compromise and use a method which although less pleasing, nevertheless leads to reliable and meaningful results while allowing the computing to be tractable. Here we have made use of the GF method in which the orbitals of each spin set are taken to be orthogonal, leading to great simplifications in the resulting wavefunctions. Since the exact many electron wavefunction forms a basis for a representation of the symmetry group of the molecule we want to retain such symmetry in the many electron GF wavefunction. This in general requires that the GF orbitals be symmetry functions. For more complicated methods such as G1, the projection operator allows for the correct many electron symmetry without requiring that the orbitals be symmetry functions. Thus the orbitals may localize into distributions which are more appealing to our chemical intuition, i.e., bonding, nonbonding orbitals, etc. In order to obtain such orbitals from a GF calculation we have made use of the freedom which we have to take unitary transformations among the orbitals of each spin set in the GF wavefunction. Such transformations do not change the wavefunction. Here we have applied an external localization criterion to take advantage of this property.

It is important that in constructing our localized orbitals we eliminate as many nonphysical restrictions as is possible. For example, in the HF method the orbitals are required to be doubly occupied. But there is no a priori reason why electrons must be spatially distributed in pairs. This restriction is relaxed in the GF method and the orbitals can be singly occupied. Thus the orbitals obtained here may be reasonable approximations to orbitals obtained using presently untractable methods based on more appropriate projection operators. As for GF such methods also utilize singly occupied orbitals leading to the correct dissociation of the wavefunction. In several of the systems discussed here, especially O and OH, this advantage of GF over HF is indeed quite important. Below we report the localized GF wavefunctions for O, OH and H_2O and we compare the changes in the orbitals as we proceed from system to system. We will see that the orbitals of these systems change in a reasonable and continuous way and lead to a perspicacious description of the bonding in H_2O and OH.

Please Note:

Pages 171-182, "Spin-Generalized SCF Wavefunctions for H_2O, OH, and O," copyright 1970 by the Journal of Chemical Physics, not microfilmed at request of author. Available for consultation at the California Institute of Technology Library.

University Microfilms.

Reprinted from THE JOURNAL OF CHEMICAL PHYSICS, Vol. 53, No. 5, 1803–1814, 1 September 1970
Printed in U. S. A.

Spin-Generalized SCF Wavefunctions for H_2O, OH, and O*

STEVEN L. GUBERMAN† AND WILLIAM A. GODDARD III‡
Arthur Amos Noyes Laboratory of Chemical Physics,§ California Institute of Technology, Pasadena, California 91109

(Received 4 February 1970)

Wavefunctions from spin-generalized SCF calculations using the GF method, are reported for H_2O, OH, and O. Three different basis sets are examined for each of these systems. The shapes and angles between the localized GF orbitals are described in some detail. It is shown that the resulting GF orbitals change in a chemically reasonable manner as we proceed from O to OH to H_2O. The dipole and quadrupole moments, electric fields, field gradients, densities, and potentials are reported for the GF wavefunctions.

I. INTRODUCTION

We have previously discussed the GF method,[1,2] a generalization of the Hartree–Fock (HF) method for electronic wavefunctions, which allows all of the spatial orbitals to be different (i.e., no double occupations), but which leads to the correct spin symmetry for the many-electron wavefunction. As discussed before,[2] the GF method leads to a wavefunction equivalent to the one which would be obtained by optimizing the orbitals of a spin-projected Slater determinant *after* the projection. Thus these orbitals are equivalent to those which would be obtained by the spin-polarized extended Hartree–Fock (SPEHF) method.[4] GF wavefunctions have been previously reported for several molecules including H_2,[3] LiH,[3] Li_2,[2] CH_2,[2] and CH_4.[2] Here we report the localized GF wavefunctions for the ground states of H_2O ($^1A_1$), OH ($^2\Pi$), and O (^3P), and compare the changes in the orbitals as we proceed from O atom to OH to H_2O. We will see that the orbitals of these systems change in a reasonable and continuous way and lead to a perspicacious description of the bonding in H_2O and OH.

II. THE WAVEFUNCTIONS

In the HF method[5] the total wavefunction is a Slater determinant

$$\mathcal{A}\Phi\chi, \tag{1}$$

where $\mathcal{A}$ is the antisymmetrizer,[6] Φ is a product of spatial orbitals

$$\Phi=\phi_{1a}(1)\phi_{2a}(2)\cdots\phi_{na}(n)\phi_{1b}(n+1)\cdots\phi_{mb}(N), \tag{2}$$

and χ is a product of one-electron spin functions

$$\chi=\alpha(1)\alpha(2)\cdots\alpha(n)\beta(n+1)\cdots\beta(N). \tag{3}$$

For the H_2O molecule we have $n=m=5$ ($N=n+m$), and in order that the wavefunction (1) be a singlet state, we force

$$\phi_{ia}=\phi_{ib}, \qquad i=1,\cdots m; \tag{4}$$

that is, we take the orbitals as doubly occupied. However, if we pull one H off to get OH+H, we need five orbitals to describe OH (four doubly occupied and one singly occupied), and one for the H. Thus the dissociated molecule requires at least six different orbitals, and since the HF wavefunction for H_2O has only five different orbitals, the HF wavefunction for H_2O cannot possibly dissociate into the HF wavefunction for OH+H. It is this improper dissociation of HF wavefunctions which has prevented detailed examinations of the nature of bonding by gradually bringing, e.g., OH and H together and following the changes which occur in the orbitals.

In order to get around this problem we replace the $\mathcal{A}$ in (1) by the group operator,[7] G_f^γ, which simultaneously takes care of both the Pauli principle and the spin symmetry. Thus we take the wavefunction as

$$G_f^\gamma\Phi\chi, \tag{5}$$

where Φ and χ are still given by Eqs. (2) and (3), but now it is not necessary to place restrictions on the orbitals of Eq. (2) as in Eqs. (4). The wavefunction in (5) has the correct spin symmetry for all choices of the orbitals ϕ_{ia} and ϕ_{ib}. The G_f^γ operator is defined in terms of Young's orthogonal units[8] O_{rf}^γ and $\omega_{\bar{r}\bar{f}}^{\bar{\gamma}}$ which operate on spatial and spin functions, respectively,[7]

$$G_f^\gamma=\sum_r \zeta_{\sigma rf} O_{rf}^\gamma \omega_{\bar{r}\bar{f}}^{\bar{\gamma}}.$$

Since the many-electron Hamiltonian, $\mathcal{H}$, is independent of spin, the total energy becomes[7]

$$E=\langle\Phi\mid\mathcal{H}\mid O_{ff}\Phi\rangle/\langle\Phi\mid O_{ff}\Phi\rangle. \tag{6}$$

That is, the spin terms immediately cancel out and the energy is the same as if the many-electron wavefunction were spinless with the form

$$O_{ff}\Phi. \tag{7}$$

The O_{ff} operator can be written as[9]

$$O_{ff}=(f^\gamma/n!m!N!)N_f P_f N_f, \tag{8}$$

where f^γ is a constant and N_f and P_f are just the Young column antisymmetrizer and row symmetrizer, respectively,[8] for the f tableau. In this case, N_f antisymmetrizes coordinates 1 through n and $n+1$ through $N=n+m$, and P_f symmetrizes 1 and $n+1$, 2 and $n+2$, 3 and $n+3$, etc. Thus we can write

$$N_f=\{1,2,\cdots n\}'\{n+1,\cdots,N\}', \tag{9}$$

$$P_f=\{1,n+1\}\{2,n+2\}\cdots\{m,n+m\}, \tag{10}$$

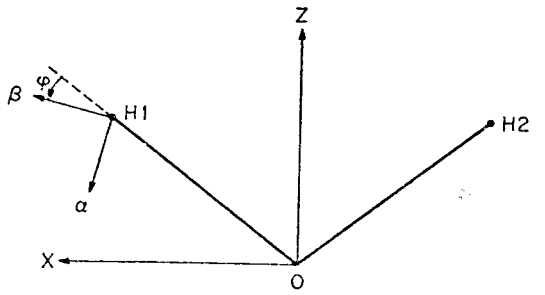

FIG. 1. Coordinates for H_2O. The Y axis is perpendicular to the plane of the molecule.

where $\{\}'$ indicates the antisymmetrizer and $\{\}$ indicates the symmetrizer. Alternative forms for (5) are[7]

$$G_f{}^\gamma\Phi\chi = f^\gamma\mathcal{A}[\Phi(\omega_{\bar{f}\bar{f}}{}^\gamma\chi)] \tag{11}$$

and

$$G_f{}^\gamma\Phi\chi = f^\gamma\mathcal{A}[(O_{ff}{}^\gamma\Phi)\chi]. \tag{12}$$

From form (11) we see that the GF wavefunction is like a Hartree–Fock wavefunction in which the spin function χ is replaced by

$$\omega_{\bar{f}\bar{f}}\chi, \tag{13}$$

which is always an eigenfunction of S^2. Here we have

$$\omega_{\bar{f}\bar{f}} = (f^\gamma/n!m!N!)P_{\bar{f}}N_{\bar{f}}P_{\bar{f}}, \tag{14}$$

where

$$P_{\bar{f}} = \{1, 2, \cdots n\}\{n+1, \cdots, N\},$$
$$N_{\bar{f}} = \{1, n+1\}'\{2, n+2\}'\cdots\{m, N\}'. \tag{15}$$

Alternatively from Eq. (12) we could view the GF wavefunction as one in which the Φ of the HF wavefunction is replaced by $O_{ff}\Phi$. Of course, using either form (11) or (12) would still result in the expression (6) for the total energy after summing over all the spins and using Eqs. (16), (17), and (4) of Ref. 7. Because of the N_f in (8), the orbitals $\{\phi_{ia}\}$ can be taken as orthogonal[1] as can the orbitals $\{\phi_{ib}\}$.

TABLE I. Coefficients and exponents for the oxygen (9s, 5p, 1d) and hydrogen (4s) Gaussian primitives.

Exponents[a]	Coefficients[a,b]	Type[d]	Contraction[b]
	Hydrogen		
19.2406[c]	0.03283	1s	
2.8992[c]	0.23121	1s	1s
0.6534[c]	0.81724	1s	
0.1776[c]	1.0	1s	1s'
	Oxygen		
7816.54	0.00203	1s	
1175.82	0.01544	1s	
273.188	0.07377	1s	1s
81.1696	0.24761	1s	
27.1836	0.61183	1s	
3.4136	0.24120	1s	
9.5322	1.0	1s	1s'
0.9398	1.0	1s	2s
0.2846	1.0	1s	2s'
35.1832	0.01958	2p	
7.9040	0.12419	2p	2$p_{x,y,z}$
2.3051	0.39473	2p	
0.7171	0.62738	2p	
0.2137	1.0	2p	2$p_{x,y,z}'$
0.760	1.0	3d_{x^2}	3d_{x^2}
0.760	1.0	3d_{y^2}	3d_{y^2}
0.760	1.0	3d_{z^2}	3d_{z^2}
0.760	1.0	3d_{xz}	3d_{xz}
0.760	1.0	3d_{yz}	3d_{yz}

[a] s and p exponents from S. Huzinaga, Ref. 18.
[b] s and p contractions from T. H. Dunning, Ref. 19.
[c] These exponents have been scaled to approximate a Slater orbital with an exponent of 1.2.
[d] By $3d_{x^2}$ we mean $Nx^2\exp(-\zeta r^2)$, where N is a normalization factor; i.e., $3d_{x^2}$ is *not* a pure d orbital. Thus $(3d_{x^2}+3d_{y^2}+3d_{z^2}) = Nr^2\exp(-\zeta r^2)$ is a (unnormalized) 3s Gaussian orbital.

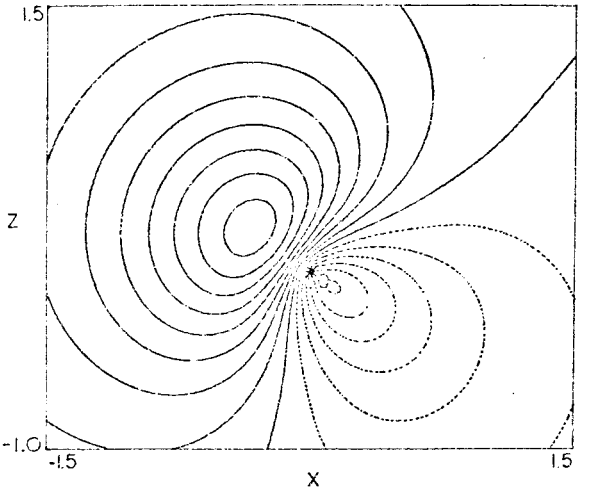

FIG. 2. One of the a LGF valence orbitals of O (plotted in the plane containing $\nabla\phi_{\bar{z}}$). The first solid contour is the node. The other solid lines are positive contours and the dashed lines are negative contours. The interval between contours is 0.1 a.u.

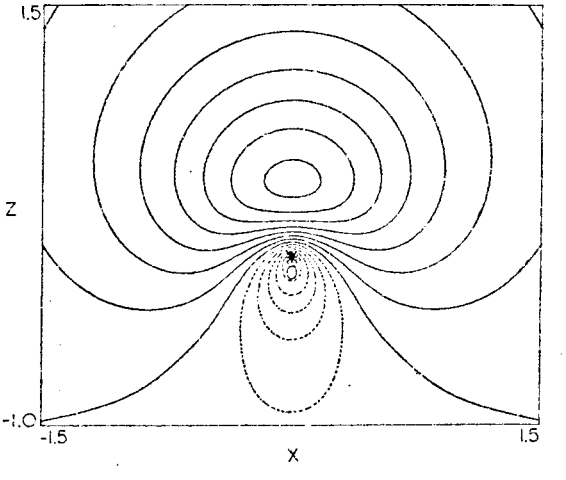

FIG. 3. One of the b LGF valence orbitals of O (plotted in the plane containing $\nabla\phi_{\bar{x}}$). See Fig. 4 for contour values.

TABLE II. The LGF orbitals for the ground state of H_2O ($^1A_1$) using the [521/2] basis.

		a orbitals			*b* orbitals		
		Core	Nonbond[a]	Bond[a]	Core	Nonbond[a]	Bond[a]
H_1	$1s$	−0.00621	0.01120	0.11743†	−0.00919	0.03229	0.45442†
	$1s'$	0.00199	0.02727	0.05282†	0.00186	0.03617	0.18589†
H_2	$1s$	−0.00621	0.01120	−0.01164†	−0.00919	0.03229	−0.03834†
	$1s'$	0.00199	0.02727	−0.02725†	0.00186	0.03617	−0.05056†
O	$1s$	0.59602	0.03332	−0.03076	0.59192	0.03258	−0.01784
	$1s'$	0.48959	0.07615	−0.06834	0.47687	0.06797	−0.03351
	$2s$	−0.10953	−0.37444	0.34759	−0.04424	−0.22865	0.10239
	$2s'$	−0.05620	−0.24236	0.12277	−0.07298	−0.44557	0.07584
	$2p_x$	0.0	0.0	0.56705*	0.0	0.0	0.23096*
	$2p_x'$	0.0	0.0	0.11940*	0.0	0.0	0.16126*
	$2p_y$	0.0	0.61435*	0.0	0.0	0.39163*	0.0
	$2p_y'$	0.0	0.15583*	0.0	0.0	0.42294*	0.0
	$2p_z$	0.00859	0.41436	0.41627	0.01869	0.22249	0.20010
	$2p_z'$	0.00431	0.10587	0.09161	0.01761	0.22915	0.18946
	$3d_{z^2}$	−0.00792	−0.02328	0.00978	0.00387	0.00543	0.01644
	$3d_{y^2}$	0.00045	0.01054	−0.01148	0.00245	−0.02018	−0.00263
	$3d_{x^2}$	−0.00237	0.03462	0.03681	0.00404	0.00677	0.02104
	$3d_{xz}$	0.0	0.0	0.03242*	0.0	0.0	0.03629*
	$3d_{yz}$	0.0	0.03757*	0.0	0.0	0.01069*	0.0

[a] Other nonbonding and bonding orbitals are obtained by changing the sign of functions denoted by * and interchanging the coefficients for H_1 and H_2 basis functions denoted by †.

In the GF method we require that the energy, Eq. (6), be stationary under variations of the orbitals in Φ. This results in the equations

$$H_a\phi_{ia}=\epsilon_{ia}\phi_{ia}, \qquad i=1, 2, \cdots, n$$

$$H_b\phi_{ib}=\epsilon_{ib}\phi_{ib}, \qquad i=1, 2, \cdots, m, \qquad (16)$$

for the optimum orbitals. That is, we have two one-particle Hamiltonians to solve, rather than one as in the HF case. The construction and solution of these equations has been discussed elsewhere.[1,2]

As shown before, the spin projected wavefunction

$$\Theta^S\mathcal{A}\Phi\chi \qquad (17)$$

can be written as

$$\Theta^S\mathcal{A}\Phi\chi=\mathcal{A}[\Phi(\omega\bar{j}j\chi)] \qquad (18)$$

for the case $M_S=S$. The optimum wavefunction of the form (17) where Φ and χ are product functions as in Eqs. (2) and (3), has been called the spin-polarized extended Hartree–Fock wavefunction,[3,4] which we see

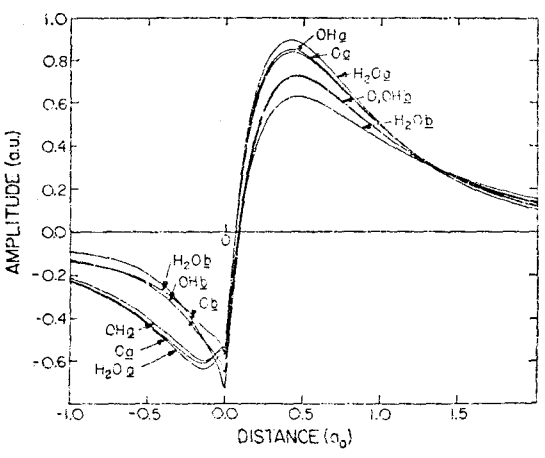

FIG. 4. The LGF orbitals of O and the LGF nonbonding orbitals of H_2O and OH (each is plotted along its axis).

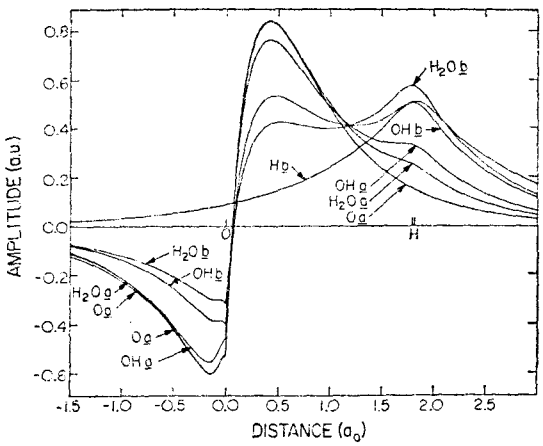

FIG. 5. The LGF bonding orbitals in H_2O and OH (each is plotted along the line connecting O and H). In addition, we show an LGF sp^2 O orbital (plotted along its axis) and the H orbital appropriate for a free hydrogen (scale 1.0).

TABLE III. The LGF orbitals for the ground state of OH ($^2\Pi$) using the [521/2] basis set.

		a orbitals				*b* orbitals		
		Core	Bond	Nonbond	Nonbond*	Core	Bond	Nonbond*
a orbitals								
H	$1s$	0.00679	0.17954	0.02342	0.02342	0.00856	0.38027	0.05009
	$1s'$	0.00464	0.02977	0.02696	0.02696	0.00428	0.20688	0.07374
O	$1s$	0.59554	−0.02652	0.03224	0.03224	0.59472	−0.02288	0.03826
	$1s'$	0.48729	−0.05715	0.07219	0.07219	0.48145	−0.04459	0.08217
	$2s$	−0.09260	0.27059	−0.33365	−0.33365	−0.06542	0.18947	−0.31433
	$2s'$	−0.06815	0.11796	−0.25812	−0.25812	−0.08047	0.01073	−0.45360
	$2p_x$	0.0	0.0	0.0	0.56187*	0.0	0.0	0.48245*
	$2p_x'$	0.0	0.0	0.0	0.22615*	0.0	0.0	0.32730*
	$2p_y$	0.0	0.0	−0.65225	0.32612	0.0	0.0	0.0
	$2p_y'$	0.0	0.0	−0.26113	0.13056	0.0	0.0	0.0
	$2p_z$	0.00888	0.64387	0.20114	0.20114	0.01723	0.40859	0.20220
	$2p_z'$	0.00309	0.20687	0.06935	0.06935	0.01078	0.19260	0.11826
	$3d_{z^2}$	−0.00268	−0.00470	−0.01085	−0.01085	0.00487	−0.00439	0.01418
	$3d_{y^2}$	−0.00268	−0.00470	−0.01085	−0.01085	0.00487	−0.00439	0.01418
	$3d_{x^2}$	0.0	0.05455	0.01870	0.01870	−0.00001	0.06755	−0.00073
	$3d_{xz}$	0.0	0.0	0.0	0.02256*	0.0	0.0	0.01763*
	$3d_{yz}$	0.0	0.0	−0.02605	0.01302	0.0	0.0	0.0

* The coefficients of another nonbonding orbital are obtained from this orbital by changing the sign of the coefficients denoted *.

from Eqs. (18) and (11) is equivalent to the GF wavefunction.

III. LOCALIZATION OF ORBITALS

It is well known that for a closed-shell singlet state the many-electron Hartree–Fock determinant remains invariant under a unitary transformation among the spatial orbitals.[10] This property has been used[11,12] to find a transformation matrix which changes the Hartree–Fock symmetry orbitals to more chemically reasonable orbitals. Lennard-Jones and Pople[12] noticed that a transformation to equivalent orbitals results in an increase in the sum of the self-repulsion integrals,

$$J[\phi]=\sum_{i=1}^{N} J_{ii}, \tag{19}$$

where

$$J_{ii}=\langle\phi_i(1)\phi_i(2)\mid 1/r_{12}\mid\phi_i(1)\phi_i(2)\rangle. \tag{20}$$

Edmiston and Ruedenberg[13] have discussed several criteria which could be used to obtain the orbitals which are most localized. Of these they especially considered

TABLE IV. The LGF orbitals for the ground state of O (^{3}P) using the [521/2] basis.

	a orbitals			*b* orbitals	
	Core	Hybrid*	Hybrid*	Core	Hybrid*
$1s$	0.59588	−0.03099	−0.03099	0.59593	0.04257
$1s'$	0.48841	−0.06950	−0.06950	0.48299	0.09119
$2s$	−0.09823	0.33011	0.33011	−0.07183	−0.35670
$2s'$	−0.06538	0.21487	0.21487	−0.08543	−0.44300
$2p_x$	0.0	0.57582*	0.0	0.0	0.0
$2p_x'$	0.0	0.21195*	0.0	0.0	0.0
$2p_y$	0.0	0.0	0.57582*	0.0	0.0
$2p_y'$	0.0	0.0	0.21195*	0.0	0.0
$2p_z$	0.0	0.40717	−0.40717	0.0	0.50361*
$2p_z'$	0.0	0.14987	−0.14987	0.0	0.30313*
$3d_{x^2}$	−0.00235	0.00520	0.00520	0.00409	0.00872
$3d_{y^2}$	−0.00235	0.00520	0.00520	0.00409	0.00872
$3d_{z^2}$	−0.00235	0.00520	0.00520	0.00409	0.00872

* Another hybrid orbital is obtained by changing the signs of the coefficients marked *.

TABLE V. Angles[a] in degrees between the LGF orbitals.

Orbitals	Slater basis (21/1)		Gaussian basis [42/2]		Gaussian basis [521/2]	
	a	*b*	*a*	*b*	*a*	*b*
O	109.5	180.0	109.5	180.0	109.5	180.0
OH						
Nonbond–Bond	105.1	108.2	107.8	110.4	107.1	112.7
Nonbond–Nonbond	113.3	143.6	111.1	139.2	111.6	134.6
H_2O						
Bond–Bond	103.2	79.2	106.9	96.5	107.4	97.8
Nonbond–Nonbond	114.4	130.5	112.1	123.1	112.0	120.9
Bond–Nonbond	109.7	108.8	109.4	108.5	109.3	108.9

[a] Angles between $\nabla\phi_i$ evaluated at the *O*.

the Lennard-Jones–Pople criterion of maximizing $J[\phi]$. In addition, they proposed a simple method for finding the corresponding transformation matrix U. Ruedenberg and coworkers applied this approach to a number of systems[12] including H_2O.[15] Pitzer applied a similar method to C_2H_6.[16]

In order to localize GF wavefunctions, we note[1] that because of the Young antisymmetrizer N_f in Eq. (8), the GF wavefunction transforms as $(\det U^a)(\det U^b)$ under unitary transformations U^a on the orbitals $\{\phi_{ia}\}$ and U_b on the orbitals $\{\phi_{ib}\}$. Thus if we consider

$$\bar{\phi}_{ia} = \sum_{j=1}^{n} \phi_{ja} U_{ji}^{a},$$

$$\bar{\phi}_{ib} = \sum_{j=1}^{m} \phi_{jb} U_{ji}^{b}, \tag{21}$$

and if we take

$$\bar{\Phi} = \bar{\phi}_{1a}\bar{\phi}_{2a}\cdots\bar{\phi}_{na}\bar{\phi}_{1b}\cdots\bar{\phi}_{mb}, \tag{22}$$

we obtain

$$O_{ff}\bar{\Phi} = (\det U^a)(\det U^b) O_{ff}\Phi \tag{23}$$

and

$$G_f\bar{\Phi}\chi = (\det U^a)(\det U^b) G_f\Phi\chi. \tag{24}$$

Consequently, the energy and all other properties of the wavefunction are unchanged[1] by the transformations of Eqs. (21).

For the GF wavefunction we determine U^a and U^b by maximizing

$$J^a[\phi] = \sum_{i=1}^{n} J_{ia,ia} \tag{25}$$

and

$$J^b[\phi] = \sum_{i=1}^{m} J_{ib,ib}, \tag{26}$$

respectively. That is, we use a natural extension of the Lennard-Jones–Pople criterion for determining U_a and U_b. For open-shell restricted Hartree–Fock wavefunctions, the orbitals could also be localized by the

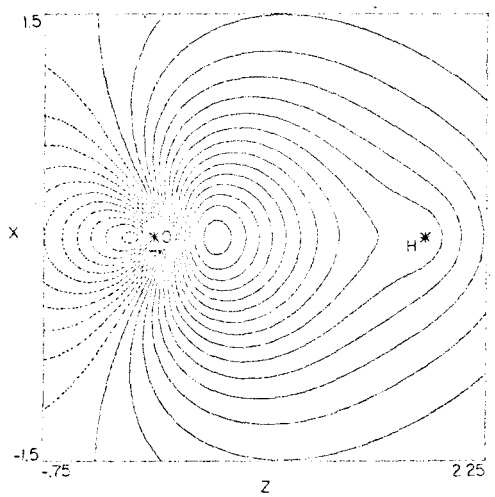

FIG. 6. The σ LGF bonding orbital of OH. The first solid contour is the node. The other solid lines are positive contours and the dashed lines are negative contours. The interval between contours is 0.05 a.u.

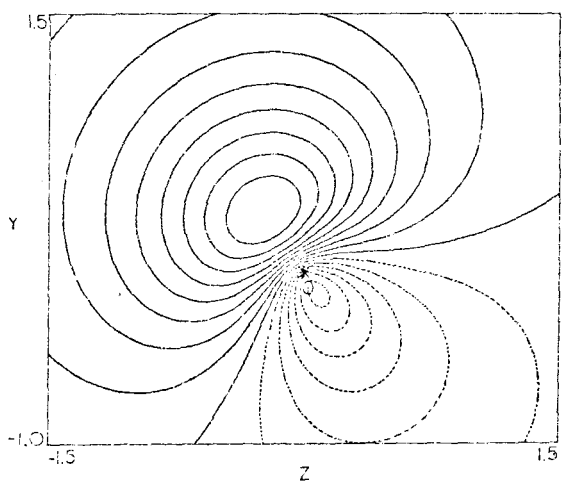

FIG. 7. One of the σ LGF nonbonding orbitals of OH (plotted in the plane containing $\nabla\varphi_i$). See Fig. 4 for contour values.

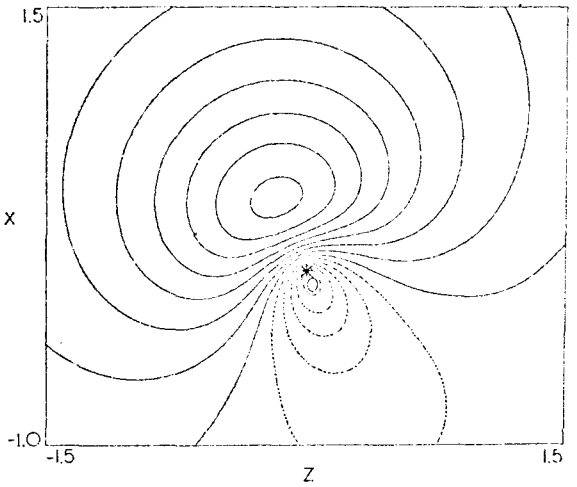

FIG. 8. One of the b LGF nonbonding orbitals of OH (plotted in the plane of these orbitals). See Fig. 4 for contour values.

above method if the doubly occupied orbitals were split and half considered as ϕ_{ia} and the other half considered as ϕ_{ib}. However, there seem to have been no such localizations reported for nonsinglet systems, such as OH and O. [*Note added in proof*: This approach has recently been applied to O_2 and NO. See D. M. Hirst and M. E. Linington, Theoret. Chim. Acta **16**, 55 (1970)].

In order to distinguish the localized GF orbitals from the canonical GF orbitals [i.e., the solutions of Eqs. (16)], we denote the former as the LGF orbitals.

IV. CALCULATIONS

The calculations were carried out for the ground states of H_2O ($^1A_1$), OH ($^2\Pi$), and O (^3P). A Slater basis set and two contracted Gaussian basis sets (centered on the nuclei) were investigated. The Slater set was a minimal basis with orbital exponents optimized for Hartree–Fock H_2O.[17] One of the Gaussian sets consisted of a $(9s5p/4s)$ primitive set of functions based on Huzinaga's[18] orbital exponents and contracted to a $[4s2p/2s]$ double-zeta-like basis set according to the Dunning principles.[19] This contraction increases the HF energy for H_2O by only 0.0040 a.u. (-76.0132 a.u. for $(9s5/4)$ and -76.0092 a.u. for $[42/2]$).[19] The second Gaussian set differed from the first in having an additional set of five d-like oxygen Gaussian orbitals, d_{x^2}, d_{y^2}, d_{z^2}, d_{xz}, and d_{yz} (see Fig. 1 for the coordinates). Here by d_{x^2} we mean $Nx^2\exp(-\zeta r^2)$, where N is a normalization factor. Thus $(d_{x^2}+d_{y^2}+d_{z^2})=Nr^2\times\exp(-\zeta r^2)$ is a (unnormalized) pure $3s$ Gaussian orbital and $(2\cdot d_{z^2}-d_{x^2}-d_{y^2})$ and $(d_{x^2}-d_{y^2})$ are (unnormalized) pure $3d$ Gaussian orbitals. Since this is equivalent to adding a $3s$ orbital and a set of $3d$ orbitals to the $[42/2]$ set, we will denote the new one as $[521/2]$ (by symmetry we know that the d_{xy} orbital cannot be used in the states considered here). The exponent of the d orbitals was optimized for the $[521/2]$ H_2O Hartree–Fock wavefunction and was found to be 0.760. These basis sets were also used in the O and OH calculations in order to allow consistent comparisons between these systems.

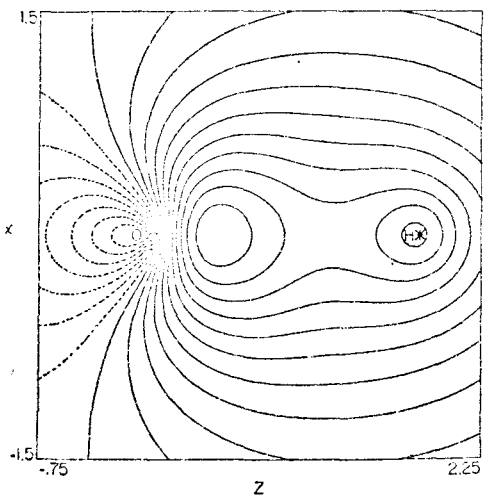

FIG. 9. The b LGF bonding orbital of OH. See Fig. 6 for contour values.

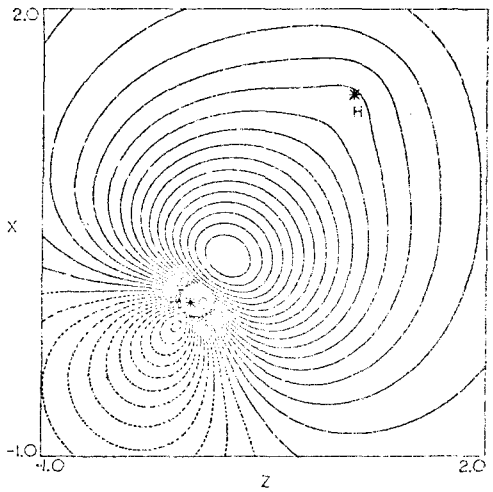

FIG. 10. One of the a LGF bonding orbitals of H_2O. See Fig. 6 for contour values.

For O and OH it was necessary to symmetry average the GF matrix Hamiltonians in order to obtain the correct spatial symmetry for the many-electron wavefunction. For these systems this is equivalent to the averaging over degenerate states used in the Roothaan open-shell formulation.[20] For OH and O this results in equivalent a type π_x and π_y orbitals and equivalent a type p_x, p_y, and p_z orbitals, respectively. As discussed below the resulting energy and properties are quite similar to those obtained when these spatial symmetry equivalence restrictions are not applied. The spatially unsymmetric wavefunctions have symmetries appropriate for the symmetry group $D_{\infty h}$ rather than SO(3) for O and C_{2v} rather than $C_{\infty v}$ for OH.

Irrespective of whether we apply the symmetry equivalence restriction, the final GF orbitals have been restricted to be symmetry functions of the appropriate group [SO(3) for O and $C_{\infty v}$ for OH] by choosing the trial vectors as symmetry functions. An exception to this occurs for the [521/2] basis where d character mixed into the O s orbitals and δ character mixed into the OH σ orbitals. In these latter cases it was necessary to apply a spatial symmetry restriction in order for the GF orbitals to be symmetry functions. For the other bases it is likely that if no symmetry restrictions whatsoever are imposed, the GF orbitals of O and OH would not be exactly s and p or σ and π, respectively. (This often occurs for the UHF and GI wavefunctions of nonsinglet systems.) However the energy improvement would be expected to be small and the resulting many-electron wavefunction would not

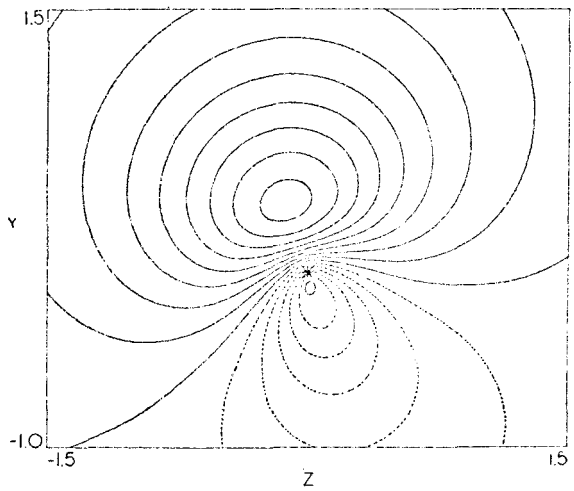

FIG. 11. One of the a nonbonding orbitals of H_2O (plotted in the plane perpendicular to the plane of the molecule). See Fig. 4 for contour values.

have the correct total symmetry (^3P for O, $^2\Pi$ for OH, and $^1A_1$ for H_2O). All the LGF orbitals reported here are those which were obtained from spatial symmetry restricted GF orbitals. In addition, for H_2O and for the OH and O wavefunctions where the symmetry equivalence restriction is applied the total wavefunction has the correct spatial symmetry.

Throughout the calculations the experimental OH and H_2O geometries have been assumed. These are 1.8342 a.u.[21] and 1.8111 a.u.[22] for the O–H distance in OH and H_2O, respectively, and 104°27 [22] for the HOH angle. The only exception to this is the Slater MBS calculation on H_2O where an O–H distance of 1.8103 a.u. was used with an HOH angle of 105°. The coordinates and geometry used for H_2O are shown in Fig. 1.

The contraction coefficients for the Gaussian bases are given in Table I. The LGF orbital coefficients in terms of these contracted coefficients for the [521/2]

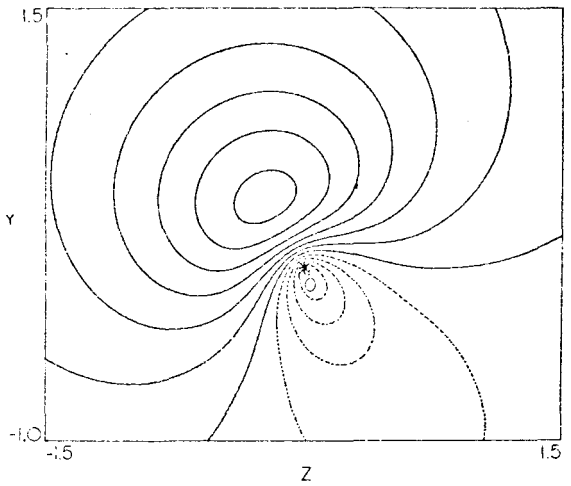

FIG. 12. One of the b nonbonding orbitals of H_2O (plotted in the plane perpendicular to the plane of the molecule). See Fig. 4 for contour values.

basis are shown in Table II for H_2O, Table III for OH, and Table IV for O.[23] In Table V we show the angles between the LGF orbitals.

V. DISCUSSION OF THE LGF ORBITALS

For all three systems, H_2O, OH, and O, there are two orbitals (ϕ_{1a} and ϕ_{1b}) which are essentially the same and are referred to as oxygen 1s-like core orbitals. Since these orbitals are similar in all three systems we will omit them from the following discussion. We will also limit the discussion to the results of the [521/2] Gaussian calculation; the results for the other basis sets are quite similar.

In Fig. 2 we show a contour plot taken in the plane bisecting one of the four tetrahedrally oriented a valence orbitals of the O atom. Each of these orbitals has 75% p character[24] and can reasonably be described as an sp^3 hybrid (the symmetry restriction requires the

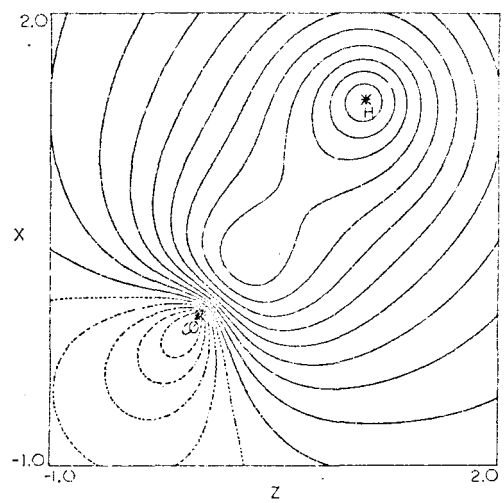

FIG. 13. One of the b LGF bonding orbitals of H_2O. See Fig. 6 for contour values.

TABLE VI. Total energies.[a]

	Basis	GF	HF	Experimental
H_2O	(10, 62/42), GTO	...	−76.03936[d]	−76.481[f]
	[521/2], GTO	−76.07804	−76.03500	
	[42/2], GTO	−76.05269	−76.0092[e]	
	(21/1), STO	−75.73384	−75.70332[g]	
OH	Cade and Huo, STO[b]	...	−75.42083	−75.780[b]
	[521/2], GTO	−75.41483	...	
	[521/2][c], GTO	−75.10992	...	
	[42/2], GTO	−75.39331	...	
	[42/2][c], GTO	−75.39321	...	
	(21/1), STO	−75.10592	−75.0600[g]	
O	(74), STO	−74.81684[j]	−74.80935[h]	−75.1101[h]
	[52], GTO	−74.81056	...	
	[52][c], GTO	−74.80548	...	
	[42], GTO	−74.80525	−74.79313[i]	
	[42][c], GTO	−74.80525	...	
	(21), STO	−74.54036	−74.54036[i]	

[a] All energies are in atomic units, 1 hartree = 27.2108 eV.
[b] P. E. Cade and W. M. Huo, Ref. 29.
[c] These wavefunctions were restricted to have the correct spatial symmetry for the many-electron wavefunction (see Sec. IV).
[d] D. Neumann and J. W. Moskowitz, Ref. 27.
[e] T. H. Dunning, Ref. 19.
[f] S. Aung, R. M. Pitzer, and S. I. Chan, Ref. 30.
[g] A. J. Freeman, Rev. Mod. Phys. 32, 273 (1960).
[h] W. A. Goddard III, Ref. 34.
[i] Reference 27. Note that the exponents and contraction scheme for the s functions differs from that reported here.
[j] E. Clementi and D. L. Raimondi, J. Chem. Phys. 38, 2686 (1963).

d orbitals to add to give only a 3s-like contribution). For the b orbitals we have two orbitals separated by 180°, each containing 50% p character. One of these orbitals is shown in Fig. 3; they will be denoted as sp hybrids. Due to the higher percentage p character, the a orbitals are more directed than the b orbitals, i.e., on the axes of the orbitals, the a orbitals have higher amplitude than the b orbitals up to about 1.4 a_0. This can be seen from inspection of Figs. 2, 3, and 4.

From Figs. 2, 5, and 6 we see that upon formation of a bond between an oxygen tetrahedral orbital and an H atom to form OH, the sp^3 hybrid loses amplitude from the region of the O to the region around the H, and the p character increases slightly to 75.5%. Note that since the GF wavefunction dissociates correctly this a bonding orbital changes continuously to an O sp^3 hybrid as the H is pulled away. Concurrent to this transfer of amplitude the axes of the remaining a orbitals rearrange by about two degrees (see Table V). Thus upon formation of the OH bond the remaining three valence a orbitals move further apart from each other (i.e., the angle between them is greater than tetrahedral) and closer to the a bonding orbital. These three a nonbonding orbitals of OH are quite similar to the a tetrahedral orbitals of O (see Figs. 2, 4, and 7) except that they have lost some p character (down to 73.5%).

In OH we have three coplanar valence b orbitals. Two of the orbitals are concentrated near the O and have an angle of 134.6° between them, instead of 180° as in the O atom. These orbitals are similar in shape to the sp hybrids of O (see Figs. 3, 4, and 8), their p character has increased to 61.2%. The remaining b orbital has high amplitude near the H and is strongly bonding to O. Once again note that since the orbitals are not doubly occupied this orbital changes continuously to an H 1s orbital as the H is withdrawn from the O. From Fig. 9 we see that this orbital is much more concentrated about the bond axis than is the a bonding orbital.

With the addition of a second H to form H_2O we now have a singlet system containing four a and four b valence orbitals. The second H approaches one of the a OH nonbonding orbitals, forming a bond with 74.2% p character (see Fig. 10). From Figs. 4 and 5 we see that the new bonding orbital is quite similar near the O to an O atom sp^3 orbital and an OH a nonbonding orbital. The a bond–bond angle in H_2O is essentially the same as (but slightly larger than) the a nonbond–bond angle in OH. Thus an a nonbonding orbital in OH stays at nearly the same angle from the bonding orbital in OH upon the approach of the second H, forming an H_2O bond and an a bond–bond angle of 107.4°. The remaining two a nonbonding orbitals in OH move about 0.5° farther apart to 112.0° forming the two a nonbonding orbitals in H_2O each having 74.2% p character. These a nonbonding orbitals (see Figs. 4 and 11), which help determine the a bond–bond angle in H_2O have higher amplitude near the oxygen than the a nonbonding orbitals in OH or the sp^3 hybrid in O. However, the b nonbonding orbitals in H_2O (see Figs. 4 and 12) have lower amplitude near the oxygen than the b nonbonding orbitals in OH or the sp hybrids in O. The two nonbonding b orbitals in OH which were in the same plane with the bonding orbital now move closer together and into a plane perpendicular

TABLE VII. Orbital energies and properties of H_2O.[a,b]

	GF [521/2]	GF [42/2]	HF [521/2]	HF [42/2][d]	N-M[e]	APC[f]	Experimental
$-\epsilon(1a_{1,a})$	20.69980	20.70711	20.55385	20.5594	20.55805	20.5654	
$-\epsilon(1a_{1,b})$	20.59129	20.59469					
$-\epsilon(2a_{1,a})$	1.57821	1.59020	1.34661	1.3613	1.35224	1.3392	
$-\epsilon(2a_{1,b})$	1.35907	1.37564					
$-\epsilon(1b_{2,a})$	0.90034	0.89903	0.71326	0.7165	0.71897	0.7283	
$-\epsilon(1b_{2,b})$	0.79428	0.80124					
$-\epsilon(3a_{1,a})$	0.77487	0.77162	0.57732	0.5668	0.58222	0.5950	
$-\epsilon(3a_{1,b})$	0.61803	0.60008					0.533±0.011[j]
$-\epsilon(1b_{1,a})$	0.70928	0.71760	0.50266	0.5063	0.50685	0.5211	
$-\epsilon(1b_{1,b})$	0.51758	0.51614					0.463±0.004[j]
T	76.10192	76.12058	76.03101	···	76.00938	75.662145	
$\langle\Sigma\, 1/r_{ij}\rangle$	37.70780	37.64824	37.83124	···	37.84784	···	
μ	0.87044	1.0331	0.89092	1.0558	0.785	0.8006	0.728[g]
Θ_{xx} (c.m.)[k]	1.83246	1.82715	1.84785	1.8302	1.882	1.96241	···
Θ_{yy} (c.m.)	−1.78654	−1.69641	−1.79664	−1.7077	−1.801	−1.92490	···
Θ_{zz} (c.m.)	−0.04592	−0.13074	−0.05121	−0.1225	−0.0805	−0.03751	···
E_z (O)	−0.12039	−0.24850	−0.11683	−0.2479	−0.010	−0.070247	0.0
E_x (H)	0.04872	0.10770	0.03892	0.1000	0.0	0.001650	0.0
E_z (H)	0.02934	0.04346	0.02150	0.0366	−0.002	−0.003488	0.0
q_{yy} (H)	0.29367	0.31335	0.29073	0.3114	0.294	0.310488	0.2660±0.0005[h]
$q_{\alpha\alpha}$ (H)	0.22630	0.24742	0.22457	0.2467	0.225	0.241506	0.2026±0.0002[h]
$q_{\beta\beta}$ (H)	−0.51997	−0.56077	−0.51531	−0.5581	−0.519	−0.551994	−0.4686±0.0002[h]
φ	0.48472°	2.81122°	0.38660°	2.71667°	0.97°	0.95°	−1.26667°[h]
q_{yy} (O)	1.83137	1.93042	1.94060	2.0517	1.852	1.834756	1.73±0.01[h]
q_{xx} (O)	−1.59238	−1.68230	−1.69955	−1.8084	−1.679	−1.680384	−1.515±0.005[h]
q_{zz} (O)	−0.23899	−0.24812	−0.24104	−0.2432	−0.173	−0.154372	−0.22±0.02[h]
$\delta(r=\mathrm{O})$	294.908	295.027	294.915	295.051	299.497	···	···
$\delta(r=\mathrm{H})$	0.40012	0.42446	0.38037	0.4147	0.392	···	···
$\langle 1/r_{\mathrm{H}}\rangle$[c]	5.76161	5.74368	5.75657	5.7384	5.795	5.744	5.744[i]
$\langle 1/r_{\mathrm{O}}\rangle$[c]	23.44354	23.43973	23.44509	23.4426	23.445	23.38	···
$\langle x^2\rangle_{\mathrm{c.m.}}$[c,k]	7.23003	7.27137	7.18537	7.2315	···	···	···
$\langle y^2\rangle_{\mathrm{c.m.}}$[c]	5.54414	5.52185	5.51648	5.4916	···	···	···
$\langle z^2\rangle_{\mathrm{c.m.}}$[c]	6.44855	6.54289	6.41768	6.5128	···	···	···
$\langle r^2\rangle_{\mathrm{c.m.}}$[c]	19.22272	19.33611	19.11954	19.2359	19.181	19.51	18.2±1.1[j]

[a] All energies and properties are in atomic units.

[b] The expressions for the operators for the properties given here can be found in Ref. 27. We denote the properties as follows: ϵ = orbital energy, μ = dipole moment, Θ_{ij} = elements of quadrupole tensor, $E_i(A)$ = components of electric field at A, $q_{ij}(A)$ = components of electric field gradient tensor at nucleus A, $\delta(r-A)$ = density at nucleus A, $\langle 1/r_A\rangle$ = electronic potential at A, T = total kinetic energy, $\langle\Sigma\, 1/r_{ij}\rangle$ = total electron repulsion energy, and $\langle r^2\rangle$ = expectation value of $\Sigma_i r_i^2$.

[c] Only the electronic contributions are given here.

[d] T. H. Dunning, Ref. 19.

[e] [10,6,2/4,2] HF calculation of Ref. 27. The geometry used here was slightly different from ours.

[f] Taken from wavefunctions IV of Ref. 30 and S. Aung, Ph.D. thesis, California Institute of Technology, 1969.

[g] W. H. Kirchhoff and D. R. Lide, Jr., Ref. 31; 1 a.u. = 2.541539 D.

[h] Calculated from quadrupole coupling constants reported in Ref. 33, assuming an ^{17}O quadrupole moment of −0.025*b* (see Ref. 34) and a *D* quadrupole moment of 0.902796*b* (see Ref. 36). φ is from Ref. 33.

[i] See Ref. 30.

[j] D. Eisenberg, J. M. Pochan, and W. H. Flygare, J. Chem. Phys. 43, 4531 (1965).

[k] c.m. denotes that this quantity was calculated with the center of mass of H_2O as the origin.

[l] W. C. Price and T. M. Sugden, Trans. Faraday Soc. 44, 108 (1948).

to the plane of the bonding orbitals upon approach of the second proton, forming the two *b* nonbonding orbitals in H_2O having a *p* character of 68.7%. These *b* nonbonding orbitals are about 9° further apart from each other than the *a* nonbonding orbitals.

Since the *b* bonding orbitals have their highest amplitude near the H, one should not place too much importance on the *b* bond–bond angles given in Table VII for H_2O since these angles were measured at the O. But the angle is indicative of the bending of the *b* bonding orbital, which can be seen in Fig. 13. One can see from Figs. 10 and 13 and from the indicated bond–bond angles from Table VII that none of the bonding orbitals of H_2O are symmetric about an OH axis.

These results for H_2O should be compared to those of Edmiston and Ruedenberg[36] who obtained 89.8° for the bond–bond angle, and 124° between nonbonding orbitals from localizing a restricted HF wavefunction composed of a minimum basis set of Slater orbitals.

It is often suggested that the bonds in H_2O are *p* bonds. Since such bonds should be at 90°, it is suggested[25] that repulsion between positive hydrogens leads to the actual bond angle of 104.5°. Our calcula-

TABLE VIII. GF orbital energies and properties of OH.[a]

	[521/2] Unsym[b]	[521/2] Sym[b]	[42/2] Unsym[b]	[42/2] Sym[b]	HF	Experimental
$-\epsilon(1\sigma_a)$	20.67152	20.67036	20.67731	20.67507	20.61811[d]	
$-\epsilon(1\sigma_b)$	20.58758	20.58550	20.58832	20.58825		
$-\epsilon(2\sigma_a)$	1.49912	1.49914	1.51150	1.51091	1.30684[d]	
$-\epsilon(2\sigma_b)$	1.21604	1.20965	1.21976	1.22005		
$-\epsilon(3\sigma_a)$	0.73871	0.73802	0.74406	0.74324	0.66041[d]	
$-\epsilon(3\sigma_b)$	0.63072	0.62820	0.61324	0.61301		
$-\epsilon(1\pi_{x,a})$	0.61390	0.80155	0.62694	0.80051	0.57215[d]	
$-\epsilon(1\pi_{x,b})$	0.49495	0.48279	0.48549	0.48797		0.4910[f]
$-\epsilon(2\pi_{y,a})$	0.67143	0.80155	0.66263	0.80051	0.57215[d]	
T	75.43989	75.43681	75.45063	75.45089		
$\langle\sum 1/r_{ij}\rangle$	32.87772	32.88330	32.84718	32.84891		
μ	0.73684	0.73775	0.83655	0.83604	0.7005[e]	0.6531[g]
Θ_{xx} (c.m.)[c]	−1.34877	−1.35575	−1.28123	−1.29285		
Θ_{yy} (c.m.)	0.12566	0.13486	0.17479	0.18750		
Θ_{zz} (c.m.)	1.22312	1.22090	1.10644	1.10533		
E_z (O)	−0.10160	−0.10198	−0.20117	−0.20113		
E_z (H)	0.05058	0.05071	0.12189	0.12182		
q_{yy} (H)	0.19305	0.19363	0.22384	0.22357		
q_{xx} (H)	0.28005	0.27941	0.30294	0.30321		
q_{zz} (H)	−0.47310	−0.47304	−0.52678	−0.52679		
q_{yy} (O)	−2.11798	−2.05698	−2.06161	−2.00819		
q_{xx} (O)	2.63851	2.56571	2.70608	2.65473		
q_{zz} (O)	−0.52054	−0.50873	−0.64447	−0.64655		
$\delta(r-\mathrm{O})$	295.786	295.797	295.893	295.884		
$\delta(r-\mathrm{H})$	0.39328	0.39333	0.42569	0.42574		
$\langle 1/r_{\mathrm{H}}\rangle$[b]	5.32241	5.32228	5.30582	5.30598		
$\langle 1/r_{\mathrm{O}}\rangle$[b]	22.84647	22.84617	22.84347	22.84356		
$\langle x^2\rangle_{\mathrm{c.m.}}$[b,c]	4.92234	4.92930	4.90125	4.90830		
$\langle y^2\rangle_{\mathrm{c.m.}}$[b]	3.93939	3.93556	3.93058	3.92141		
$\langle z^2\rangle_{\mathrm{c.m.}}$[b]	3.20775	3.21153	3.30947	3.30953		
$\langle r^2\rangle_{\mathrm{c.m.}}$[b]	12.06948	12.07659	12.14130	12.13924		

[a] All energies and properties are in atomic units.

[b] These include only the electric contribution.

[c] c.m. denotes that this property was calculated with the center of mass of OH as origin.

[d] P. E. Cade and W. M. Huo, Ref. 29.

[e] P. E. Cade and W. M. Huo, J. Chem. Phys. 45, 1063 (1966).

[f] P. G. Wilkinson, Astrophys. J. 138, 778 (1963).

[g] F. X. Powell and D. R. Lide, Jr., Ref. 32.

[h] Sym implies that equivalence restrictions were imposed on the π_x and π_y orbitals and the d_{x^2}, d_{y^2}, and d_{z^2} basis functions (see Sec. IV). Unsym implies that these symmetry restrictions were not imposed.

tions do not support either of these suggestions. We saw that the a bonding orbitals have about 75% p character and can reasonably be considered as sp^2 orbitals. Thus the assumption of p bonds is not justified. In addition, we saw that the angle between the bonding and nonbonding orbitals of OH did not change appreciably when the H was bonded to the nonbonding orbital. If H repulsions were important, we would have expected this angle to increase. Although the GF orbitals lead to a reasonable explanation of the bonding in H_2O, a significant test will be whether it also does so for molecules such as H_2S, where the bonding angle is much different (92°).

In recent years Linnett[26] has proposed a novel model of bonding in which the familiar Lewis octet is replaced by a double quartet, one quartet for each spin. In Linnett's model a quartet of electrons of the same spin should be at the vertices of a tetrahedron in order to minimize the electron repulsion energy. The electrons of the molecule are then shared in such a way as to complete tetrahedral quartets about each atom often leading to a Lewis octet. Although this model is based on nonquantitative semiclassical reasoning, it does lead to compelling descriptions of some molecules, especially nonsinglet states such as O_2. It is interesting to note here that for H_2O and a number of other systems which we have considered (e.g., C_2H_2, NH, HF), the LGF orbitals are distributed in space in a way qualitatively similar to Linnett's quartets. Of course the LGF orbitals are not centered on just one atom and the bonding orbitals are paired with one orbital more near one center than the other. Water is not the best system for discussing this since there is only one octet (however note that for O, OH, and H_2O the a quartet is always within 3° of tetrahedral); C_2H_2 and BF are more appropriate and especially for C_2H_2 the results are consistent with Linnett's model. This will be discussed in more detail in a future paper,

TABLE IX. GF orbital energies and properties of O.[a]

	[521] Unsym[b]	[521] Sym[b]	[42] Unsym[b]	[42] Sym[b]	(74) STO[d]	Experimental
$-\epsilon(1s_a)$	20.73566	20.73570	20.73683	20.73677	20.73879	•••
$-\epsilon(1s_b)$	20.62570	20.62490	20.62368	20.62368	20.62834	•••
$-\epsilon(2s_a)$	1.53034	1.53072	1.52990	1.52983	1.53886	•••
$-\epsilon(2s_b)$	1.06748	1.06192	1.06237	1.06239	1.06471	•••
$-\epsilon(2p_{x,a})$	0.64725	0.84521	0.65838	0.84456	0.66813	•••
$-\epsilon(2p_{x,b})$	0.51003	0.49748	0.49743	0.49759	0.49695	0.50052[e]
$-\epsilon(2p_{y,a})$	0.71096	0.84521	0.70597	0.84456	0.71279	•••
$-\epsilon(2p_{z,a})$	0.71096	0.84521	0.70597	0.84456	0.71279	•••
T	74.81115	74.80732	74.79849	74.79850	74.81776	
$\langle\Sigma\, 1/r_{ij}\rangle$	28.44441	28.45090	28.45233	28.45242	28.42636	
Θ_{xx}	−0.94745	−0.93257	−0.93019	−0.93155	•••	
Θ_{yy}	0.47372	0.46628	0.46510	0.46578	•••	
Θ_{zz}	0.47372	0.46628	0.46510	0.46578	•••	
$q_{yy}(O)$	−1.66604	−1.65357	−1.65846	−1.65550	−1.71153	−1.777[c]
$q_{xx}(O)$	3.33208	3.30713	3.31692	3.31101	3.42306	3.554[c]
$q_{zz}(O)$	−1.66604	−1.65357	−1.65846	−1.65550	−1.71153	−1.777[c]
$\delta(r=O)$	296.516	296.530	296.519	296.518	311.5249	•••
$\langle 1/r_O\rangle$	22.25828	22.25797	22.25710	22.25711	22.25762	•••
$\langle x^2\rangle$	4.31752	4.30971	4.30665	4.30751	•••	
$\langle y^2\rangle$	3.37008	3.37714	3.37646	3.37596	•••	
$\langle z^2\rangle$	3.37008	3.37714	3.37646	3.37596	•••	
$\langle r^2\rangle$	11.05768	11.06399	11.05957	11.05943	11.24470	

[a] All energies and properties are in atomic units.

[b] Sym implies that equivalence restrictions were imposed on the p orbitals of O and the d_{x^2}, d_{y^2}, and d_{z^2} basis functions (see Sec. IV). Unsym implies that such restrictions were not imposed.

[c] Using $Q = -0.025b$ and $qQ = 0.04442$ from Ref. 34.

[d] W. A. Goddard III, Ref. 34.

[e] C. E. Moore, Natl. Bur. Std. Circ. 467, Vol. 1 (1949).

but we note here that the LGF orbitals may provide the theoretical foundation for Linnett's model and in any case should lead to a quantitative description of bonding in terms of interpretable orbitals.

VI. DISCUSSION OF THE ENERGIES AND PROPERTIES

The GF total energies for H_2O, OH, and O are given in Table VI and compared with the HF results. We see that the [521/2] GF H_2O energy is 0.019 hartree (0.5 eV) lower than that obtained by Neumann and Moskowitz[27] (hereafter NM), the best previously reported value. Note that NM used a larger uncontracted (10, 6/2, 4/2) basis. Comparing the GF and HF results for the [521/2] and [42/2] bases, we see that the GF energy is lower by 0.043 hartree in both cases, indicating that for the (10, 6/2, 4/2) basis the GF energy would be about −76.102 hartree.

The bond dissociation energy of H_2O, D_e(H–OH),[28] is calculated from the [521/2] GF wavefunctions to be 0.1632 a.u. or 81% of the experimental value, 0.201 a.u.[29,30] The [521/2] total binding energy of H_2O is calculated to be 0.2675 a.u. which is 72% of the experimental value, 0.371 a.u.[29,30]

In Tables VII, VIII, and IX we show the orbital energies and several properties for H_2O, OH, and O, respectively. We see that using Koopmans' theorem,[5] the calculated first ionization potential is too large by about 12% for H_2O, 1% for OH, and 2% for O (using the [521/2] basis).

Neumann and Moskowitz[27] have already pointed out the importance of d basis functions on the O, and p basis functions on the H, for describing the dipole moment μ. Comparing the HF results we see that the inclusion of one set of O d functions accounts for about 61% of the difference between the [42/2] and NM H_2O dipole moments. The GF dipole moment was 0.02 a.u. lower than the corresponding HF value for both Gaussian sets and hence would probably be about 0.765 a.u. for the (10, 6, 2/4, 2) basis. This compares to an experimental value of 0.728 a.u.[31] The calculated OH dipole moment also decreases significantly upon adding d basis functions but is still larger than the experimental value of 0.653 a.u.[32] For both H_2O and OH the inclusion of d basis functions significantly decreases $\langle z^2\rangle_{c.m.}$.

Comparing the symmetry restricted and unrestricted GF calculations on OH, we see that the symmetry restrictions significantly decrease $\epsilon_{1\pi x,a}$ and $\epsilon_{1\pi y,a}$ but lead to small changes in the other properties in Table VIII (largest change is 7% in θ_{yy} and 3% in $q_{yy}(O)$ and $q_{xx}(O)$ for the [521/2] basis). This indicates that the charge distribution is not appreciably altered by the symmetry restrictions.

As has been observed before[33] the potentials at the O

and H are rather insensitive to changes in the basis. These potentials are related to the diamagnetic shielding by $\sigma_A^d = (e^2/3mc^2)(\sum 1/r_A)$.

For H_2O the experimental values of the elements of the electric field gradient tensor, q_{ii}, were computed from the experimental quadrupole coupling constants of Verhoeven *et al.*[33] using the O^{17} quadrupole moment of $-0.025b$ from Goddard[34] (Schaefer *et al.*[35] obtained $-0.0256b$) and the D quadrupole moment of $+0.0027966b$ from Narumi and Watanabe.[36] Here x, y, and z are the principal axes of the electric field gradient tensor at the O, α, β, and γ are the principal axes at the H, and φ is the orientation angle (see Fig. 1). The resulting $q_{ii}(O)$ from the GF wavefunctions for H_2O are all closer to experiment than those from the HF wavefunctions of Neumann and Moskowitz[27] and Aung *et al.*[30] The GF values of $q_{ii}(H)$ in H_2O are quite similar to the HF values from Neumann and Moskowitz, and are more sensitive to the addition of O d functions than are the $q_{ii}(O)$.

VII. SUMMARY

We find that the LGF orbitals lead to a lucid description of the changes in bonding as we proceed from O to OH to H_2O. It appears that this same approach will generally lead to equally useful results in other systems. In particular, these calculations indicate that the LGF orbitals may provide a theoretical foundation for Linnett's double-quartet model of bonding.

ACKNOWLEDGMENTS

We thank Professor R. M. Pitzer and Professor W. E. Palke for the use of their localization program (which was modified for these calculations) and for the use of their version of the Cambridge (Harvard–MIT) Slater Integrals program. In addition, we thank Dr. T. H. Dunning and Dr. M. Geller for the use of the Geller Gaussian Integrals Program and Dr. R. M. Stevens for the use of the Nesbet–Stevens Diatomic Integrals Program. We thank W. J. Hunt and Dr. H. Basch for the use of the Hunt version of the Basch Polyatomic Integrals Program. Finally we thank C. Melius for help with calculation of the properties.

* Partially supported by Grants GP-6965 and GP-15423 from the National Science Foundation. Page charges supported by California Institute of Technology.

† Woodrow Wilson Fellow, 1967–1968; NDEA Fellow, 1969–1970.

‡ Alfred P. Sloan Fellow.

§ Contribution No. 4012.

[1] W. A. Goddard III, J. Chem. Phys. **48**, 450 (1968).
[2] W. A. Goddard III, J. Chem. Phys. **48**, 5337 (1968).
[3] W. A. Goddard III, Phys. Rev. **157**, 81 (1967).
[4] P.-O. Löwdin, Advan. Chem. Phys. **2**, 207 (1959); Phys. Rev. **97**, 1509 (1955).
[5] J. C. Slater, *Electronic Structure of Molecules* (McGraw-Hill, New York, 1963).
[6] $G = (1/N!)\sum_{\tau}\xi_{\tau}$, where the sum is over all $\tau \in S_N$ and ξ_{τ} is the parity of τ.
[7] W. A. Goddard III, Phys. Rev. **157**, 73 (1967).
[8] D. E. Rutherford, *Substitutional Analysis* (Edinburgh University Press, London, 1948).
[9] W. A. Goddard III, Phys. Rev. **169**, 120 (1968).
[10] V. Fock, Z. Physik **61**, 126 (1930).
[11] C. A. Coulson, Trans. Faraday Soc. **38**, 433 (1942); J. E. Lennard-Jones, Proc. Roy. Soc. (London) **A198**, 14 (1949); G. G. Hall and J. E. Lennard-Jones, *ibid.* **A202**, 155 (1950); J. A. Pople, Quart. Rev. **11**, 273 (1957).
[12] J. E. Lennard-Jones and J. A. Pople, Proc. Roy. Soc. (London) **A202**, 166 (1950).
[13] C. Edmiston and K. Ruedenberg, Rev. Mod. Phys. **35**, 457 (1963); K. Ruedenberg, *Modern Quantum Chemistry*, edited by O. Sinanoğlu (Academic, New York, 1965), Vol. 1, p. 85.
[14] C. Edmiston and K. Ruedenberg, J. Chem. Phys. **43**, S97 (1965).
[15] C. Edmiston and K. Ruedenberg, *Quantum Theory of Atoms Molecules and Solids*, edited by P. O. Löwdin (Academic, New York, 1966), p. 263.
[16] R. M. Pitzer, J. Chem. Phys. **41**, 2216 (1964).
[17] R. M. Pitzer and D. P. Merrifield, J. Chem. Phys. **52**, 4782 (1970).
[18] S. Huzinaga, J. Chem. Phys. **42**, 1293 (1965).
[19] T. H. Dunning, "Molecular Quantum Mechanics," Miscellaneous Tech. Rept. No. 2, A. A. Noyes Laboratory, California Institute of Technology (unpublished).
[20] C. C. J. Roothaan, Rev. Mod. Phys. **32**, 179 (1960).
[21] G. Herzberg, *Spectra of Diatomic Molecules* (Van Nostrand, New York, 1950).
[22] W. S. Benedict, N. Gailar, and E. K. Plyler, J. Chem. Phys. **24**, 1139 (1956).
[23] Coefficient vectors for the other basis sets are available upon request.
[24] In defining the p character of one orbital, we approximate the functions centered on H expanding them in terms of the basis functions centered on O and define the p character as the total fraction of the orbital contained in the p components.
[25] See, for example, J. D. Roberts and M. C. Caserio, *Basic Principles of Organic Chemistry* (Benjamin, New York, 1964), p. 132–133, and L. Pauling, *The Nature of the Chemical Bond* (Cornell U. P., New York, 1960).
[26] J. W. Linnett, *The Electronic Structure of Molecules* (Wiley, New York, 1964); J. Am. Chem. Soc. **83**, 2643 (1961).
[27] D. Neumann and J. W. Moskowitz, J. Chem. Phys. **49**, 2056 (1969).
[28] G. Herzberg, *Electronic Spectra and Electronic Structure of Polyatomic Molecules* (Van Nostrand, New York, 1966), p. 585.
[29] P. E. Cade and W. M. Huo, J. Chem. Phys. **47**, 614 (1967).
[30] S. Aung, R. M. Pitzer, and S. I. Chan, J. Chem. Phys. **49**, 2071 (1968).
[31] W. H. Kirchoff and D. R. Lide, Jr., as quoted in Refs. 27 and 30.
[32] F. X. Powell and D. R. Lide, Jr., J. Chem. Phys. **42**, 4201 (1965).
[33] J. Verhoeven, A. Dymanus, and H. Bluyssen, J. Chem. Phys. **50**, 3330 (1969).
[34] W. A. Goddard III, Phys. Rev. **182**, 48 (1969).
[35] H. F. Schaefer III, R. A. Klemm, and F. E. Harris, Phys. Rev. **176**, 49 (1969).
[36] H. Narumi and T. Watanabe, Bull. Am. Phys. Soc. **9**, 11 (1964).